UNIVERSITAT POLITÈCNICA DE VALÈNCIA

INSTITUTO INTERUNIVERSITARIO DE INVESTIGACIÓN DE RECONOCIMIENTO MOLECULAR Y DESARROLLO TECNOLÓGICO

Nanostructured supports for detection of pathogens and biomolecules of interest based on molecular gates with oligonucleotides

PhD. THESIS

Submitted by

María Nieves Aranda Sobrino

PhD. Supervisors:

Prof. Ramón Martínez Máñez

Dra. Elena Aznar Gimeno

Valencia, September 2024

RAMÓN MARTÍNEZ MÁÑEZ, Ph.D. in Chemistry and Professor at the *Universitat Politècnica de València* and ELENA AZNAR GIMENO, Ph.D. in Chemistry and Lecturer at the U*niversitat Politècnica de València*.

CERTIFY:

That the work ***"Nanostructured supports for detection of pathogens and biomolecules of interest based on molecular gates with oligonucleotides"*** has been developed by María Nieves Aranda Sobrino under their supervision in the Instituto Interuniversitario de Investigación de Reconocimiento Molecular y Desarrollo Tecnológico (IDM) of the *Universitat Politècnica de València*, forming part of the Unidad Mixta UPV-IISLAFE de Nanomedicina y sensores, as a Thesis Project in order to obtain the degree of Ph.D. in Chemistry at the *Universitat Politècnica de València*

Valencia, September 2024

Prof. Ramón Martínez Máñez
Director

Dra. Elena Aznar Gimeno
Director

A mis padres

Uno nunca se da cuenta de lo que ha hecho;

Uno solo puede ver lo que le queda por hacer.

Marie Curie

Acknowledgements

Agradecimientos

Una vez escuché que “la paciencia es la madre de la ciencia”, y no podría estar más de acuerdo. Esta tesis ha sido un claro ejemplo de ello, especialmente en su etapa final, de la cual HOY me siento MUY orgullosa. Sin embargo, llegar hasta aquí no habría sido posible sin el apoyo de mi gente, quienes fueron clave en todas las fases de esta aventura llamanda *Programa de Doctorado en Química de la UPV.*

En la primera etapa, mis directores de tesis, Ramón y Elena, fueron fundamentales al darme la oportunidad de contribuir a la investigación básica. Agradezco a Ramón por su constante confianza en mi trabajo y por todo lo que me enseñó en estos casi 4 años, no solo en ciencia, sino también en gestión de proyectos y relaciones laborales. A Elena, le doy las gracias por su apoyo incondicional, por su fe en que los experimentos saldrían bien y por no rendirse nunca, sin importar las dificultades. Admiro profundamente tu fortaleza en los momentos más complicados, y por fin podemos decir, ¡lo logramos!

También quiero agradecer al equipo administrativo del IDM, especialmente a Eva Brun, por asegurar que todo estuviera a tiempo y facilitar los trámites con el mejor trato posible, y a Tania, cuya alegría es contagiosa, por su infinita paciencia y ayuda en todas las gestiones.

Quiero agradecer al mítico COMANDO FE: Luis, Sara, Moloud y Mari Carmen, quienes me abrieron las puertas del lab 6.30 y me enseñaron a dar mis primeros pasos en *Nanomedicina y sensores*. ¡Ha sido un HONOR trabajar con vosotros! Y Marina, calienta que sales. El antiguo 2.6 también me acogió con los brazos abiertos: Paula, Xente, Serena, Toni Llopis, Marcia, Juanfran, Iris (nuestro súper artículo *is coming*) Angy (la primera persona que me sentó a su lado, y no creo que haya sido casualidad) y Eva (la mejor organizadora de planes en pandemia). También agradezco el cálido recibimiento de las chicas veteranas del CIPF, Alba G., Araceli, Gema y Alejandra. ¡Qué pena no haber coincidido más!

La segunda etapa, la más significativa para mí, estuvo marcada por mi familia valenciana. Laura, desde el primer día en Valencia te convertiste en mi hermana; aún me sorprende la SUERTE que tuve de encontrarte. Y tú también, Clem. Cualquier plan para vernos siempre ha sido un chute de energía y ha sido fundamental para llegar hasta aquí. Carla, mi alumna estrella y descubrimiento en pandemia, gracias por ser mi persona vitamina (y mi FM favorita) junto con Marta. Y recordad, ¡los mejores planes están SIEMPRE por llegar! Marina fue la primera bio-staff que vi en un laboratorio de químicos. No contentas con eso, decidimos conquistar lo que se convertiría en nuestro hogar-lab durante 3 años: el CONVENTO FE. Sigo maravillada de tu forma de dar consejos, de ser crítica y saber decirme lo que no quería escuchar. No he podido tener mejor compi predoc desde el principio. Y si alguna vez escucháis que lo mejor está por venir, creedlo: un día, la sevillana más guapa, inteligente y aventurera de Carmona entró por la puerta del 6.30. Isa, lo nuestro fue amor a primera *pipeta*, y desde el primer momento supe que conquistaríamos el mundo juntas, ¡ya llevamos 3 continentes! Es INCALCULABLE el número de horas que hemos pasado juntas en la poyata, y siempre has estado AHÍ en TODO. Eres un deseo cumplido. Alba, esto también va para ti. No podría haber dado lo mejor de mí sin tu apoyo incondicional, tus consejos de hermana y tus planes *cuquis*. Ahora sé lo que significa tener lab-sis (± gym bro). Esta tesis también lleva vuestros nombres. Sin olvidarme de los otros dos pilares que han hecho posible que yo esté aquí: Andy, por venir a "salvarnos" cuando más lo necesitábamos; todos deberíamos de tener a alguien como tú en nuestras vidas. Y Andrea, no podríamos haber llevado a la Fe a su *peak* sin ti, ¡sigue brillando donde quiera que vayas! Con mención especial al lab del CIPF, que además de tener una campana extractora, había dos investigadoras de las cuales tengo que hablar. Blanca, has sido LO MEJOR en tiempos de pandemia, destacando cómo un ratito contigo puede hacerte desconectar de todo, ya sea en Pamplona, Agadir, Teruel o cualquier rincón de la ciudad. Y como ya casi casi lo tienes… ¡Ve pensado tu viaje fin de tesis! Y Elena, desde que te conocí supe que eras un SÍ: sí a escucharme, a ayudarme, a cualquier nueva actividad (deportiva o no, con o sin nieve), y lo más importante, a apoyarme en todo momento.

También agradecer al resto del equipo separado al "nacer". Guille, no se me ocurre mejor ejemplo de buenrrollísmo que tú. ¡Volveré para cerrar con Andy, con Isa y contigo cualquier celebración del grupo! Yoel, gracias por demostrar que los cambios son para mejor. ¡Siempre tendrás tu sitio en la Fe! Al nuevo equipo del CIPF: Javi, David A., David B., Jenny, Maria (*best TFG ever*), Alba O., Juanjo y Sandra Clara, ¡ha sido un placer coincidir con vosotros! Y por último, pero no menos importante, al increíble equipo del poli, encabezado por Vicente, Estela y Andrea Bernardos, Hicke, Öznur, Tayfun, Andrea Escudero, Miguel, Eduardo, Giovanni, Jordi y Carol. ¡Espero veros pronto!

Mención especial a *los de siempre,* los cuales han estado presente en TODAS las etapas de esta tesis. Gracias a mis amigos del cole, INSEPARABLES desde el PRINCIPIO: Ali, Ángela A., Inma, Fran, Pau y (un poco menos) Raúl. Si hoy estoy aquí, es por culpa de vosotros. Gema y María, habéis sido mis *life-saving sisters* tanto en los momentos más difíciles como en los mejores bombardeos. Contando SIEMPRE los días para veros. Pilar, siempre confiándote mi vida (tanto en las pista de esquí como cuidando mi tesis) y tú siempre tan salvavidas. Te debo las que quieras. Yeyi, no recuerdo NI UNA SOLA VEZ que no hayas sido mi *persona vitamina*. Por favor, síguelo siendo siempre. Isita, aunque estemos a 2220 km de distancia, no sé de una en la que no hayas estado ahí presente. Juli, no habría llevado estos últimos meses (ni *the head of the intro*) igual sin nuestros gym y ñam con Ángela P. (la + tocha y + mejó y + vitamina). Nuria y Mari Carmen, no se me ocurre apoyo más incondicional que el vuestro. Desde tercero de la E.S.O. he sido INCAPAZ de soltaos. María Sobrino, te he visto bailar manchegas y desfilar en Nueva York. ¿Qué más podría pedirle al destino que tener a mi modelo de pasarela y de vida favorita? Ali N., ahora es tu turno de demostrar de lo que eres capaz; Elx está MUY orgulloso de nosotras, y yo, aún MÁS. También de ti, Lucía. El nanomáster no hubiera tenido valor si no te hubiera conocido. Lusan, Carcha, Marpla y Mamba, gracias por SIEMPRE encontrar tiempo para recargarme de energía con cualquier plan, y también a mis chicos, Alfonso y Pedro, ya que sin vustro apoyo INCONDICIONAL no habría sido capaz de llegar tan lejos. Mario, gracias por preocuparte tanto en la etapa más durilla. Tus cafeses y nuestros *push press* me han salvado. Miguel, Pepe, Ángela, Sara, Juli, Beto, Javi y Blanco, gracias por vuestro apoyo incondicional. Esto va por vosotros, mis Anacardos. ¡OS QUIERO! Alberto y

Alejandro, gracias por preocupaos por mi y picarme al CrossFit. ¡Los post entreno han sido lo mejor! A mis bioquímicos, Raúl (partner in crime since always), Sara (apoyando esta tesis con nuestras videollamadas internacionales), Noelia (dándome el último empujón cantando desde Aranda), Mari Ángeles, Manolo, Álvaro, Ana y Mariate (la mejor sorpresa valenciana) los cuales acertaron (salvo Andrea y Ana, ¡ya casi lo tenéis!) en no hacer una tesis doctoral pero me han apoyado en todo momento. Nerea, gracias por no soltarme en 10 años y ser familia. También quiero agradecer a quienes formaron parte de este camino pero ya no lo continúan. Julia, Jaime y Adrián, gracias por aguantarme en la etapa más peleona de la tesis y hacer que vivir con vosotros fuese tan fácil. Gracias a mis casi doctoras sevillanas, Clara y Carmen, y a Noe, la fallera alborayense *més millor*, conoceros ha sido más bonico que las hortensias de *São Miguel*. Tamara y Nuria, gracias por estar hasta para cualquier emergencia. De cada uno de vosotros he aprendido aún más, si cabe.

Finalmente, gracias mis tíos, tías, primos y primas, sabéis lo duro que ha sido y no habéis dejado de preocupaos. Y, sobre todo, a mis padres, a quienes quiero y admito a partes iguales y cuyo apoyo INCONDICIONAL ha sido lo que me ha hecho llegar hoy hasta AQUÍ. Papá, mamá, os lo debo todo.

Resumen:

La tesis doctoral "Nanostructured supports for the detection of pathogens and biomolecules of interest based on molecular gates with oligonucleotides" se enfoca en el diseño y desarrollo de nanomateriales híbridos orgánico-inorgánicos como biosensores. Dichos sistemas se basan en puertas moleculares ancladas en alúmina mesoporosa como sistemas innovadores que pueden usarse en aplicaciones relacionadas con el diagnóstico de enfermedades y el monitoreo de la calidad ambiental.

El primer capítulo de la tesis introduce los principios básicos en los que se basan los estudios realizados y los materiales desarrollados: química supramolecular, reconocimiento molecular, materiales híbridos orgánicos-inorgánicos y su aplicación en procedimientos de identificación molecular. Los objetivos generales de la tesis se describen brevemente en el segundo capítulo.

En el tercer capítulo se ha diseñado y optimizado un nuevo dispositivo para la detección rápida y selectiva del ADN del virus del papiloma humano (VPH). Utilizando películas nanoporosas de alúmina anódica recubiertas de oligonucleótidos, se desarrollaron sensores fluorogénicos cargados con el indicador rodamina B (RhB) y protegidos con secuencias cortas de ADN monocatenario complementarias a secuencias de bases que coinciden con la composición genética de varias cepas de VPH de alto riesgo. Estas secuencias de oligonucleótidos específicas recubren el soporte nanoporoso e impiden que la RhB se difunda a la fase líquida en ausencia de ADN del VPH. Sin embargo, cuando un determinado ADN del virus está presente en el medio, las puertas moleculares se abren y se libera el fluoróforo, cuya presencia en solución puede medirse mediante fluorescencia. Este trabajo también ha mejorado el proceso de síntesis, enfocándose en una producción a gran escala con altos niveles de eficiencia y reproducibilidad. La superficie del sensor se ha caracterizado por Microscopía Electrónica de Barrido de Emisiones de Campo de Alta Resolución (HR-FESEM), Microscopía de Fuerza Atómica (AFM) y Espectroscopia de Rayos X de Dispersión de energía (EDXS). Se prepararon nueve biosensores diferentes para la detección precisa de 14 VPH diferentes y se validaron en 43 muestras clínicas.

El cuarto capítulo desarrolla un nanodispositivo diseñado para detectar específicamente la bacteria *Vibrio vulnificus*. El crecimiento del patógeno zoonótico relacionado con la acuicultura se está generalizando cada vez más como resultado del calentamiento global. La mayor presencia y actividad de esta bacteria, favorecida por condiciones ambientales más cálidas y salinas, se atribuye a los cambios climáticos, incluyendo el aumento de la temperatura del agua, las variaciones en los patrones de precipitación y los eventos climáticos extremos. Para el diseño del biosensor, el colorante se cargó en los poros de alúmina anódica nanoporosa y luego se bloqueó con una secuencia nucleotídica específica que reconoce la secuencia génica estructural de citolisina vvhA 5 de *V. vulnificus*. La apertura del material cerrado y la liberación de RhB se observó en presencia de ADN de la bacteria. Sin necesidad de procesos previos de extracción o amplificación de ADN, se analizaron muestras de agua para detectar *V. vulnificus* logrando su detección a concentraciones tan bajas como 100 UFC/mL en solo una hora. El sistema ofrece una técnica simple y asequible para realizar análisis de muestras de bacterias *Vibrio vulnificus* con un alto nivel de eficiencia en medios reales.

El quinto capítulo trata del desarrollo de un biosensor compuesto de alúmina nanoporosa, cargada de RhB y recubierta de una secuencia específica de ADN diseñada para detectar miR-4732-3p, una molécula vinculada a pacientes de cáncer que experimentaron cardiotoxicidad inducida por antraciclina. Este procedimiento permitió la detección de miRNA 4732-3p a baja concentración en muestras séricas de pacientes y se ha conseguido en menor tiempo que los métodos clásicos estándar como qPCR. El biosensor es muy prometedor para la detección temprana de cardiotoxicidad.

El sexto capítulo concluye con un análisis de los resultados obtenidos en los capítulos anteriores, así como de las posibles aplicaciones de los sistemas desarrollados.

Estos sistemas de alta sensibilidad y especificidad son rápidos y económicos, fáciles de usar y no requieren personal especializado, mientras que se pueden transportar fácilmente al sitio de muestreo para realizar pruebas. Todos los sensores desarrollados han sido validados con muestras reales, confirmando su viabilidad para un mayor desarrollo y comercialización.

Resum:

La tesi doctoral "Nanostructured supports for the detection of pathogens and biomolecules of interest based on molecular gates with oligonucleotides" s'enfoca en el disseny i desenvolupament de nanomaterials híbrids orgànic-inorgànics com biosensors. Estos sistemes es basen en portes moleculars ancorades en alúmina mesoporosa com a sistemes innovadors que poden usar-se en aplicacions relacionades amb el diagnòstic de malalties i el monitoratge de la qualitat ambiental.

El primer capítol de la tesi introduïx els principis bàsics en els quals es basen els estudis realitzats i els materials desenvolupats: química supramolecular, reconeixement molecular, materials híbrids orgànics-inorgànics i la seua aplicació en procediments d'identificació molecular. Els objectius generals de la tesi es descriuen breument en el segon capítol.

En el tercer capítol s'ha dissenyat i optimitzat un nou dispositiu per a la detecció ràpida i selectiva de l'ADN del virus del papil·loma humà (VPH). Utilitzant pel·lícules nanoporosas d'alúmina anòdica recobertes de oligonucleòtid, es van desenvolupar sensors fluorogénicos carregats amb l'indicador rodamina B (RhB) i protegits amb seqüències curtes monocatenaries d'ADN complementàries a seqüències de bases que coincidixen amb la composició genètica de diversos ceps de VPH d'alt risc. Estes seqüències de oligonucleòtids específiques recobrixen el suport nanoporos i impedixen que la RhB es difonga a la fase líquida en absència d'ADN del VPH. No obstant això, quan un determinat ADN del virus és present en el mig, les portes moleculars s'obrin i s'allibera el fluoróforo, la presència en solució del qual pot mesurar-se mitjançant fluorescència. Este treball també ha millorat el procés de síntesi, enfocant-se en una producció a gran escala amb alts nivells d'eficiència i reproducibilitat. La superfície del sensor s'ha caracteritzat per Microscòpia Electrònica d'Escombratge d'Emissions de Camp d'Alta Resolució (HR-FESEM), Microscòpia de Força Atòmica (AFM) i Espectroscòpia de Raigs X de Dispersió d'Energia (EDXS). Es van preparar nou biosensors diferents per a la detecció precisa de 14 VPH diferents i es van validar en 43 mostres clíniques.

El quart capítol desenvolupa un nanodispositiu dissenyat per a detectar específicament el bacteri *Vibrio vulnificus*. El creixement del patogen zoonòtic relacionat amb l'aqüicultura s'està generalitzant cada vegada més com a resultat del calfament global. La major presència i activitat d'este bacteri, afavorida per condicions ambientals més càlides i salines, s'atribuïx als canvis climàtics, incloent-hi l'augment de la temperatura de l'aigua, les variacions en els patrons de precipitació i els esdeveniments climàtics extrems. Per al disseny del biosensor, el colorant es va carregar en els poros d'alúmina anòdica nanoporosa i després es va bloquejar amb una seqüència específica de nucleòtids que reconeix la seqüència gènica estructural de citolisina vvhA 5 de *V. vulnificus*. L'obertura del material tancat i l'alliberament de RhB es va observar en presència d'ADN del bacteri. Sense necessitat de processos previs d'extracció o amplificació d'ADN, es van analitzar mostres d'aigua per a detectar *V. vulnificus* aconseguint la seua detecció a concentracions tan baixes com 100 UFC/mL en només una hora. El sistema oferix una tècnica simple i assequible per a realitzar anàlisi de mostres de bacteris *Vibrio vulnificus* amb un alt nivell d'eficiència en mitjans reals.

El quint capítol tracta del desenvolupament d'un biosensor compost d'alúmina nanoporosa, carregada de RhB i recoberta d'una seqüència específica d'ADN dissenyada per a detectar miR-4732-3p, una molècula vinculada a pacients de càncer que van experimentar cardiotoxicitat induïda per antraciclina. Este procediment va permetre la detecció de miRNA 4732-3p a baixa concentració en mostres sèriques de pacients i s'ha aconseguit en menor temps que els mètodes clàssics estàndard com qPCR. El biosensor és molt prometedor per a la detecció precoç de cardiotoxicitat.

El sext capítol conclou amb una anàlisi dels resultats obtinguts en els capítols anteriors, així com de les possibles aplicacions dels sistemes desenvolupats.

Estos sistemes d'alta sensibilitat i especificitat són ràpids i econòmics, fàcils d'usar i no requerixen personal especialitzat, mentres que es poden transportar fàcilment al lloc de mostreig per a realitzar proves. Tots els sensors desenvolupats han sigut validats amb mostres reals, confirmant la seua viabilitat per a un major desenvolupament i comercialització.

Abstract:

The doctoral thesis "Nanostructured supports for the detection of pathogens and biomolecules of interest based on molecular gates with oligonucleotides" focuses on the design and development of organic-inorganic hybrid nanomaterials as biosensors. Such systems are based on molecular gates anchored on mesoporous alumina as innovative systems that can be used in applications related to disease diagnosis and environmental quality monitoring.

The first chapter of the thesis introduces the basic principles on which the studies carried out and the materials developed are based: supramolecular chemistry, molecular recognition, hybrid organic materials-inorganic substances and their application in molecular identification procedures. The general objectives of the thesis are briefly described in the second chapter.

In the third chapter, a new device has been designed and optimized for the rapid and selective detection of DNA of human papillomavirus (HPV). Using nanoporous oligonucleotide-coated anodic alumina films, fluorogenic sensors loaded with the rodamine B indicator (RhB) have been developed and capped with short single-stranded DNA sequences complementary to taget equences that match the genetic composition of several high-risk HPV strains. These specific oligonucleotide sequences cap the nanoporous support and prevent RhB from diffusing to the liquid phase in the absence of HPV DNA. However, when a certain DNA of the virus is present in the medium, the molecular gates open and the fluorophore is released, the presence of which in solution can then be measured by fluorescence. This work has also improved the synthesis process focused on potental large-scale production with high levels of efficiency and reproducibility. The surface of the sensor has been characterized by High-Resolution Field Emission Scanning Electron Microscopy (HR-FESEM), Atomic Force Microscopy (AFM) and Energy Dispersion X-ray Spectroscopy (EDXS). Nine different biosensors were prepared for the precise detection of 14 different HPV and were validated in 43 clinical samples.

The fourth chapter develops a nanodevice designed to specifically detect *Vibrio vulnificus* bacteria. The growth of the aquaculture-related zoonotic pathogen is becoming increasingly widespread as a result of global warming. The increased presence and activity of this bacterium, favored by warmer and saline environmental conditions, is attributed to climate changes, including increased water temperatures, variations in precipitation patterns and extreme weather events. For the design of the biosensor, RhB was loaded on the nanopores of mesoporous anodic alumina and then blocked with a specific nucleotide sequence that recognizeds the cytolysine *vvhA 5* structural gene sequence of *V. vulnificus*. The opening of the gated material and RhB release was observed in the presence of bacterial DNA. Without the need for previous DNA extraction or amplification processes, water samples were tested for *V. vulnificus* achieving its detection at concentrations as low as 100 CFU/mL in just one hour. The system offers a simple and affordable technique for performing sample analyses of *Vibrio vulnificus* bacteria with a high level of efficiency in real media.

The fifth chapter deals with the development of a biosensor consisting of nanoporous alumina, loaded with RhB and capped with a specific DNA sequence designed to detect miR-4732-3p, a molecule related to cancer patients who experienced anthracycline-induced cardiotoxicity. This procedure allowed the detection of miRNA 4732-3p at low concentration in serum samples from patients and has been achieved in less time than standard classical methods such as qPCR. The biosensor is very promising for early detection of cardiotoxicity.

The sixth chapter concludes with a discussion of the results obtained in the previous chapters, as well as the possible applications of the systems developed.

These high sensitive and specific systems are fast and inexpensive, easy to use and do not require specialised personnel, while they can be easily transported to the sampling site for testing. All sensors developed have been validated with real samples, confirming their feasibility for further development and commercialisation.

Publications:

The research described in the thesis, together with additional contributions, has resulted in the following scientific publications:

Hernández-Montoto, A., **Aranda, M. N**., Caballos, I., López-Palacios, A., Tormo-Mas, M. Á., Pemán, J., Prieto Rodríguez, M., Picornell, C., Aznar, E., & Martínez-Máñez, R. (**2023**). Human papilloma virus DNA detection in clinical samples using fluorogenic probes based on oligonucleotide gated nanoporous anodic alumina films. *Advanced Healthcare Materials*, 2203326.

Submited publications:

Aranda, M. N., Caballos, I., López-Palacios, A., Carmona-Salido, H., Sanjuan, E., Aznar, E., Amaro, C., Ramón Martínez-Máñez, R., & Hernández-Montoto, A. Development of an Innovative Fluorogenic Biosensor for Direct Detection of *Vibrio vulnificus*, a Climate Change Biomarker.

Aranda, M. N., Caballos, I., López-Palacios, A., Hernández-Montoto, A., Gómez-Ferrer, M., Ontoria-Oviedo, I., Aznar, E., Sepúlveda, P. & Ramón Martínez-Máñez, R. Nanoporous Oligonucleotide-Capped Alumina Sensors for Rapid Screening of miR-4732-3p.

Other contributions:

Caballos, I., **Aranda, M. N.,** López-Palacios, A., Pla, L., Santiago-Felipe, S., Hernández-Montoto, A., Tormo-Mas, M. Á., Pemán, J., Gómez-Ruíz, M.D., Calabuig, E., Sánchez-Sendra, B., Francés-Gómez, C., Geller, R., Aznar, E. & Martínez-Máñez, R. (**2023**). Aptamer-Capped Nanoporous Anodic Alumina for SARS-CoV-2 Spike Protein Detection. *Advanced Materials Technologies*, 2201913.

Abbreviations and Acronyms:

A

AAO	Aluminum anodic oxide
ADP	Adenosine 5'-diphosphate
APSs	Activatable photosensitizers
APTES	(3-Aminopropyl)triethoxysilane
ATP	Adenosine 5'-triphosphate
AuNPs	Gold nanoparticles

B

BPA	Bisphenol A

C

CIBER-BBN	Centro de Investigación Biomedical En Red de Bioingeniería, Biomateriales y Nanomedicina
c.a.	Approximately
CTP	Camptothecin
COF	Covalent organic frameworks
CUR	Curcumin
CVD	Cardiovascular disease

D

DNA	Deoxyribonucleic acid
Dd	Nanopore diameter

E

EXC	Excitation

ELISA	Enzyme-linked immunosorbent assay
F	
FDA	Food and drug administration
FESEM	Field emision scanning electronic microscopy
FEN1	Flap endonuclease 1
H	
h	Hours
HAc	Acetic acid
HPV	Human papillomavirus
I	
ICPTS	3-(Triethoxysilyl)propyl isocyanate
IDM	Instituto Inveruniversitario de Investigación de Reconocimiento Molecular y Desarrollo Tecnológico
IDT	Integrated DNA Technologies
IUPAC	International union pure and applied chemistry
L	
LOD	Limit of detection
M	
M_2-AChR	Muscarinic acetylcholine repector
MDMA	3,4-methylenedioxymethamphetamine
MDPV	Methylenedioxypyrovalerone

min	Minutes
miRNA	Micro RNA
MOF	Metal–organic frameworks
MPTS	(3-mercaptopropyl)triethoxysilane

N

NAA	Nanoporous anodic alumina

P

PBA	3-phenoxybenzoic acid
PBS	Phosphate buffer saline
PcC4	Phthalocyanine derivative
PCR	Polymerase chain reaction
PDT	Photodynamic therapy
ppm	Parts per million

R

RhB	Rhodamine B
RNA	Ribonucleic acid
rpm	Revolutions per minute

S

SCP	Scopolamine
SMS	Silica mesoporous support
SRG	Sulforhodamine G
SOPMOs	Self-ordered porous metal oxides

T

T	Temperature
TEA	Triethylamine
TRIS	Tris(hydroxymethyl)aminomethane

U

UV	Ultraviolet
UCF	Unite forming colony

V

VBNC	Viable but not cultivable

W

WHO	World Health Organization

General index

General introduction

1. Supramolecular chemistry

Chemistry is the science that studies matter, its composition, structure, properties and the transformations it undergoes. In other words, chemistry is responsible for understanding how things are formed around us, how they change and how we can use them for our benefit, being present in everything around us (from the air we breathe to the food we eat, the clothes we wear and the medicines we take). Even our own body is made up of molecules and chemical reactions.

In the 1960s, a group of chemists ventured beyond simple covalent bonds in search of new discoveries. Although his knowledge was rooted in coordination chemistry and catalysis, it was in the 1970s that the concept of "supramolecular" began to make sense. One of the key points was the discovery and research of cyclodextrins by the French chemist Jean-Marie Lehn in the 1970s.[1] These compounds, formed by glucose units, had the ability to form inclusion complexes with other molecules, it made the way for a new field of study focused on non-covalent interactions between molecules. But the real recognition came in the 1980s, when Jean-Marie Lehn, along with his distinguished colleagues Donald J. Cram and Charles J. Pedersen, were awarded the Nobel Prize in Chemistry in 1987.[2] Their brilliant contributions to the development of molecules with specific recognition structures and his studies on the chemistry of macromolecules established supramolecular chemistry as a crucial and rapidly growing field of research.

Unlike traditional chemistry, which focuses on the formation of covalent chemical bonds, supramolecular chemistry uses intermolecular forces to assemble and organize molecules into specific and functional patterns, including hydrogen bonds, dipole-dipole, and hydrophobic forces, among others. This field, also known as "chemistry beyond

[1] Boger, J., Corcoran, R. J., & Lehn, J. M. (1978). *Cyclodextrin chemistry. Selective modification of all primary hydroxyl groups of α-and β-cyclodextrins.* Helvetica Chimica Acta, 61(6), 2190-2218.

[2] Lehn, J. M. (1988*). Supramolecular chemistry—scope and perspectives molecules, supermolecules, and molecular devices (Nobel Lecture).* Angewandte Chemie International Edition in English, 27(1), 89-112.

molecules", involves molecular self-assembly and reversible targeted recognition of unitary molecules.[3] Supramolecular assemblies can take various forms, such as host-guest complexes, polymers, and nanomaterials. In addition, since these are dynamic interactions, a substantial part of supramolecular chemistry will revolve around the chemical equilibrium in solution, and the control of variables such as temperature, concentration or solvent are decisive in the displacement of said equilibrium. The non-covalent interactions between the different units determine the structural and functional properties of supramolecular systems, as well as their macroscopic properties.[4]

Size plays a crucial role in supramolecular chemistry applications, where sensing systems are typically small, simple, and require limited molecular interactions, while complex molecular assemblies may involve many molecules.[5] For example, integrating these systems with mesoporous materials holds promise for developing new functional systems, leveraging unique properties not found in individual entities. This approach, based on molecules or supermolecules on preorganized surfaces, offers significant potential across various applications.

2. Molecular recognition

A broad aspect of supramolecular chemistry is the study of how two or more molecules interact to form more complex structures. What distinguishes it from molecular chemistry is its focus on non-covalent interactions and the phenomenon of self-assembly, where molecules spontaneously come together to recognize each other. These non-covalent interactions are fundamental for the reversible formation of supramolecular assemblies, allowing both molecular recognition and self-assembly. Self-assembly leads to the organization of smaller units into larger, more ordered patterns, which decreases

[3] Lehn, J. M. (2009). *Towards complex matter: supramolecular chemistry and self-organization*. European Review, 17(2), 263-280.

[4] Nussbaumer, A. L., Studer, D., Malinovskii, V. L., & Häner, R. (2011). *Amplification of chirality by supramolecular polymerization of pyrene oligomers.* Angewandte Chemie, 123(24), 5604-5608.

[5] Ariga, K. (2016). *Supermolecules*. In Biomaterials Nanoarchitectonics (pp. 25-40). William Andrew Publishing.

the free energy of the system and reaches thermodynamic equilibrium. As described by H. E. Fischer in 1894, supramolecular recognition chemistry occurs for example when the enzyme substrate interacts with the host or receptor by forming a "lock and key" relationship in which the guest has a complementary geometric size or shape (Figure 1). In 1987, the synthesis and evaluation of crown ethers, later expanded to cryptands and other polycyclic compounds, brought J.M. Lehn and molecular recognition to a whole new level and was worthy of the Nobel Prize.[6]

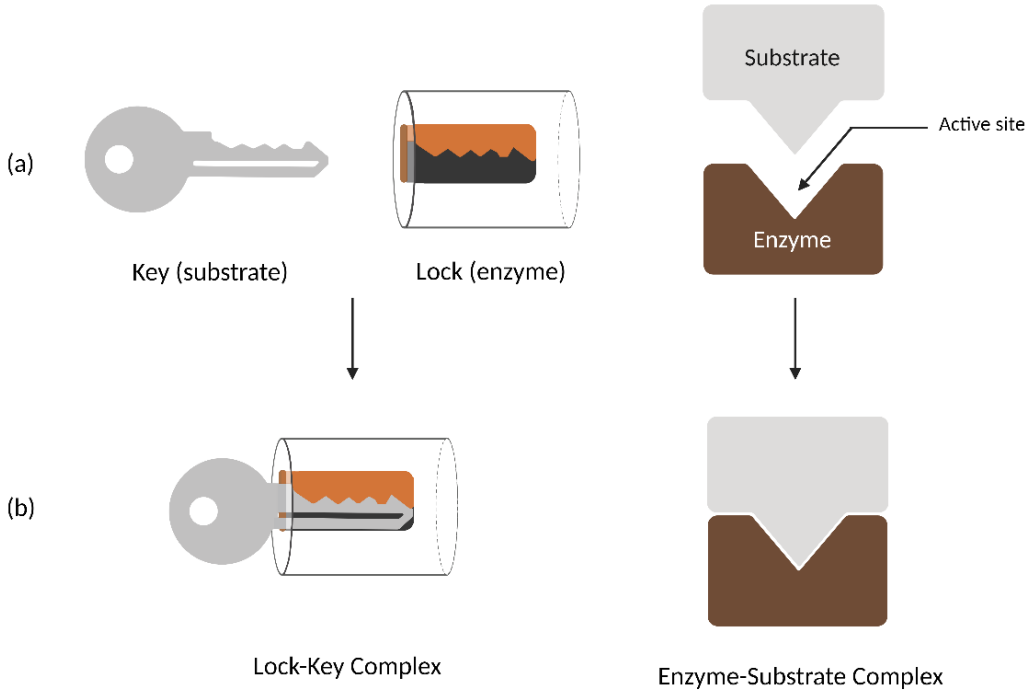

Figure 1. *Schematic of a molecular recognition event illustrated as a "lock and key" mechanism, where there is a specific interaction between a host (enzyme) and a host (substrate).*

[6] Lehn, J. M. (1988). *Supramolecular chemistry—scope and perspectives molecules, supermolecules, and molecular devices (Nobel Lecture).* Angewandte Chemie International Edition in English, 27(1), 89-112.

A fundamental application of supramolecular chemistry is the development of "molecular sensors", devices capable of detecting and recording physical or chemical properties, especially at very low concentrations. Inspired by biological processes, these sensors mimic the recognition mechanisms used by living organisms to detect a wide range of molecules, from nutrients to toxins and hormones. This similarity to nature has laid the foundation for the design and development of these sensors and their main components.[7] In these chemosensors, a macroscopic signal is produced along with molecular recognition events, usually through a reporting remainder, to indicate the presence of the analyte. This phenomenon requires selectivity and rapid response for practical applications. While chemical sensors rely on coordinating forces for host bonding, the term "chemidosimeter" is used when specific irreversible reactions occur between the host and the guest. In short, a molecular chemical sensor consists of at least two units:

- **Recognition subunit:** region of a molecule designed to interact with another specific molecule. Its essential characteristics include high specificity, ensuring binding only to the desired target through precise complementarity in size, shape and charge; sensitivity to detect even small amounts of the target, generating notable changes in the signal; resolution, with the signal proportional to the target quantity; and a wide dynamic range, operating at various concentrations.
- **Signaling subunit**: this part of the molecular sensor is responsible for changes in physical or chemical parameters (e.g. fluorescence variations, electrochemical reactions or redox processes), since it macroscopically transduces the signal produced by the detection event at the microscopic level.

[7] Zhang, J. X., & Hoshino, K. (2018*). Molecular sensors and nanodevices: principles, designs and applications in biomedical engineering.* Academic Press.

Various types of chemosensors have been developed based on changes in electrical quantities, such as redox potentials[8] or electrical capacities.[9] However, the most common are those that are based on optical changes, such as the absorption or emission of electromagnetic radiation[10]. Optical methods have perhaps been the most widely used due to their high sensitivity, fast response time, use of simple facilities, and low cost.[11] By coupling optical signaling units with specific binding sites, molecular sensors that are both chromogenic[12] and fluorogenic/luminescent[13] can be developed. Luminescent sensors undergo changes in the photophysical properties of the signaling unit when a certain analyte is present, whereas chromogenic sensors experience a color change in response to the analyte (for example, changes in the wavelength of the emission maximum, in quantum yield or a change in the ratio of luminescence emitters) after binding with the selected target. To be specific, the ease in which fluorescence spectra are recorded, the wide variety of fluorescent molecules (polycyclic aromatic hydrocarbons and organic heterocycles) and the low detection limits achieved compared to colorimetric techniques (below 10^{-6} M) make optical fluorogenic probes widely attractive.

Chromofluorogenic chemosensors are generally constructed by applying one of the following three approaches depending on how the recognition site is organized with the signaling subunit:

[8] Sancenón, F., Benito, A., Hernández, F. J., Lloris, J. M., Martínez-Máñez, R., Pardo, T., & Soto, J. (2002). *Difunctionalised chemosensors containing electroactive and fluorescent signalling subunits*. European Journal of Inorganic Chemistry, 2002(4), 866-875.

[9] Delaney, T. L., Zimin, D., Rahm, M., Weiss, D., Wolfbeis, O. S., & Mirsky, V. M. (2007). *Capacitive detection in ultrathin chemosensors prepared by molecularly imprinted grafting photopolymerization.* Analytical chemistry, 79(8), 3220-3225.

[10] a) Turro, N. J. (1991). *Modern molecular photochemistry. University science books*. b) D. Jawale Patil, P., D. Ingle, R., M. Wagalgave, S., S. Bhosale, R., V. Bhosale, S., P. Pawar, R., & V. Bhosale, S. (2019). *A naphthalimide-benzothiazole conjugate as colorimetric and fluorescent sensor for selective trinitrophenol detection.* Chemosensors, 7(3), 38.

[11] Martínez-Máñez, R., Sancenón, F., Hecht, M., Biyikal, M., & Rurack, K. (2011). *Nanoscopic optical sensors based on functional supramolecular hybrid materials.* Analytical and bioanalytical chemistry, 399, 55-74.

[12] Martinez-Máñez, R., & Sancenon, F. (2003). *Fluorogenic and chromogenic chemosensors and reagents for anions*. Chemical reviews, 103(11), 4419-4476.

[13] Martínez-Máñez, R., & Sancenón, F. (2005). *New advances in fluorogenic anion chemosensors*. Journal of Fluorescence, 15, 267-285.

- **Binding site-signaling subunit approach:** In this case, a covalent bond links both units. As a result of interacting with the binding site, a target molecule changes the electronic properties of the signaling subunit (a dye or a fluorophore), modulating color or emission (see Figure 2a).[14] Changes in fluorescence intensity/absorption may occur, as well as changes in wavelength. This is the most widely used method to build optical sensors, however the synthesis of the probes following this approach is usually complex.
- **Displacement approach:** In this protocol, binding sites and signaling subunits form a supramolecular ensemble that is not covalently linked (see Figure 2b). When the target molecule is coordinated with the binding site, a displacement reaction occurs, and the signaling subunit returns to solution. In the sensing ensemble, the signaling subunit presents a different color or emission than when it is free in solution, resulting in an optical response. [15]
- **"Chemodosimeter" approach:** It differs from other approaches in that it is a specific and irreversible chemical reaction that generates color or fluorimetric changes. Reactions induced by specific analytes, which break or form bonds with the designed probe, rapidly cause large chemical changes in the sensor, are usually highly selectivity and can be performed in aqueous media for most reactions.[16]

[14] a) Amendola, V., Esteban-Gómez, D., Fabbrizzi, L., & Licchelli, M. (2006*). What anions do to N– H-containing receptors*. Accounts of Chemical Research, 39(5), 343-353.. b) Bell, T. W., & Hext, N. M. (2004). *Supramolecular optical chemosensors for organic analytes*. Chemical Society Reviews, 33(9), 589-598. c) Gunnlaugsson, T., Glynn, M., Tocci, G. M., Kruger, P. E., & Pfeffer, F. M. (2006*). Anion recognition and sensing in organic and aqueous media using luminescent and colorimetric sensors.* Coordination chemistry reviews, 250(23-24), 3094-3117.

[15] Nguyen, B. T., & Anslyn, E. V. (2006). *Indicator–displacement assays*. Coordination chemistry reviews, 250(23-24), 3118-3127.

[16] Xu, Z., Chen, X., Kim, H. N., & Yoon, J. (2010). *Sensors for the optical detection of cyanide ion*. Chemical Society Reviews, 39(1), 127-137.

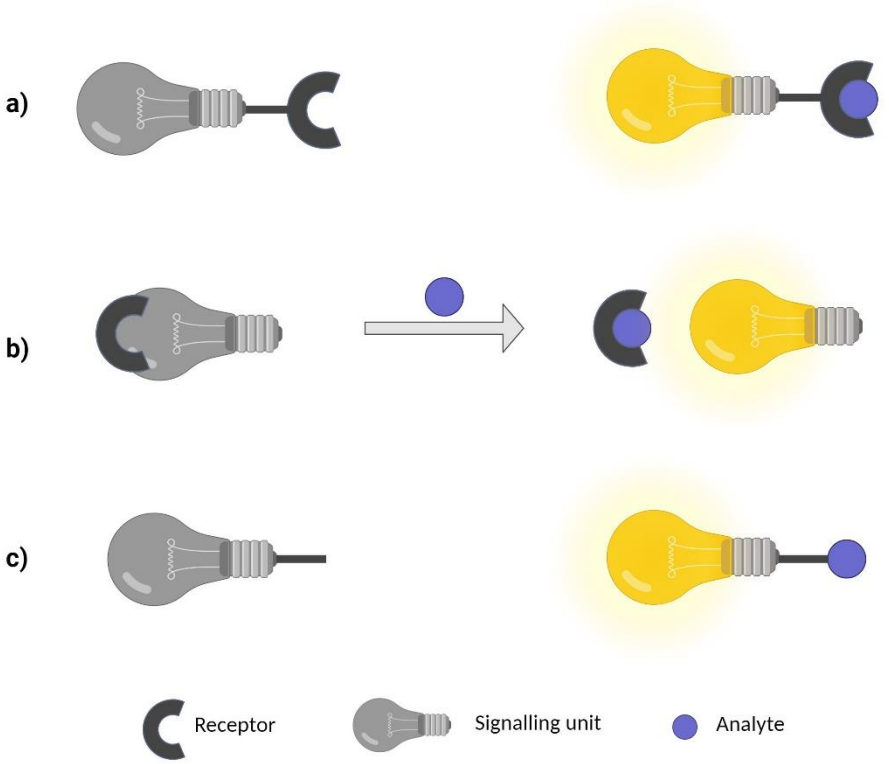

Figure 2. *Schematic representation of three possible optical chemosensor approaches: (a) binding site-signalling subunit; (b) displacement; (c) chemodosimeter.*

3. Nanotechnology: future sensors are one step closer

During a conference in 1959, Dr. Richard Feynman discussed the possibility of directly manipulating atoms and molecules and made the first conceptual reference of the concept of *Nanotechnology*. Moreover, in 1974 Dr. Norio Taniguchi specified that nanotechnology is related to the *"production technology to extra high accuracy and ultra-fine dimensions, that is, the preciseness and fineness on the order of 1 nm, 10^{-9} m, in length"* thus defining this new branch of technology.[17] Since then, nanotechnology has

[17] Taniguchi N. (1974). *On the basic concept of 'nano-technology'. Proc Intl Conf Prod Eng Tokyo, Part II*, Japan Society of Precision Engineering, (5–10).

grown and evolved into the study and application of functional structures designed on an atomic or molecular scale with at least one characteristic dimension measured in nanometers.[18] The scale of 1 to 100 nanometers (nm) represents a range of extremely small dimensions, where objects are thousands of times smaller than the width of a human hair. In this range, we find several examples, such as viruses, with sizes between 20 and 300 nm, biological molecules such as proteins and carbohydrates, ranging from 1 to 10 nm, DNA with a diameter of about 2 nm, carbon nanotubes of about 1 nm, T2 phages between 50 and 150 nm, nanotransistors around 10 nm[19] and nanoparticles, with sizes between 1 and 100 nm (Figure 3).

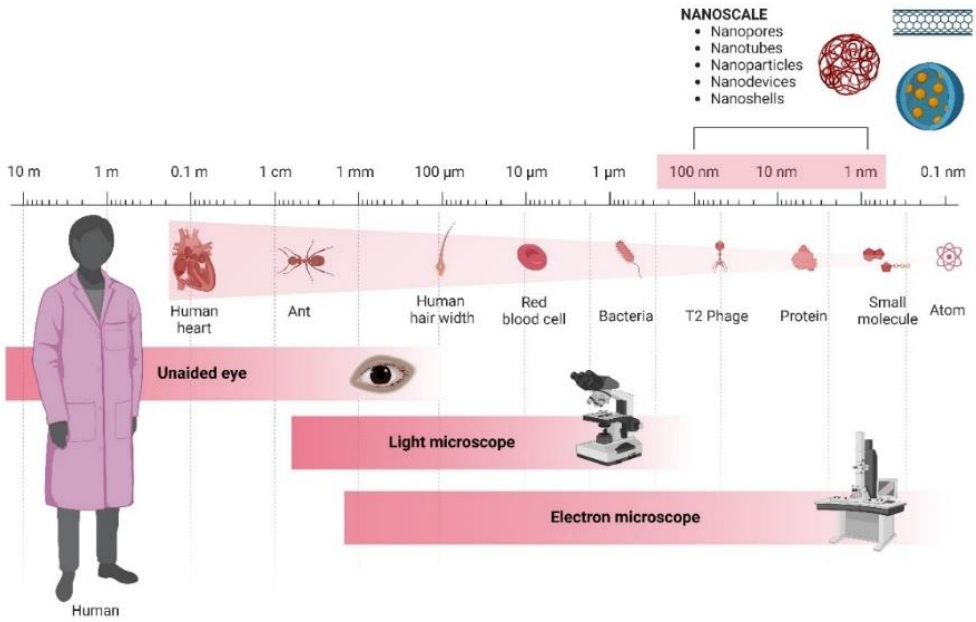

Figure 3. *Diagram illustrating the size range of common objects.*

[18] Kumar, N., & K*umbha*t, S. (2016). *Essentials in nanoscience and nanotechnology*. John Wiley & Sons.

[19] Li, J., Li, Y., Zhou, N., Xiong, W., Wang, G., Zhang, Q., y Radamson, HH (2020). *Study of silicon nitride inner spacer formation in process of gate-all-around nano-transistors.* Nanomaterials , 10 (4), 793.

Almost in all research fields and industrial areas there are currently applications related the the use of nanotechnology, which can be defined as any technology offering practical applications at the nanoscale. Nanobiotechnology, nanomaterials, nanoelectronics, nanomagnetism, nanophotonics and nanoelectronics, among other areas, have developed and continue developing systems based on nanoparticles or nanostructured surfaces. In addition to providing additional functionality to new nanomaterials, supramolecular chemistry and molecular recognition have been central in the development of this field.

As a subclass of nanomaterials, nanoporous materials are widely used in materials science and biomedicine: solids with nanoporous structures (pores less than 100 nm) that can be crystalline or amorphous.[20] Nanoporosity provides materials with a range of novel properties in the chemical, physical, electrical, mechanical and thermal fields, including low density, large specific surfaces, surface functionality feasibility and high load capacity. [21] The use of inorganic porous supports to recognize biomolecules of interest is described in the following sections.

4. Organic-inorganic hybrid porous materials

The coupling of supramolecular concepts with nanoscopic solid structures allows the design of new hybrid detection systems with improved sensitivity and selectivity for certain analytes, which is particularly valuable for challenging targets where selectivity is difficult to achieve using current methods. [22] These hybrid materials, which combine

[20] Xu, Q. (Ed.). (2013). *Nanoporous materials: synthesis and applications*. CRC press.

[21] Thommes, M., & Schlumberger, C. (2021). *Characterization of nanoporous materials.* Annual Review of Chemical and Biomolecular Engineering, 12, 137-162.

[22] a) Drechsler, U., Erdogan, B., & Rotello, V. M. (2004). *Nanoparticles: Scaffolds for molecular recognition*. Chemistry–A European Journal, 10(22), 5570-5579; b) Mancin, F., Rampazzo, E., Tecilla, P., & Tonellato, U. (2006). *Self-assembled fluorescent chemosensors.* Chemistry–A European Journal, 12(7), 1844-1854; c) Willner, I., Basnar, B., & Willner, B. (2007). *From molecular machines to microscale motility of objects: application as "smart materials", sensors, and nanodevices*. Advanced Functional Materials, 17(5), 702-717; d) Descalzo, A. B., Martínez-Máñez, R., Sancenon, F., Hoffmann, K., & Rurack, K. (2006). *The supramolecular chemistry of organic–inorganic hybrid materials.* Angewandte Chemie International Edition,

organic and inorganic components in a synergistic interaction on a nanometric scale, and are often obtained by anchoring organic functional groups into nanoscopic inorganic materials as support platforms. According to Professor Clément Sanchez, "*hybrid organic inorganic materials are not simply physical mixtures. They can be broadly defined as nano-composites with (bio)organic and inorganic components, intimately mixed where at least one of the component domains has a dimension ranging from a few Å to several nanometers. Consequently, the properties of hybrid materials are not only the sum of the individual contributions of both phases, but the role of their inner interfaces could be predominant*."[23]

In the field of host-guest interactions, ans specifically when recognition protocols are purged, anchoring organic molecules on solid supports offers several significant advantages:

- Interaction with the target analyte is maximized by preorganizing the receptor, which leads to the formation of a dense monomolecular layer of binding or coordination sites arranged specifically on the solid surface.
- The properties of the hybrid material can be modulated by means of multifunctionalization.
- The recognition process is improved by restricting the movement of the receiver when anchored to the solid surface.
- The detection system can be reused several times if coordination processes are reversible.
- Selectivity and sensitivity can be improved by controlling the size, shape and surface area, resulting in changes in the physical and chemical properties of the inorganic surface.

45(36), 5924-5948.

[23]Gomez-Romero, P., & Sanchez, C. (2005). *State of the art developments in functional hybrid materials*. Journal of Materials Chemistry, 15, 3557-3558.

The final properties and structure of the nanomaterial are mainly determined by the choice of the inorganic support, the organic groups anchored on its surface and the reaction conditions employed during its synthesis. Some of these materials can be obtained by simple interaction of organic molecules on inorganic nanoscopic structures. In fact, this thesis focuses on the design and development of new organic-inorganic hybrid nanodisposers using this general approach.

Typical examples of nanoporous materials include activated carbon, zeolites, mesoporous silica, porous metal nanoparticles, ceramics, porous carbon, different polymers and metal-organic frameworks, among others. During the fabrication and/or functionalization of porous nanomaterials, it is crucial to simultaneously control multiple length scales, purity, morphology and chemical composition. A nanoporous solid's properties largely determine its potential applications as a sensor, physisorbent, catalyst and therapeutic agent. In terms of applications, such as photonics, actuators, and biomedical materials or devices, three-dimensionally ordered macroporous structures with internal nanostructured features, large surface area, the interconnectivity of the pores, and the fully accessible inner surface are appealing. The aim of the next section will be to describe porous scaffolds as an important component for building organic-inorganic hybrid nanomaterials.

4.1. Types of porous materials

Based on the pore diameter, porous materials are categorized under three groups: (i) microporous (pore size less than 2 nanometers), (ii) mesoporous (pore size between 2-50 nanometers), and (iii) macroporous (pore size greater than 50 nanometers) as shown in Figure 4.[24] In this area many advancements have been made in processing

[24] Chaudhary, V., & Sharma, S. (2017). *An overview of ordered mesoporous material SBA-15: synthesis, functionalization and application in oxidation reactions.* Journal of Porous Materials, 24, 741-749.

aspects of porous solids, in the stability of mesoporous materials, in structural, compositional, and morphological control, as well as in existing and novel applications[25].

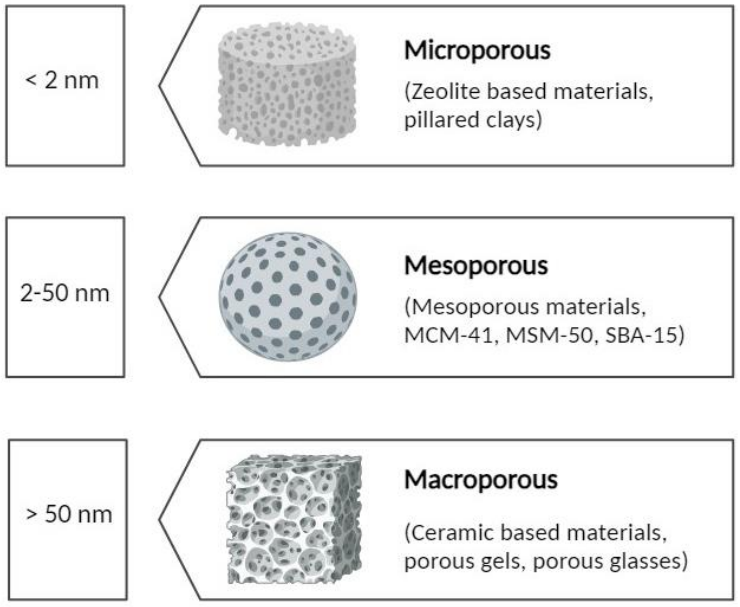

Figure 4. *Porous materials according to the IUPAC classification.*

Particularly, silica mesoporous supports (SMSs), such as microporous zeolites, mesoporous silica or metal–organic frameworks (MOFs), are available in a variety of diameters, from micrometric to nanometric, with homogenous pores. Additionally, they exhibit great inertness, are simple to functionalize using conventional chemistries, and

[25] a) De Vos, D. E., Dams, M., Sels, B. F., & Jacobs, P. A. (2002). *Ordered mesoporous and microporous molecular sieves functionalized with transition metal complexes as catalysts for selective organic transformations.* Chemical Reviews, 102(10), 3615-3640; b) Vallet-Regí, M., Colilla, M., & Izquierdo-Barba, I. (2008). *Bioactive mesoporous silicas as controlled delivery systems: application in bone tissue regeneration*. Journal of Biomedical Nanotechnology, 4(1), 1-15; c) Pla Blasco, L. (2021). *New nanostructured supports with signal amplification features for the detection of molecules and biomolecules of interest (Doctoral dissertation, Universitat Politècnica de València)*; d) Jane, A., Dronov, R., Hodges, A., & Voelcker, N. H. (2009). *Porous silicon biosensors on the advance*. Trends in biotechnology, 27(4), 230-239.

have a remarkable load capacity due to their extremely large specific surface area and specific volume.

In 1756, stilbite was identified as the first natural zeolite, and in the 1940s it was artificially synthesized. Zeolites are microporous materials well known for their regularity in pore size, stability and high selectivity,[26] making them valuable in sustainable chemical applications such catalusis, energy storage, biomass conversion and CO_2 capture. [27]

Mesoporous materials, more recent in development but equally noted for their broad specific surface area and diverse applications, emerged with the discovery of mesoporous silica MCM-41 in 1992. [28] Unlike zeolites, these materials have larger pores (2-50 nm) and more varied chemical compositions, which has made them valuable in fields such as enzymatic immobilization,[29] drug delivery[30] or catalysis,[31] among other fields.[32]. On the other hand, porous crystalline materials such as MOF and COF are more recent innovations, formed by covalent or coordination connections between

[26]a) Perego, C., & Millini, R. (2013). *Porous materials in catalysis: challenges for mesoporous materials*. Chemical Society Reviews, 42(9), 3956-3976. b) Johnson, S. A., Brigham, E. S., Ollivier, P. J., & Mallouk, T. E. (1997). *Effect of micropore topology on the structure and properties of zeolite polymer replicas.* Chemistry of Materials, 9(11), 2448-2458.

[27] Yu, J., Corma, A., & Li, Y. (2020). *Functional porous materials chemistry.*

[28] a) Taguchi, A., & Schüth, F. (2005). *Ordered mesoporous materials in catalysis*. Microporous and mesoporous materials, 77(1), 1-45. b) Perego, C., & Millini, R. (2013*). Porous materials in catalysis: challenges for mesoporous materials.* Chemical Society Reviews, 42(9), 3956-3976.

[29] Vallet-Regí, M., Colilla, M., & Izquierdo-Barba, I. (2008*). Bioactive mesoporous silicas as controlled delivery systems: application in bone tissue regeneration.* Journal of Biomedical Nanotechnology, 4(1), 1-15.

[30] a) De La Torre, C., Casanova, I., Acosta, G., Coll, C., Moreno, M. J., Albericio, F., & Martínez-Máñez, R. (2015). *Gated mesoporous silica nanoparticles using a double-role circular peptide for the controlled and target-preferential release of doxorubicin in CXCR4-expresing lymphoma cells.* Advanced Functional Materials, 25(5), 687-695. b) Bhat, R., Ribes, A., Mas, N., Aznar, E., Sancenon, F., Marcos, M. D., & Martinez-Máñez, R. (2016). *Thrombin-responsive gated silica mesoporous nanoparticles as coagulation regulators.* Langmuir, 32(5), 1195-1200. c) Vallet-Regí, M., Balas, F., & Arcos, D. (2007). *Mesoporous materials for drug delivery.* Angewandte Chemie International Edition, 46(40), 7548-7558.

[31] Mavrogiorgou, A., Baikousi, M., Costas, V., Mouzourakis, E., Deligiannakis, Y., Karakassides, M. A., & Louloudi, M. (2016). *Mn-Schiff base modified MCM-41, SBA-15 and CMK-3 NMs as single-site heterogeneous catalysts: Alkene epoxidation with H2O2 incorporation*. Journal of Molecular Catalysis A: Chemical, 413, 40-55.

[32] a) Pawar, R. R., Kevadiya, B. D., Brahmbhatt, H., & Bajaj, H. C. (2013). *Template free synthesis of mesoporous hectorites: Efficient host for pH responsive drug delivery.* International journal of pharmaceutics, 446(1-2), 145-152. b) Lebeau, B., Galarneau, A., & Linden, M. (2013). *Introduction for 20 years of research on ordered mesoporous materials.* Chemical Society Reviews, 42(9), 3661-3662.

inorganic/organic nodes and organic bonds. This peculiarity allows precise control over the shape and size of nanopores, which makes them promising in applications such as biomedicine, catalysis, gas separation and storage, and energy conversion.

The following section will be focused on nanoporous anodic alumina (NAA) supports, since it is used in this thesis as porous support.

4.1.1. Nanoporous Anodic Alumina

Porous anodic alumina was discovered in the 1930s, but it was from the 1950s to the 1970s that efforts eventually led to its development.[33] In 1995, the formation of nanoporous anodic alumina with a highly ordered 2D hexagonal porous structure was confirmed, and since then, nanoscience researchers have recognized the potential of three-dimensional nanostructures to improve the performance of of biodevices.[34]

Keller was the first to characterize the NAA using electron microscopy, describing it as arrays of hexagonally arranged nanometric pores, where the interpor distance is directly related to the anodizing voltage.[34] Over time, it has been established that control of shape and geometry depends primarily on the anodizing voltage or current strength. Other factors such as anodizing time, electrolyte type/concentration, pH and temperature also influence the resulting material.[35]

---

[33] a)Keller, F., Hunter, M. S., & Robinson, D. L. (1953). *Structural features of oxide coatings on aluminum*. Journal of the Electrochemical Society, 100(9), 411; b) O'sullivan, J. P., & Wood, G. C. (1970). *The morphology and mechanism of formation of porous anodic films on aluminium.* Proceedings of the Royal Society of London. A. Mathematical and Physical Sciences, 317(1531), 511-543.

[34] a) Wang, J., Karnaushenko, D., Medina-Sánchez, M., Yin, Y., Ma, L., & Schmidt, O. G. (2019*). Three-dimensional microtubular devices for lab-on-a-chip sensing applications.* ACS sensors, 4(6), 1476-1496; b) Amouzadeh Tabrizi, M., Ferre-Borrull, J., & Marsal, L. F. (2020). *Advances in optical biosensors and sensors using nanoporous anodic alumina.* Sensors, 20(18), 5068; c) Domagalski, J. T., Xifre-Perez, E., & Marsal, L. F. (2021*). Recent advances in nanoporous anodic alumina: Principles, engineering, and applications.* Nanomaterials, 11(2), 430.

[35] a) Lee, W., & Park, S. J. (2014). *Porous anodic aluminum oxide: anodization and templated synthesis of functional nanostructures.* Chemical reviews, 114(15), 7487-7556; b) Zaraska, L., Brudzisz, A., Wierzbicka, E., & Sulka, G. D. (2016). *The effect of electrolyte change on the morphology and degree of nanopore order of porous alumina formed by two-step anodization.* Electrochimica Acta, 198, 259-267.

Self-ordered porous metal oxides (SOPMOs) are a class of three-dimensional nanostructure platforms formed through the electrochemical anodization of metals such as titanium,[36] iron,[37] stainless steel,[38] silicon,[39] and aluminum[40] in acidic solutions. In this process, the metal is immersed in an electrolyte and an electric current is applied to the system. In the context of this thesis, the focus is on aluminum, which serves as the anode, hence the term "anodizing." Through this method, an amorphous oxide layer can be grown on the surface of aluminum, resulting in NAA.

Anodizing of materials is a widely used process in various industries due to its durability, easy functionalization, high surface area, biocompatibility, and cost-effectiveness[41]. Furthermore, it enhances the mechanical properties and chemical resistance of metals by providing a robust oxide layer[42]. However, under carefully

[36] Anitha, V. C., Goswami, A., Sopha, H., Nandan, D., Gawande, M. B., Cepe, K., & Macak, J. M. (2018). *Pt nanoparticles decorated TiO2 nanotubes for the reduction of olefins*. Applied Materials Today, 10, 86-92.

[37] Martin-Gonzalez, M., Martinez-Moro, R., Aguirre, M. H., Flores, E., & Caballero-Calero, O. (2020). *Unravelling nanoporous anodic iron oxide formation.* Electrochimica Acta, 330, 135241.

[38] Dhawan, U., Pan, H. A., Shie, M. J., Chu, Y. H., Huang, G. S., Chen, P. C., & Chen, W. L. (2017*). The spatiotemporal control of osteoblast cell growth, behavior, and function dictated by nanostructured stainless steel artificial microenvironments.* Nanoscale Research Letters, 12, 1-10.

[39] Elia, P., Nativ-Roth, E., Zeiri, Y., & Porat, Z. E. (2016). *Determination of the average pore-size and total porosity in porous silicon layers by image processing of SEM micrographs*. Microporous and Mesoporous Materials, 225, 465-471.

[40] Lee, W., & Park, S. J. (2014). *Porous anodic aluminum oxide: anodization and templated synthesis of functional nanostructures.* Chemical reviews, 114(15), 7487-7556.

[41] a) Santos, A., Balderrama, V. S., Alba, M., Formentín, P., Ferré-Borrull, J., Pallarès, J., & Marsal, L. F. (2012). *Nanoporous anodic alumina barcodes: toward smart optical biosensors*. Advanced Materials, 24(8), 1050-1054; b) Kumeria, T., Rahman, M. M., Santos, A., Ferre-Borrull, J., Marsal, L. F., & Losic, D. (2014). *Structural and optical nanoengineering of nanoporous anodic alumina rugate filters for real-time and label-free biosensing applications*. Analytical chemistry, 86(3), 1837-1844; c) Jani, A. M. M., Losic, D., & Voelcker, N. H. (2013*). Nanoporous anodic aluminium oxide: Advances in surface engineering and emerging applications*. Progress in materials science, 58(5), 636-704; d) Mey, I., Steinem, C., & Janshoff, A. (2012). *Biomimetic functionalization of porous substrates: towards model systems for cellular membranes.* Journal of Materials Chemistry, 22(37), 19348-19356.

[42] a) Surmenev, R. A., Chernozem, R. V., Pariy, I. O., & Surmeneva, M. A. (2021*). A review on piezo-and pyroelectric responses of flexible nano-and micropatterned polymer surfaces for biomedical sensing and energy harvesting applications*. Nano Energy, 79, 105442; b) Rajeev, G., Prieto Simon, B., Marsal, L. F., & Voelcker, N. H. (2018). *Advances in nanoporous anodic alumina-based biosensors to detect biomarkers of clinical significance: a review*. Advanced Healthcare Materials, 7(5), 1700904; c) Mijangos, C., Hernández, R., & Martin, J. (2016). *A review on the progress of polymer nanostructures with modulated morphologies and properties, using nanoporous AAO templates*. Progress in Polymer Science, 54, 148-182.

controlled conditions, the resulting structure can exhibit a highly ordered pattern. This ordered structure, along with the inherent chemical and physical properties of the material, offers numerous possibilities for diverse applications, including biosensors,[43] sensors,[44] template-based fabrication of nanowires and nanotubes[45] and drug delivery systems[46].

The unique chemical properties of aluminum oxide enable the attachment of a wide range of biomolecules or other compounds to the outer surface of NAA.[47] Among all the possibilities, incorporation of gating mechanisms in this supports transforms NAA-based materials into powerful tools for detection and diagnostics, providing precise detection capabilities.[48]

---

[43] a) Rajeev, G., Prieto Simon, B., Marsal, L. F., & Voelcker, N. H. (2018). *Advances in nanoporous anodic alumina-based biosensors to detect biomarkers of clinical significance: a review.* Advanced Healthcare Materials, 7(5), 1700904: b) Álvarez, J., Sola, L., Cretich, M., Swann, M. J., Gylfason, K. B., Volden, T., & Hill, D. (2014). *Real time optical immunosensing with flow-through porous alumina membranes.* Sensors and Actuators B: Chemical, 202, 834-839; c) Tanvir, S., Pantigny, J., Boulnois, P., & Pulvin, S. (2009). *Covalent immobilization of recombinant human cytochrome CYP2E1 and glucose-6-phosphate dehydrogenase in alumina membrane for drug screening applications*. Journal of Membrane Science, 329(1-2), 85-90.

[44] a) Carneiro, J. O., Machado, F., Pereira, M., Teixeira, V., Costa, M. F., Ribeiro, A., & Samantilleke, A. P. (2018). *The influence of the morphological characteristics of nanoporous anodic aluminium oxide (AAO) structures on capacitive touch sensor performance: a biological application.* RSC advances, 8(65), 37254-37266; b) Hong, C., Chu, L., Lai, W., Chiang, A. S., & Fang, W. (2011). *Implementation of a new capacitive touch sensor using the nanoporous anodic aluminum oxide (np-AAO) structure*. IEEE Sensors journal, 11(12), 3409-3416; c) Salamat, A., & Islam, T. (2020). *Fabrication of an anodized porous alumina relative humidity sensor with improved sensitivity.* Instrumentation Science & Technology, 48(2), 128-145.

[45] a) Peng, F., Tu, Y., & Wilson, D. A. (2017). *Micro/nanomotors towards in vivo application: cell, tissue and biofluid.* Chemical Society Reviews, 46(17), 5289-5310; b) Domagalski, J. T., Xifre-Perez, E., Santos, A., Ferre-Borrull, J., & Marsal, L. F. (2020). *Tailor-engineered structural and physico-chemical properties of anodic alumina nanotubes by pulse anodization: A step forward*. Microporous and Mesoporous Materials, 303, 110264.

[46] a) Porta-i-Batalla, M., Xifré-Pérez, E., Eckstein, C., Ferré-Borrull, J., & Marsal, L. F. (2017). *3D nanoporous anodic alumina structures for sustained drug release.* Nanomaterials, 7(8), 227; b) Wang, Y., Santos, A., Kaur, G., Evdokiou, A., & Losic, D. (2014). *Structurally engineered anodic alumina nanotubes as nano-carriers for delivery of anticancer therapeutics.* Biomaterials, 35(21), 5517-5526.

[47] Baranowska, M., Slota, A. J., Eravuchira, P. J., Macias, G., Xifré-Pérez, E., Pallares, J., & Marsal, L. F. (2014*). Protein attachment to nanoporous anodic alumina for biotechnological applications: influence of pore size, protein size and functionalization path.* Colloids and Surfaces B: Biointerfaces, 122, 375-383.

[48] a) García-Fernández, A., Aznar, E., Martínez-Máñez, R., & Sancenon, F. (2020*). New advances in in vivo applications of gated mesoporous silica as drug delivery nanocarriers*. Small, 16(3), 1902242; b) Castillo, R. R., Baeza, A., & Vallet-Regí, M. (2017*). Recent applications of the combination of mesoporous silica nanoparticles with nucleic acids: Development of bioresponsive devices, carriers and sensors*. Biomaterials

5. Gated materials

Gated materials are designed to finely control the delivery of chemical or biochemical species between the voids of porous supports and a solution, in response to a specific stimulus. In line with this concept, numerous research groups have focused on synthesizing and characterizing innovative nanodevices, where the release of a stored cargo can be triggered by applying specific external stimuli.[49] These gated materials typically consist of two main components: (i) molecular or supramolecular combinations that can be "opened" and "closed" based on specific stimuli, and (ii) an inorganic porous support in which a load is encapsulated (Figure 5).[50]

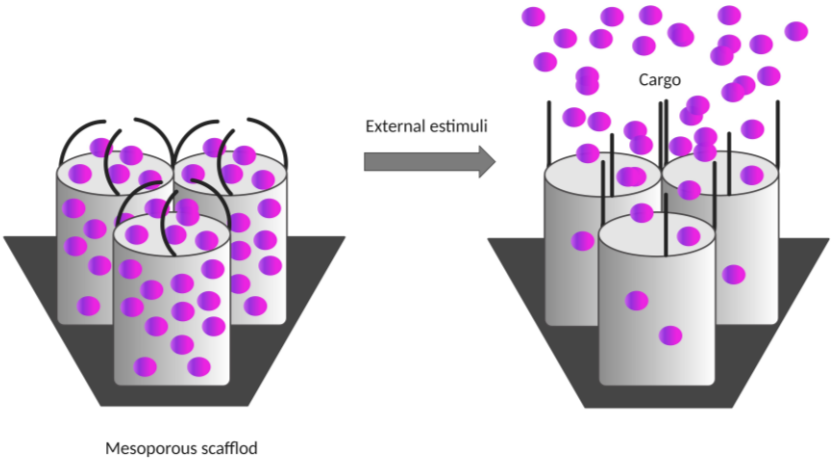

Figure 5. *Gated material function scheme.*

science, 5(3), 353-377.

[49] a) Aznar, E., Martínez-Máñez, R., & Sancenón, F. (2009). *Controlled release using mesoporous materials containing gate-like scaffoldings*. Expert opinion on drug delivery, 6(6), 643-655; b) Cotí, K. K., Belowich, M. E., Liong, M., Ambrogio, M. W., Lau, Y. A., Khatib, H. A., & Stoddart, J. F. (2009). *Mechanised nanoparticles for drug delivery.* Nanoscale, 1(1), 16-39.

[50] Aznar, E., Oroval, M., Pascual, L., Murguía, J. R., Martinez-Máñez, R., & Sancenon, F. (2016). *Gated materials for on-command release of guest molecules.* Chemical reviews, 116(2), 561-718.

Mesoporous solids are widely used as an inorganic support for the fabrication of gated nanodevices. These materials can be prepared in various shapes, ranging from micrometer to nanometer sizes, and possess custom pore diameters from 2 to 10 nm, along with exceptionally large specific surface areas of up to 1200 $m^2 \cdot g^{-1}$.[51] These remarkable characteristics allow mesoporous materials to display high loading capacity, as well as simple functionalization.[52]

The NAA stands out as a mesoporous material of growing importance in nanoscience and nanotechnology. In this thesis, it will be used as a base material due to its highly organized structure of nanometric pores and its ability to develop new hybrid materials. In addition, this type of nanomaterial has shown promise in areas such as nanomanufacturing, biotechnology and biosensorization, which drives us to explore its potential in the design of hybrid materials for applications in molecular recognition and biomolecule detection.

In addition, the design of controlled delivery materials involves the rigorous selection of two key elements: (i) the stimulus that triggers the release of the load and (ii) the molecular gate that responds to this stimulus.

[51] a) Stein, A. (2003). *Advances in microporous and mesoporous solids—highlights of recent progress*. Advanced Materials, 15(10), 763-775; b) Valtchev, V., & Tosheva, L. (2013). *Porous nanosized particles: preparation, properties, and applications*. Chemical Reviews, 113(8), 6734-6760.

[52] a) Soler-Illia, G. J., & Azzaroni, O. (2011). *Multifunctional hybrids by combining ordered mesoporous materials and macromolecular building blocks.* Chemical Society Reviews, 40(2), 1107-1150.; b) Kickelbick, G. (2004). *Hybrid inorganic–organic mesoporous materials.* Angewandte Chemie International Edition, 43(24), 3102-3104.

i. External stimuli fall into two main categories: physical and (bio)chemical. Physical stimuli, such as light, [53] temperature[54] and magnetic fields, [55] offer the advantage of simplifying optimization by not requiring the addition of additional substances. However, the amount of bio-organic molecules controllable by physical stimuli is limited, which complicates the development of materials sensitive to these stimuli. On the other hand, (bio)chemical stimuli cover a wide variety of examples and applications, including small molecules,[56] oligonucleotides,[57] small molecules

[53] a) Aznar, E., Casasus, R., García-Acosta, B., Marcos, M. D., Martínez-Máñez, R., Sancenón, F., & Amorós, P. (2007). *Photochemical and chemical two-channel control of functional nanogated hybrid architectures.* Advanced Materials, 19(17), 2228-2231; b) Zhao, L., Song, X., Fan, D., Liu, X., Wang, H., Wei, Q., & Wu, D. (2023). *Highly efficient signal on/off electrochemiluminescence gel aptasensor based on a controlled release strategy for the sensitive detection of prostate specific antigen*. Analytical Chemistry, 95(13), 5695-5701; c) Croissant, J., Chaix, A., Mongin, O., Wang, M., Clément, S., Raehm, L., & Zink, J. I. (2014). *Two-Photon-Triggered Drug Delivery via Fluorescent Nanovalves.* Small, 10(9), 1752-1755.

[54] a) Luo, B., Wang, W., Zhao, Y., & Zhao, Y. (2023). *Hot-Electron Dynamics Mediated Medical Diagnosis and Therapy.* Chemical Reviews, 123(17), 10808-10833; b) Yu, Z., Li, N., Zheng, P., Pan, W., & Tang, B. (2014). *Temperature-responsive DNA-gated nanocarriers for intracellular controlled release.* Chemical communications, 50(26), 3494-3497.

[55] a) Baeza, A., Guisasola, E., Ruiz-Hernandez, E., & Vallet-Regí, M. (2012*). Magnetically triggered multidrug release by hybrid mesoporous silica nanoparticles.* Chemistry of Materials, 24(3), 517-524; b) Hojjati, S. M., Salehi, Z., & Akrami, M. (2024*). MRI-traceable multifunctional magnetic mesoporous silica nanoparticles (MMSN) capped with graphene quantum dots (GQD) as a theragnostic system in colorectal cancer treatment.* Journal of Drug Delivery Science and Technology, 96, 105700.

[56] a) Climent, E., Marcos, M. D., Martinez-Máñez, R., Sancenón, F., Soto, J., Rurack, K., & Amorós, P. (2009). *The determination of methylmercury in real samples using organically capped mesoporous inorganic materials capable of signal amplification.* Angewandte Chemie (International ed. in English), 48(45), 8519-8522; b) Huang, Y., Guo, X., Wu, Y., Chen, X., Feng, L., Xie, N., & Shen, G. (2024). *Nanotechnology's frontier in combatting infectious and inflammatory diseases: prevention and treatment*. Signal Transduction and Targeted Therapy, 9(1), 34; c) Casasús, R., Aznar, E., Marcos, M. D., Martínez-Máñez, R., Sancenón, F., Soto, J., & Amorós, P. (2006*). New methods for anion recognition and signaling using nanoscopic gatelike scaffoldings.* Angewandte Chemie International Edition, 45(40), 6661-6664; d) Candel, I., Bernardos, A., Climent, E., Marcos, M. D., Martínez-Máñez, R., Sancenon, F., & Parra, M. (2011). *Selective opening of nanoscopic capped mesoporous inorganic materials with nerve agent simulants; an application to design chromo-fluorogenic probes*. Chemical Communications, 47(29), 8313-8315.

[57] a) El Sayed, S., & Otri, I. (2023). *Silica nanoparticles for sensing applications. In Fundamentals of Sensor Technology* (pp. 591-630). Woodhead Publishing; b) Climent, E., Bernardos, A., Martinez-Máñez, R., Maquieira, A., Marcos, M. D., Pastor-Navarro, N., & Amoros, P. (2009). *Controlled delivery systems using antibody-capped mesoporous nanocontainers*. Journal of the American Chemical Society, 131(39), 14075-14080.

with redox activity,[58] saccharides,[59] metal cations,[60] peptides,[61] pH changes, [62] metal ions and enzymes.[63] The choice of appropriate stimulus depends on the specific application of the controlled delivery material, considering aspects such as reversibility, specificity, sensitivity and biocompatibility.

ii. The design of the molecular gate must respond selectively to the chosen stimulus and allow controlled mass transport. Aspects such as stimulus affinity, permeability and mechanical stability are key considerations in this process. In addition, aspects such as biodegradability, toxicity and cost of production should also be taken into account in the design of controlled release materials.[64]

---

[58] a) Lozano-Torres, B., Pascual, L., Bernardos, A., Marcos, M. D., Jeppesen, J. O., Salinas, Y., & Sancenón, F. (2017). *Pseudorotaxane capped mesoporous silica nanoparticles for 3, 4-methylenedioxymethamphetamine (MDMA) detection in water.* Chemical Communications, 53(25), 3559-3562; b) Monreal Trigo, J. (2023). *Electronic devices for the combination of electrically controlled drug release, electrostimulation, and optogenetic stimulation for nerve tissue regeneration* (Doctoral dissertation, Universitat Politècnica de València).

[59] a) Bernardos, A., Mondragon, L., Aznar, E., Marcos, M. D., Martinez-Manez, R., Sancenon, F., & Amoros, P. (2010). *Enzyme-responsive intracellular controlled release using nanometric silica mesoporous supports capped with "saccharides".* ACS nano, 4(11), 6353-6368.; b) Mal, N. K., Fujiwara, M., & Tanaka, Y. (2003). *Photocontrolled reversible release of guest molecules from coumarin-modified mesoporous silica*. Nature, 421(6921), 350-353.

[60] Zhou, Y., Tan, L. L., Li, Q. L., Qiu, X. L., Qi, A. D., Tao, Y., & Yang, Y. W. (2014). *Acetylcholine-triggered cargo release from supramolecular nanovalves based on different macrocyclic receptors.* Chemistry–A European Journal, 20(11), 2998-3004; b) Wang, Z., Chen, J., Gao, R., Jiang, L., Zhang, G., Zhao, Y., & Shi, Y. (2024). *Spatiotemporal manipulation metal–organic frameworks as oral drug delivery systems for precision medicine.* Coordination Chemistry Reviews, 502, 215615.

[61] a) Coll, C., Mondragón, L., Martínez-Máñez, R., Sancenón, F., Marcos, M. D., Soto, J., & Pérez-Payá, E. (2011). *Enzyme-mediated controlled release systems by anchoring peptide sequences on mesoporous silica supports.* Angewandte Chemie International Edition, 50(9), 2138-2140; b) Li, R., Mei, X., Li, X., Zhang, C., & Ruan, L. (2021). *A bolt-like-blocking nanovalve on mesoporous silica nanoparticles for controlled release.* Microporous and Mesoporous Materials, 317, 111007.

[62] a) Casasús, R., Marcos, M. D., Martínez-Máñez, R., Ros-Lis, J. V., Soto, J., Villaescusa, L. A., & Latorre, J. (2004). *Toward the development of ionically controlled nanoscopic molecular gates.* Journal of the American Chemical Society, 126(28), 8612-8613; b) Ruiz-Rico, M., Pérez-Esteve, É., Lerma-Garcia, M. J., Marcos, M. D., Martinez-Máñez, R., & Barat, J. M. (2017). *Protection of folic acid through encapsulation in mesoporous silica particles included in fruit juices.* Food Chemistry, 218, 471-478.

[63] a) Pascual, L., El Sayed, S., Marcos, M. D., Martínez-Máñez, R., & Sancenón, F. (2017*). Acetylcholinesterase-capped mesoporous silica nanoparticles controlled by the presence of inhibitors*. Chemistry–An Asian Journal, 12(7), 775-784; b) Llopis-Lorente, A., Lozano-Torres, B., Bernardos, A., Martínez-Máñez, R., & Sancenón, F. (2017). *Mesoporous silica materials for controlled delivery based on enzymes.* Journal of Materials Chemistry B, 5(17), 3069-3083.

[64] Coll, C., Bernardos, A., Martinez-Máñez, R., & Sancenon, F. (2013*). Gated silica mesoporous supports for*

Over the years, gated ensembles have evolved from simple molecules to complex supermolecules. In 2003, Fujiwara et al. introduced the concept of gated material using MCM-41 mesoporous silica nanoparticles (MSNs) loaded with the steroid cholestane.[65] The authors successfully demonstrated the regulation of photochemical uptake, storage, and release of the cargo (Figure 6). To achieve this, the pores of the MSNs were loaded with cholestane, and the external surface was functionalized with 7-[(3-triethoxysilyl)-propoxy]coumarin. Under irradiation with wavelengths longer than 310 nm, the coumarin derivative underwent a [2+2] photodimerization reaction, forming bulky cyclobutane dimers in an anti-head-to-head conformation. This conformation blocked the pore entrances, inhibiting cholestane release. The dimerization process was reversible, and irradiation at 250 nm restored the monomer conformation, allowing cholestane release (Figure 6). Similar results were achieved with other cargos such as pyrene, phenanthrene, and progesterone, demonstrating the control over pore accessibility and cargo release.

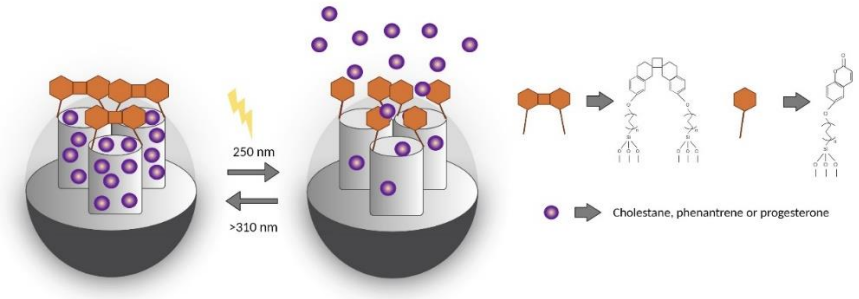

Figure 6. *Diagram of the photo-driven nanovalve that uses MSNs to dimerize coumarin. Selected cargos were released and coumarin monomers were produced after exposure to radiation at 250 nm.*

controlled release and signaling applications. Accounts of Chemical Research, 46(2), 339-349.

[65] a) Mal, N. K., Fujiwara, M., & Tanaka, Y. (2003*). Photocontrolled reversible release of guest molecules from coumarin-modified mesoporous silica.* Nature, 421(6921), 350-353; b) Mal, N. K., Fujiwara, M., Tanaka, Y., Taguchi, T., & Matsukata, M. (2003). *Photo-switched storage and release of guest molecules in the pore void of coumarin-modified MCM-41*. Chemistry of materials, 15(17), 3385-3394.

In 2004, R. Casasús, R. Martínez-Máñez et al. reported on a pH-controlled silica mesoporous support, which represents the first example of gated systems operating in an aqueous environment.[66] While most gated materials focus on delivery applications, this particular example aimed to ionically control the entry of a specific pH-sensitive molecule, squaraine dye, into the internal pores of the mesoporous scaffold. The researchers used an MCM-41 micromeric support functionalized on the outer surface with 3-[2-(2-aminoethylamino)ethylamino]propylmethoxysilane, a linear polyamine, and with mercaptopropyl chains grafted into the pores (see Figure 7). At neutral pH, the nitrogen atoms of the polyamine molecules are not protonated, so there are no coulombic repulsions between the ammonium groups and the conformation adopted is relaxed, thus allowing the squaraine dye to enter the internal pores. The reaction that takes place within the pores results in a colorless derivative. On the other hand, under acidic conditions, the nitrogen atoms of the polyamine molecules were protonated, adopting a rigid conformation due to the coulombic repelling forces and consequent blockage of the pores, preventing the squaraine from accessing the thiol residues and thus maintaining the blue color of the initial solution. The device thus demonstrates how simple pH-sensitive molecules can be used to regulate mass transport.

[66] Casasús, R., Marcos, M. D., Martínez-Máñez, R., Ros-Lis, J. V., Soto, J., Villaescusa, L. A., & Latorre, J. (2004). *Toward the development of ionically controlled nanoscopic molecular gates.* Journal of the American Chemical Society, 126(28), 8612-8613.

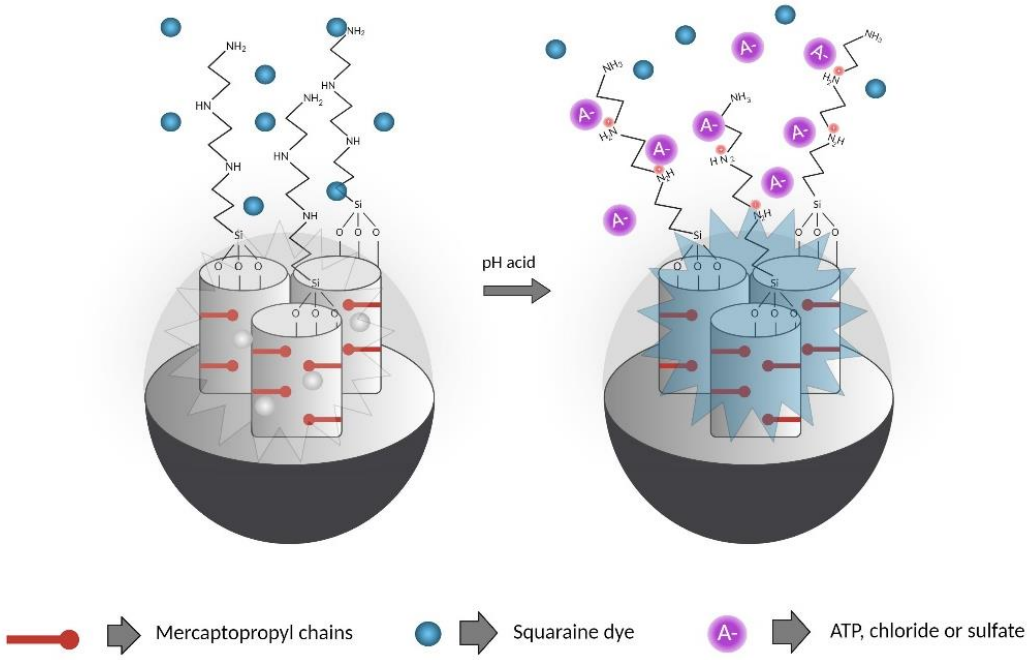

Figure 7. *Micrometric MCM-41 support featuring mercaptopropyl groups on the inner surface and polyamines on the outer surface. Access to the pores by squaraine was regulated by pH changes.*

More recently, the development of materials controlled by biomolecules that respond to external signals has gained great interest. Among them, the highly sensitive and precise detection of various analytes by means of nanoporous chemical biosensors stands out, especially from the clinical point of view. This area of research introduces new opportunities in the field of early identification and, consequently, disease prevention.

This is possible due to the high number of biomolecules that can block pores in mesoporous supports, such as DNA,[67] peptides,[68] aptamers[69] or enzymes.[70]

In addition to the aforementioned cases, a multitude of gating systems using mesoporous silica nanoparticles as containers have been documented so far. One representative is that of Wei et al. in 2022, in which they illustrate the potential of MSNs as promising carriers of a wide range of substances, including drugs and fluorescence molecules.[71] Specifically, they took advantage of amino-functionalized mesoporous silica nanoparticles (NH_2-MSN), characterized by a highly porous structure, to encapsulate rhodamine 6G (Rh6G) molecules, to obtain fluorescent nanoprobes. Using specific single-stranded DNA-conjugated gold nanoparticles (AuNPs-ssDNA) as a molecular gate, they coated the surface of NH_2-MSN (Figure 8). The fluorescence signal is practically negligible when the fluorescence molecules were blocked by the AuNPs-ssDNA. Upon introduction of the flap endonuclease-1 (FEN1) stimulus, flap endonuclease 1 recognized and cleaved the particular ssDNA sequence, thereby releasing Rh6G from NH_2-MSN and leading to emission of fluorescence signals. Consequently, the controlled release of Rh6G allowed sensitive detection of FEN1 activity. In particular, the fluorescence signal showed a strong

[67] Zhang, Y., Yuan, Q., Chen, T., Zhang, X., Chen, Y., & Tan, W. (2012). *DNA-capped mesoporous silica nanoparticles as an ion-responsive release system to determine the presence of mercury in aqueous solutions*. Analytical chemistry, 84(4), 1956-1962.

[68] Coll, C., Mondragón, L., Martínez-Máñez, R., Sancenón, F., Marcos, M. D., Soto, J., & Pérez-Payá, E. (2011). *Enzyme-mediated controlled release systems by anchoring peptide sequences on mesoporous silica supports.* Angewandte Chemie International Edition, 50(9), 2138-2140.

[69] a) Zhu, C. L., Lu, C. H., Song, X. Y., Yang, H. H., & Wang, X. R. (2011*). Bioresponsive controlled release using mesoporous silica nanoparticles capped with aptamer-based molecular gate.* Journal of the American Chemical Society, 133(5), 1278-1281; b) Pla, L., Martínez-Bisbal, M. C., Aznar, E., Sancenón, F., Martínez-Máñez, R., & Santiago-Felipe, S. (2021). *A fluorogenic capped mesoporous aptasensor for gluten detection.* Analytica Chimica Acta, 1147, 178-186.

[70] Patel, K., Angelos, S., Dichtel, W. R., Coskun, A., Yang, Y. W., Zink, J. I., & Stoddart, J. F. (2008). Enzyme-responsive snap-top covered silica nanocontainers. Journal of the American Chemical Society, 130(8), 2382-2383.

[71] Tang, Y., Zhang, D., Lu, Y., Liu, S., Zhang, J., Pu, Y., & Wei, W. (2022). *Fluorescence imaging of FEN1 activity in living cells based on controlled-release of fluorescence probe from mesoporous silica nanoparticles*. Biosensors and Bioelectronics, 214, 114529.

linear correlation with log FEN1 activity, ranging from 0.05 to 1.75 units of enzyme activity (U), and demonstrated a detection threshold of 0.03 U.

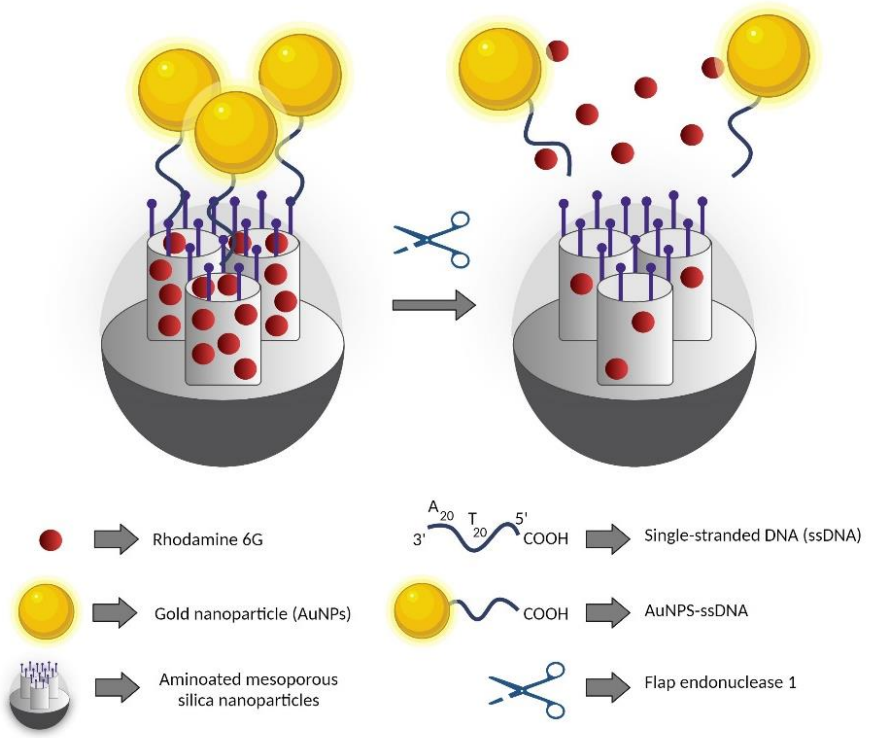

Figure 8. *Diagram depicting the nanoprobes MSNs@AuNPs-ssDNA loaded with Rhodamine 6G (Rh6G) for the identification of FEN1.*

5.1. Gating materials for sensing propouses

The application of gated materials in recognition protocols has merged as a new area of development in recent years.[72] A diverse range of (bio)molecules have been chosen to trigger the release of entrapped cargos from mesoporous supports.[73] As we

[72] Aznar, E., Martínez-Máñez, R., & Sancenón, F. (2009). *Controlled release using mesoporous materials containing gate-like scaffoldings*. Expert opinion on drug delivery, 6(6), 643-655.

[73] Sancenón, F., Pascual, L., Oroval, M., Aznar, E., & Martínez-Máñez, R. (2015*). Gated silica mesoporous*

have sen in the example above, the core idea behind applying gated materials to sensing protocols is to load the support with a reporter and design the capping mechanism in a way that a target analyte (cation,[74] anion,[75] small neutral molecule[76] or biomolecule)[77] can selectively trigger uncapping and the delivery of the cargo.[78] This concept differs from classic supramolecular systems where the recognition and signalling steps are interconnected, making the signal amount independent on the host-guest interaction.[79] That is, the system can achieve amplification through its large loading capacity, enabling the release of a significant quantity of signaling molecules upon the detection of just a few analyte molecules. Furthermore, these gated systems offer flexibility and adaptability to different applications, as they can be implanted in different types of supports and utilize various molecules as reporters.

DNA sequences are especially attractive for the design of gated nanosensors due to their high specificity, chemical stability, ease of modification, biocompatibility, signal

materials in sensing applications. ChemistryOpen, 4(4), 418-437.

[74] Climent, E., Marcos, M. D., Martínez-Máñez, R., Sancenón, F., Soto, J., Rurack, K., & Amorós, P. (2009). *The determination of methylmercury in real samples using organically capped mesoporous inorganic materials capable of signal amplification.* Angewandte Chemie (International ed. in English), 48(45), 8519-8522.

[75] Hou, L., Zhu, C., Wu, X., Chen, G., & Tang, D. (2014). *Bioresponsive controlled release from mesoporous silica nanocontainers with glucometer readout.* Chemical communications, 50(12), 1441-1443.

[76] a) Salinas, Y., Agostini, A., Pérez-Esteve, E., Martínez-Máñez, R., Sancenón, F., Marcos, M. D., & Amorós, P. (2013). *Fluorogenic detection of Tetryl and TNT explosives using nanoscopic-capped mesoporous hybrid materials.* Journal of Materials Chemistry A, 1(11), 3561-3564; b) Díez, P., Sánchez, A., Gamella, M., Martínez-Ruíz, P., Aznar, E., De La Torre, C., & Pingarron, J. M. (2014). *Toward the design of smart delivery systems controlled by integrated enzyme-based biocomputing ensembles.* Journal of the American Chemical Society, 136(25), 9116-9123; c) El Sayed, S., Giménez, C., Aznar, E., Martínez-Máñez, R., Sancenón, F., & Licchelli, M. (2015). *Highly selective and sensitive detection of glutathione using mesoporous silica nanoparticles capped with disulfide-containing oligo (ethylene glycol) chains.* Organic & biomolecular chemistry, 13(4), 1017-1021; d) R. Villalonga, P. Díez, A. Sánchez, E. Aznar, R. Martínez-Máñez, J. M. Pingarrón, Chem. Eur. J., 2013, 19, 1017-1021; e) E. Climent, R. Martínez-Máñez, A. Maquieira, F. Sancenón, M.D. Marcos, E.M. Brun, J. Soto, P. Amorós, ChemistryOpen, 2012, 1, 251-259.

[77] Oroval, M., Climent, E., Coll, C., Eritja, R., Aviñó, A., Marcos, M. D., & Amorós, P. (2013*). An aptamer-gated silica mesoporous material for thrombin detection.* Chemical Communications, 49(48), 5480-5482.

[78] Coll, C., Bernardos, A., Martinez-Máñez, R., & Sancenon, F. (2013). *Gated silica mesoporous supports for controlled release and signaling applications.* Accounts of Chemical Research, 46(2), 339-349.

[79] Santos-Figueroa, L. E., Moragues, M. E., Climent, E., Agostini, A., Martínez-Máñez, R., & Sancenón, F. (2013). *Chromogenic and fluorogenic chemosensors and reagents for anions.* A comprehensive review of the years 2010–2011. Chemical society reviews, 42(8), 3489-3613.

amplification ability and versatility. These characteristics allow the design of chromogenic or fluorogenic nanosensors, where the selective recognition of a strand of nucleic acid in the presence of complementary oligonucleotide releases the trapped load. This approach can facilitate rapid and accurate identification of DNA genomic sequences. As proof of concept, the team of Professor Ramón Martínez-Mañez developed a gated material for the direct and rapid detection of nucleotide sequences of bacterium *Mycoplasma*[80]. In this work, a solid based on mesoporous silica nanoparticles loaded with rodamine B was developed for the detection of *Mycoplasma* in contaminated cell culture media, without the use of PCR and reaching a detection limit of 70 copies of DNA per mL (Figure 9). A conserved sequence of the *Mycoplasma* genome was used, specifically a fragment of the 16S subunit of ribosomal RNA (O1), where the presence of *Mycoplasma* genomic DNA causes the release of the dye trapped by the solid. This methodology is distinguished by being easier to handle, considerably faster (60 min vs 250 min PCR), economical (requires only one UV lamp) and prevents amplification errors. The innovative strategy of combining an indicator release with specific biochemical recognition positions this approach as a competitive alternative to PCR methods in critical areas such as point-of-care diagnosis and contamination detection specific biological agents with pathogens.

[80] Climent, E., Mondragon, L., Martínez-Máñez, R., Sancenon, F., Marcos, M. D., Murguía, J. R., & Pérez-Payá, E. (2013*). Selective, highly sensitive, and rapid detection of genomic DNA by using gated materials: Mycoplasma detection*. Angewandte Chemie International Edition, 52(34).

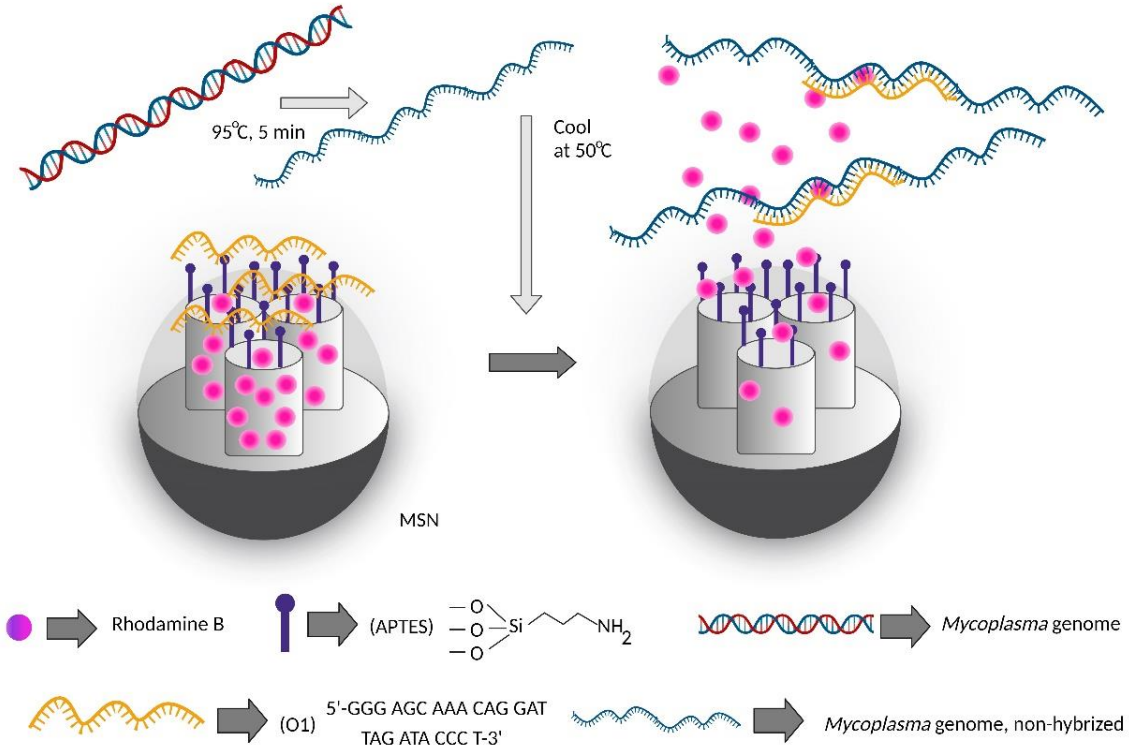

Figure 9. *Representation of the gated material S1-O1, first functionalized with APTES and then capped with a single-strand oligonucleotide (O1). The release of dye rhodamine B occurs selectively in the presence of the complementary non-hybridised 16S ribosomal RNA chain.*

Then, another use of gated materials in mesoporous nanoparticles was explored for nucleotide recognition applications, focusing on the detection of adenosine diphosphate (ADP) and adenosine triphosphate (ATP), as illustrated in Figure 10.[81] In this study, mesoporous silica nanoparticles were functionalized on their external surface with

[81] Casasús, R., Aznar, E., Marcos, M. D., Martínez-Máñez, R., Sancenón, F., Soto, J., & Amorós, P. (2006*). New methods for anion recognition and signaling using nanoscopic gatelike scaffoldings.* Angewandte Chemie International Edition, 45(40), 6661-6664.

polyamines, and the nanopores were loaded with the dye tris(2,2'-bpyridyl)ruthenium(II) chloride [$Ru(bpy)_3Cl$]. When the system was exposed to anions such as fluoride, chloride, bromide, iodide, nitrate, phosphate, sulfate, acetate, and carbonate, the pores remained open, and the release of the dye was observed. However, in the presence of ADP and ATP nucleotides, no dye release was fund. This lack of release was attributed to a capping effect caused by strong electrostatic and hydrogen bonding interactions between the bulky anions (ADP and ATP) and the protonated amines anchored on the nanoparticle surface. These interactions hindered the delivery of the dye cargo. The strength of the interaction was further enhanced by the preorganization effect resulting from grafting the polyamine moieties onto the inorganic support.

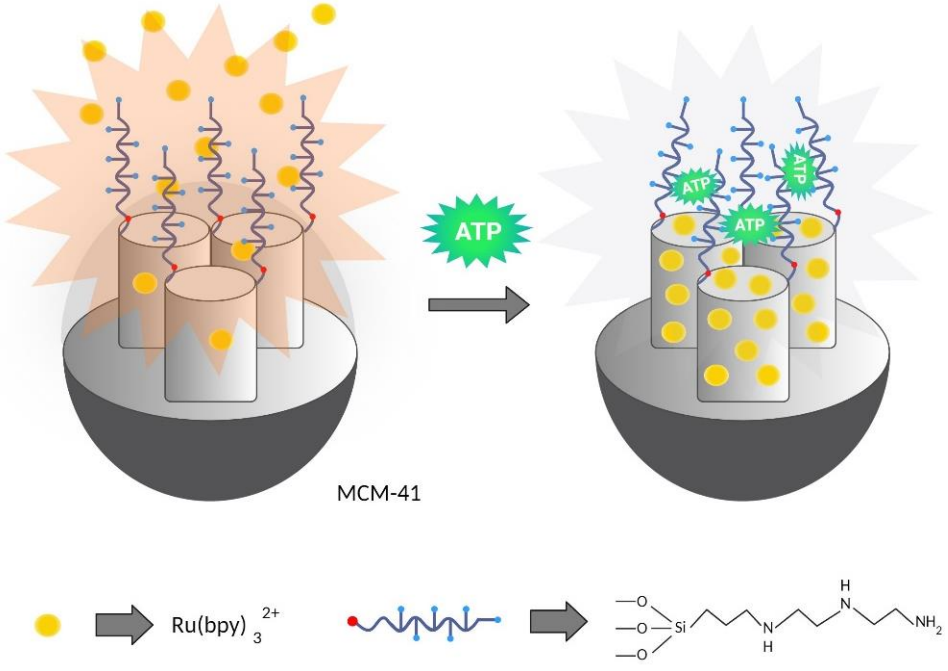

Figure 10. *MSN with polyamine caps are used to specifically detect ATP via chromo-fluorescence.*

Starting from the aforementioned concepts, this thesis is focused in the design, development and application of detection systems based on gated materials. In particular, four different systems aimed at the recognition of species and biomolecules have been conceptualized, developed and tested. As it hs been reported, this detection approach shows remarkable adaptability, and high potential to prepare sensors to detect a wide range of molecules, such as drugs, toxins, bacteria and viruses for applications in different fields such as clinical diagnosis or food or environmental quality.

5.1.1. Sensors for environmental monitoring and safety applications

The development of an almost unlimited number of new supports with a wide variety of properties has been possible thanks to the combination of various inorganic solids with organic compounds. Controlled nanodevices that can release a encapsulated load in the presence of specific external stimuli are promising materials in this area. A recent example of this concept is the work of Ribes and collaborators in 2017, where they demonstrated that the combination of NAA supports and selected aptamers can be used to prepare gated systems to detect specific molecules.[82] In particular, they loaded a NAA support with rhodamine B and capped it with a specific aptamer capable of sensitively and selectively recognize bisphenol A (BPA) in water (Figure 10). The capped nanomaterial facilitated rapid and accurate identification of BPA in tap water. This achievement was the first time in which mesoporous supports capped with aptamers was successfully used for the detection of this molecule.

[82] Ribes, À., Aznar, E., Bernardos, A., Marcos, M. D., Amorós, P., Martínez-Máñez, R., & Sancenón, F. (2017). *Fluorogenic sensing of carcinogenic bisphenol A using aptamer-capped mesoporous silica nanoparticles*. Chemistry–A European Journal, 23(36), 8581-8584.

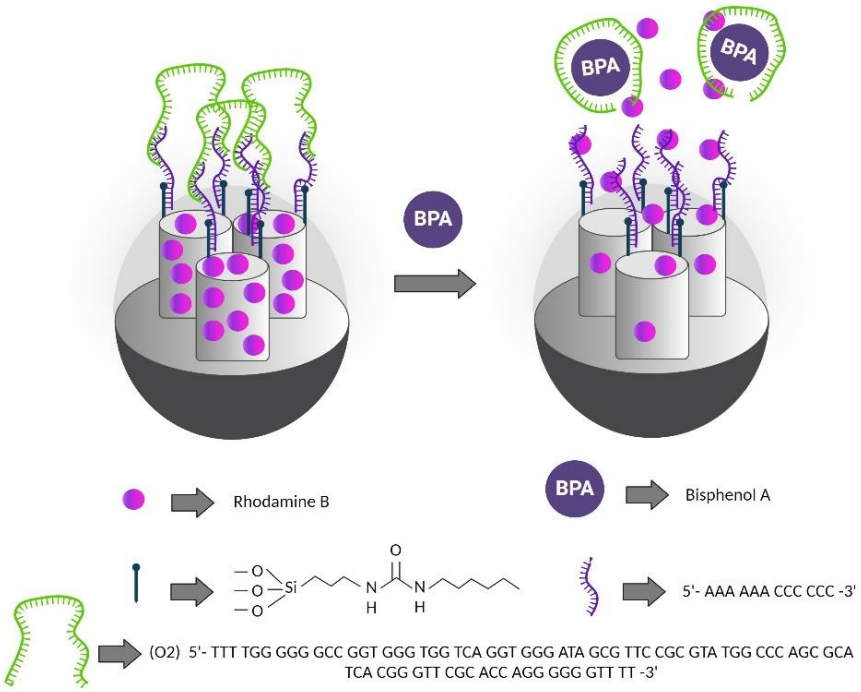

Figure 10. *Illustration of the gated material with an oligonucleotide O2 cap. By the interaction of O2 with the BPA molecule, the released dye (rhodamine B) was only detected in the presence of BPA.*

Rurack and co-workers reported in 2020 another example of gated material for sensing applications in this case for the detection of pyrethroids using a simple dipstick assay[83]. This system utilized antibody-triggered reporter-releasing hybrid materials. Figure 11 depicts the material's architecture and its operational principle. The employed scaffold was SBA-15 mesoporous silica particles with a pore diameter of 9 nm. The outer surface of the silica support underwent functionalization using short-chain PEG silanes. This modification enhanced the material's stability, biocompatibility, and reduced non-

[83] Costa, E., Climent, E., Ast, S., Weller, M. G., Canning, J., & Rurack, K. (2020). *Development of a lateral flow test for rapid pyrethroid detection using antibody-gated indicator-releasing hybrid materials*. Analyst, 145(10), 3490-3494.

specific molecule adsorption. Next, an hapten was selectively grafted solely onto the upper edge of the inner surface of the pores. This precise and controlled placement of hapten molecules within the material optimized their interaction with the target analytes. For detection purposes, sulforhodamine G (SRG) was loaded into the mesopores of the material as a reporter dye. SRG served as a visual signal indicating the presence of the target analytes. Furthermore, retention of SRG in the pores was achieved through binding with an anti-pyrethroid antibody, that they were specifically generated against the 3-phenoxybenzoic acid (PBA) fraction of pyrethroids. This strategic choice of antibodies and hapten enables the detection of all type I pyrethroids, which share the common (3-phenoxybenzyl)oxy group. Since the original design in 2020, further advancements in nanodevices for chemical detection have been made. These ongoing efforts continue to push the boundaries of nanotechnology, ultimately leading to more sophisticated and efficient detection systems that contribute to environmental monitoring, public health, and safety.

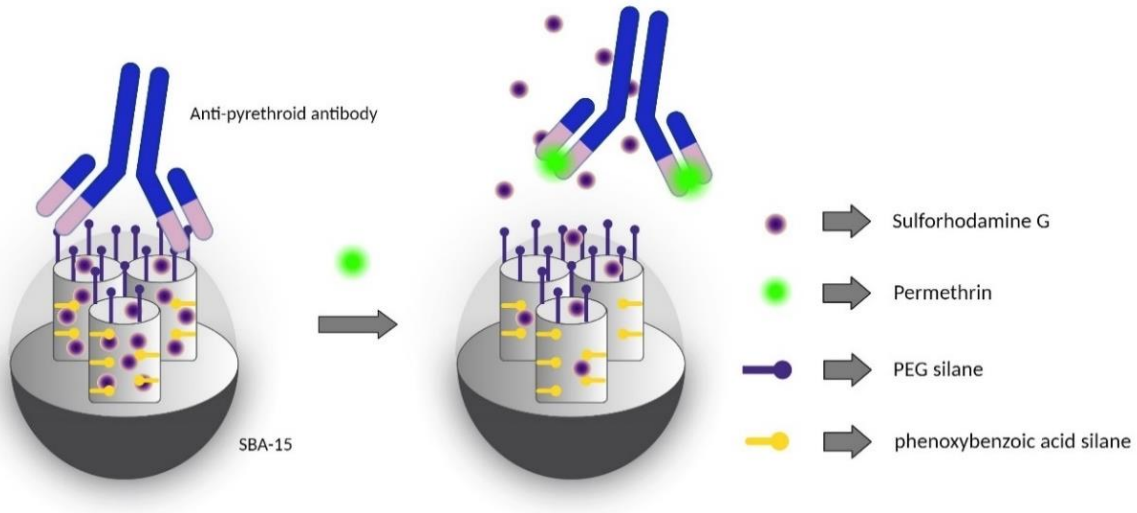

Figure 11. *Diagram illustrating the detection strategy, showing the hapten units along the inner pore walls.*

In the field of biosafety, E. Garrido et al. developed a smartphone-based rapid strip-based test utilizing bioinspired hybrid nanomaterials for the *in situ* detection of the drug scopolamine (SCP).[84] SCP is a psychoactive substance associated with drug-facilitated sexual assault, where victims are incapacitated and unable to provide consent due to drug administration. The nanosensor employed rhodamine B-loaded mesoporous silica nanoparticles, which were functionalized with bethanechol, a potent agonist of the recombinant human M_2 muscarinic acetylcholine receptor (M_2-AChR). Interaction between M_2-AChR and the anchored bethanechol derivative led to the pore-blocking effect. The detection mechanism relied on SCP binding to M_2-AChR, resulting in the opening of the nanopores and subsequent release of the trapped rhodamine B reporter molecule. Notably, other drugs such as cocaine, heroin, morphine, and 3,4-methylenedioxymethamphetamine (MDMA) had minimal impact on cargo release (Figure 12a). The material was incorporated into strips for lateral flow assays, which could be easily read using a smartphone without the need for additional treatment or conditioning (Figure 12b). The assay demonstrated rapid response times, typically less than 15 minutes, and exhibited excellent selectivity and sensitivity. The limit of detection (LOD) achieved was as low as 0.04 µM in aqueous solutions and 18.7 µM in extracted saliva samples. Additionally, a dualplex lateral flow assay (LFA) was developed, enabling the simultaneous *in situ* detection of both SCP and the "cannibal drug" MDPV.

[84] Garrido, E., Climent, E., Marcos, M. D., Sancenón, F., Rurack, K., & Martínez-Máñez, R. (2022). *Dualplex lateral flow assay for simultaneous scopolamine and "cannibal drug" detection based on receptor-gated mesoporous nanoparticles.* Nanoscale, 14(37), 13505-13513.

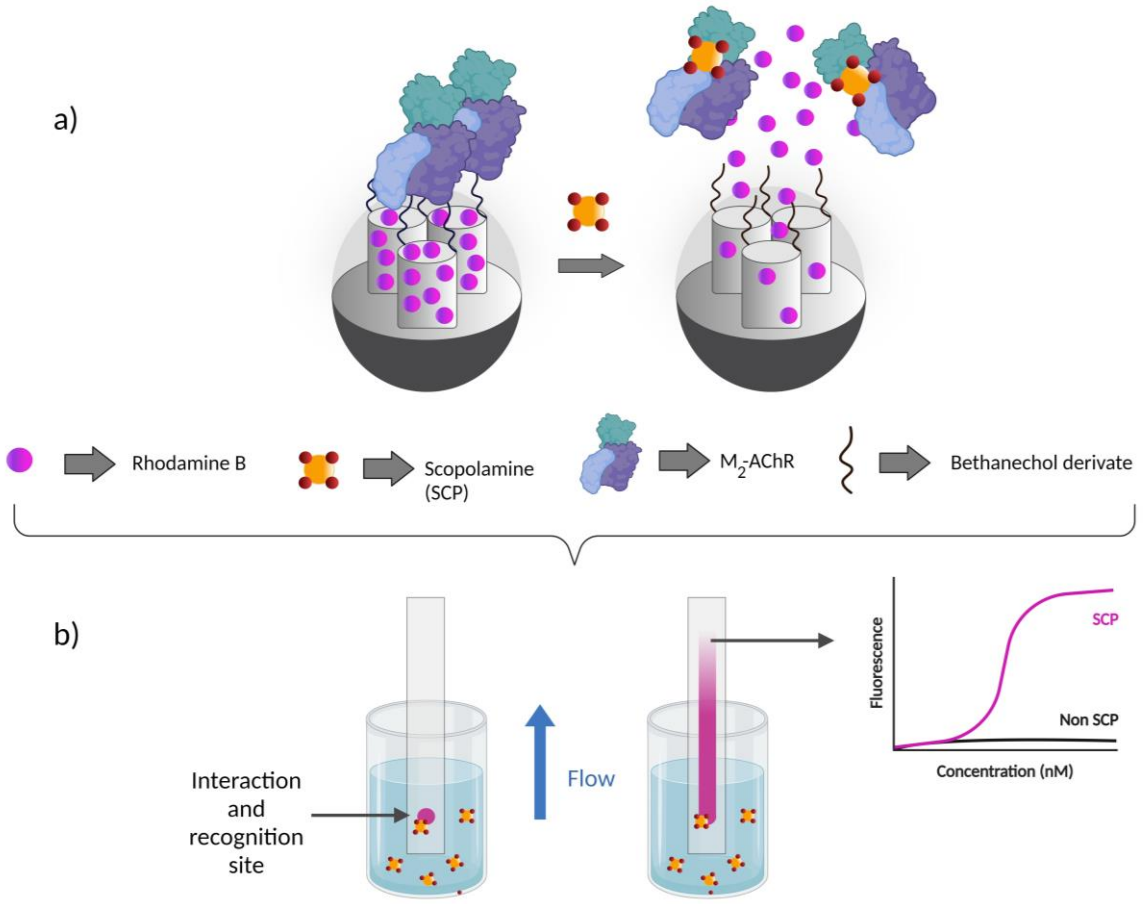

Figure 12. *a) Performance of M2-AChR-gated nanoparticles when SCP is present. b) Schematic illustration of the created test-strip lateral-flow assay for SCP detection.*

5.1.2. Nanomaterials for cancer diagnostics

In the fight against cancer, early detection is crucial for effective treatment, but traditional methods have limitations. MSNs are promising in cancer therapy because of their unique properties: ordered porous structure, biocompatibility, stability and adjustable pores with a wide surface. In addition, its surface can be functionalized with

molecules that act as molecular gates, which enables the controlled release of its content in response to specific stimuli, such as proteins or ligands.

Recently, a promising approach to cancer-specific treatment involves photodynamic therapy (PDT) using activatable photosensitizers (aPS). In this context, Li et al. presented a photosensitizer sequentially active and sensitive to proteins called PcC4-MSN-O1 (Fig. 13).[85] The success of PcC4-MSN-O1 in PDT lies in its skilful use of selective molecular recognition events, where a novel photosensitizer with an inherent "biological gate" was designed, allowed by sequential interaction with specific biomolecules. This innovation involves encapsulating the zinc(II) phthalocyanin derivative (PcC4), the photosensitizer, within MSN to suppress its photoactivity. The posterior envelope of MSN with DNA (O1) forms a molecular recognition element that interacts selectively with target molecules. The activation process involves a two-step recognition cascade: initially bonding with telomerase triggers the release of PcC4 from MSN, followed by interaction with albumin, activating the photodynamic potential of PcC4. This meticulously designed recognition sequence ensures minimal phototoxicity in healthy tissues while promoting powerful PDT action within tumors. PcC4-MSN-O1 preferentially accumulates in HeLa tumors, and subsequent laser irradiation is effectively directed to cancer cells, facilitated by the triggered photodynamic activity. The process of controlled activation within the tumor and the rapid elimination of PcC4-MSN-O1 improve the safety profile of therapy.

[85]Li, X., Fan, H., Guo, T., Bai, H., Kwon, N., Kim, K. H., & Tan, W. (2019). *Sequential protein-responsive nanophotosensitizer complex for enhancing tumor-specific therapy*. ACS nano, 13(6), 6702-6710.

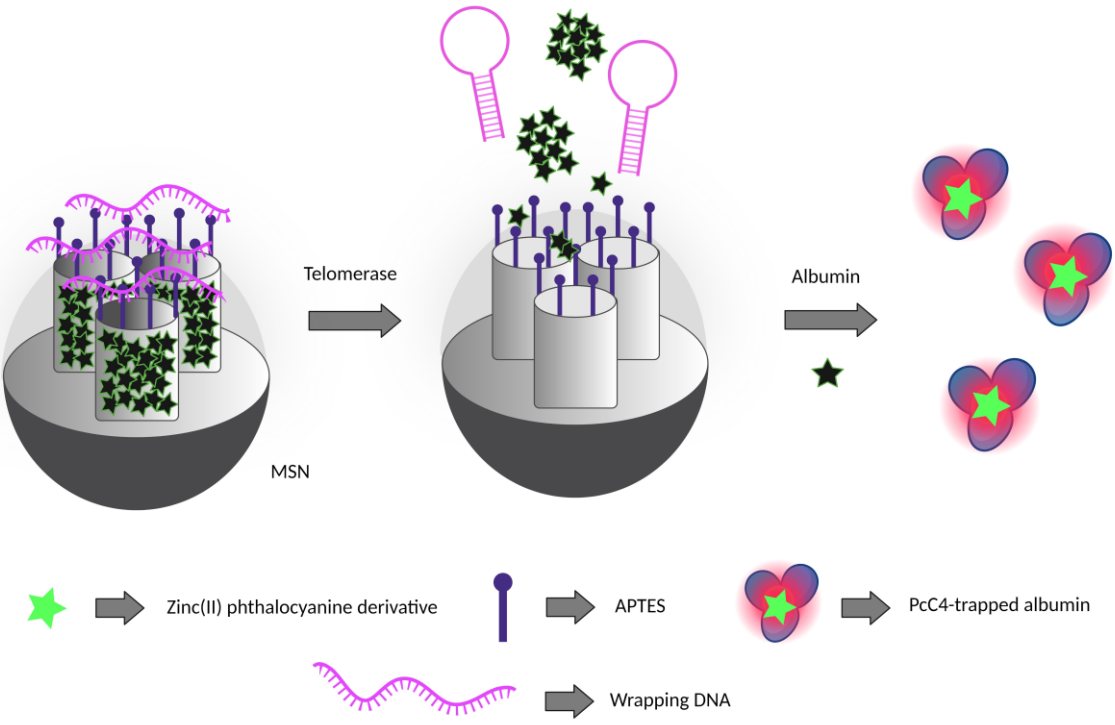

Figure 13. *Illustration depicting the sequential responsive processes driven by dual proteins and the activatable photoactivity of PcC4-MSN-O1.*

In addition to the use of proteins in "molecular gates," nucleic acids have also been used as protective pore barriers and have shown a good response to stimuli associated with MSN. For example, in 2013, Willner's team developed a method in which controlled release of the MSN load depended on DNA, achieved through cooperative stimulation involving ATP and endonucleases.[86] The NPs were initially modified with open nucleic acid hairpin structures (90 °C). This structure allowed loading the pores of the nanoparticles with rhodamine B. At a lower temperature of 25 °C, strand adopted a

[86] Zhang, Z., Balogh, D., Wang, F., Sung, S. Y., Nechushtai, R., & Willner, I. (2013). *Biocatalytic release of an anticancer drug from nucleic-acids-capped mesoporous SiO2 Using DNA or molecular biomarkers as triggering stimuli.* ACS nano, 7(10), 8455-8468.

hairpin structure comprising the ATP aptamer sequence and a single-stranded sequence at the 3'-end. This hairpin structure effectively capped the nanoparticle pores and protected them from hydrolytic degradation by Exo III, an endonuclease. In the presence of ATP, the hairpin structure underwent reconfiguration, forming a secondary ATP/ATP aptamer complex. This complex provided a duplex structure that was susceptible to hydrolytic digestion by Exo III. Consequently, the ATP/ATP aptamer complexes were destabilized, resulting in the release of RhB as a biomarker. The release of ATP in turn triggered the opening of another hairpin structure. Figure 14 demonstrates that the effective release of Rh B occurred only when both ATP and Exo III were present, supporting the proposed mechanism. Importantly, the triggered release from the nanocarriers was selective to ATP, as the presence of other nucleotides did not affect the unlocking of the nanoparticle pores.

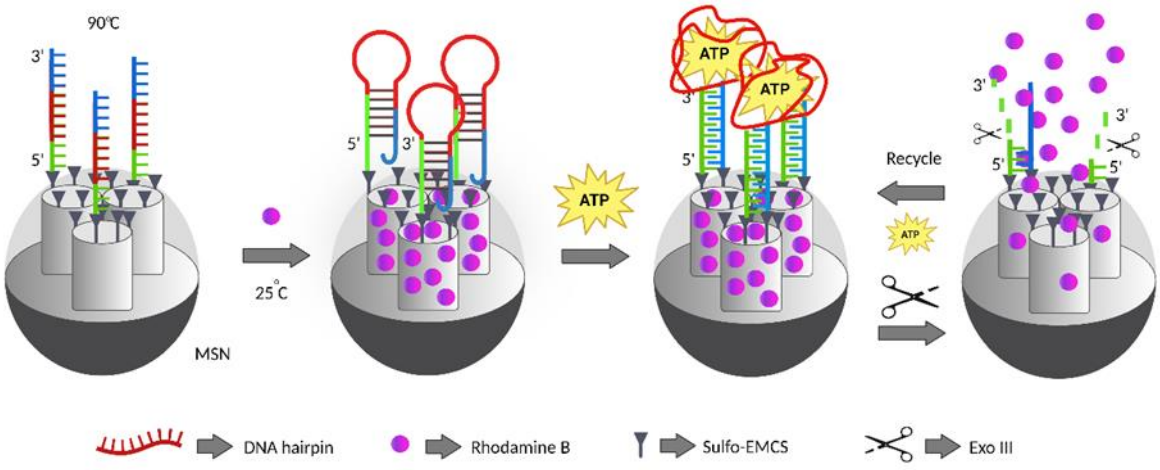

Figure 14. *Pores of DNA hairpin-capped MSNs were unlocked, leading to the release of rhodamine B by employing an analyte-DNA biomarker as trigger for open them. Additionally, Exonuclease III was utilized as a biocatalyst for regenerating the DNA-biomarker.*

In addition to proposing a method of recognition, the anticancer application of MSNs activated by ATP aptmers included the loading of the drug camptotecine (CTP). This resulted in a remarkable 65% reduction in the viability of MDA-MB-231 breast cancer cells. The observed increase in cancer cell death induced by CPT correlated positively with the enhanced ATP synthesis in cancer cells. These promising preliminary results underscore the significance of developing MSN that are loaded with both fluorophores signaling molecules and chemotherapeutic drugs, as these can be specifically unlocked and released specifically within target cancer cells by utilizing an intracellular biomarker (ATP). This study introduces a new paradigm for cancer therapy, offering potential advancements in the field.

5.1.3. Cancer and disease detection

In order to detect different diseases through biosensors, it is essential to have highly specific biomarkers, in addition to non-invasive or minimally invasive techniques. It is also necessary to have adequate control to differentiate between markers associated with different pathologies. These biosensors are essential to quickly assess the patient's health status, detect the onset of disease and the need to act as soon as possible.

Recently, a variety of medical applications have benefited from the development of fluorescence-based biosensors based on gated materials. One of these was the study done in 2021 by Pla and colleagues, which showed the quick, accurate, and focused detection of a particular aptasensor of an oncological marker of colorectal cancer.[87] The aptasensor is composed of a NAA support that is loaded with RhB and functionalized with a molecular gate based on an aptamer bonded by amines (APTES). When the 8-oxo-dG target molecule, abundant in cancer due to oxidative stress in the nucleophile bases of DNA, binds to the aptamer, displacement occurs and allows the delivery of RhB (Figure

[87] Pla, L., Sancenon, F., Martinez-Bisbal, M. C., Banuls, C., Estan, N., Botello-Marabotto, M., Aznar, E., Sáez, G., Santiago-Felipe, S., & Martinez-Máñez, R. (2021). *A new 8-oxo-7, 8-2' deoxyguanosine nanoporous anodic alumina aptasensor for colorectal cancer diagnosis in blood and urine*. Nanoscale, 13(18), 8648-8657.

15). In the absence of 8-oxo-dG, the release of RhB is limited. This aptasensor was evaluated in several real matrices, including serum and urine, after an optimization process. It demonstrated a detection capacity of 8-oxo-dG in the range of 1-50 nM in one hour, without the need for preconcentration or prior treatment. Subsequently, it was verified with a set of 38 serum and urine samples, comparing the results with those of a commercial ELISA kit as a reference. In serum samples, the aptasensor showed a sensitivity of 95.73% and a specificity of 80%, with an accuracy greater than 93%. In urine samples, both sensitivity and specificity were 100%.

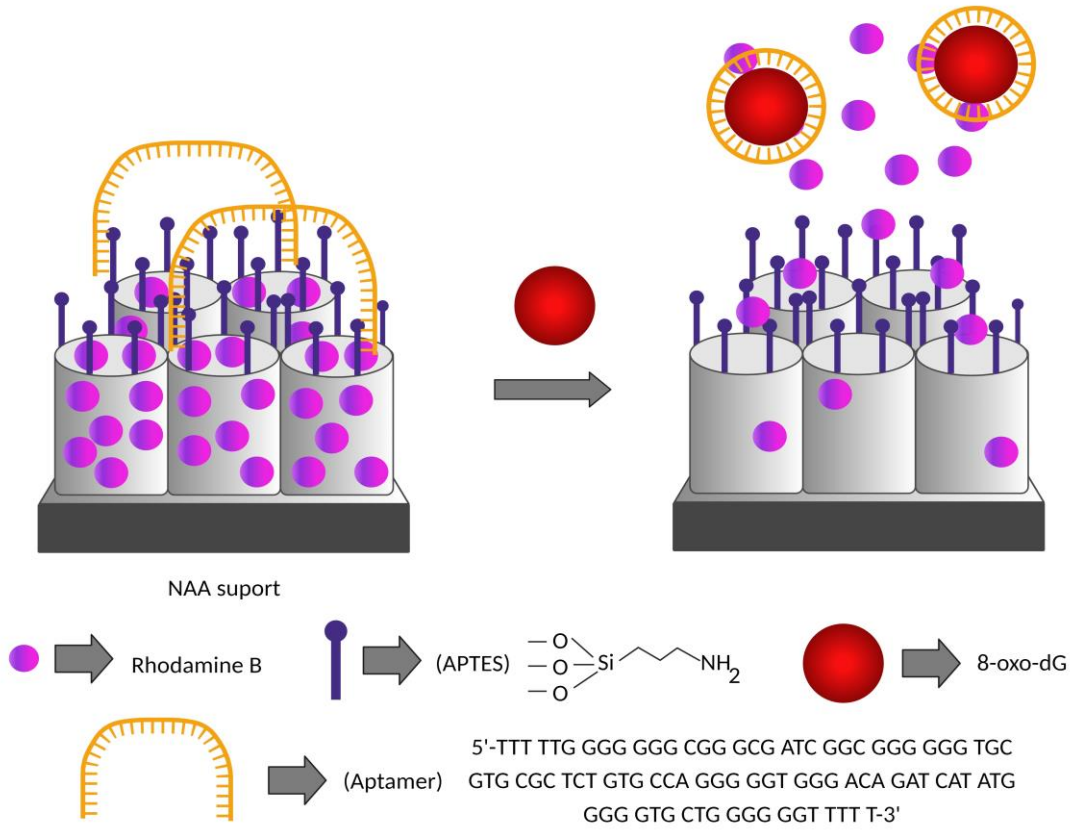

Figure 15. *Diagram showing how the capped sensor functions with and without the 8-oxo-dG target. Displacement of aptamer sequences causes cargo delivery when the oncological marker is present.*

Additionally, Özalp et al. also developed aptamer-capped MSNs, that opened in the presence of nucleolin.[88] Nucleoline is a multifunctional protein that interacts with DNA and RNA and is highly concentrated in the nucleolus and cytoplasms of healthy cells, as well as on the surface of actively proliferative cancer cells. To design this system, the researchers first prepared a nucleoline-specific amino acid modified aptamer (AS1411) and conjugated it to the surface of MSNs using (3-mercaptopropyl)trietoxisilane (MPTS) to effectively block pores, as shown in Figure 16. In their in vitro release studies, researchers observed that when incubated with isolated cell membrane fragments of MDA-MB-231 cells (which overexpress nucleoline), nanoparticles remained intact and fluorescein was released significantly. The interaction of the aptmer with the nucleoline on the surface of the cancer cells induced a conformational change in the aptmer, which opened the pores of the MSN and allowed the release of the encapsulated load.

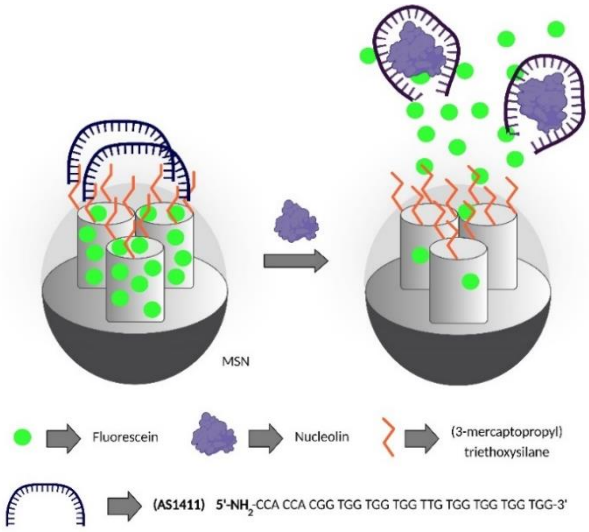

***Figure 16**. Fluorescein-loaded MSNs and capped aptamers that recognize and bind nucleolin. Cargo delivery was activated in the presence of nucleolin.*

[88] Hernandez, F. J., Hernandez, L. I., Pinto, A., Schäfer, T., & Özalp, V. C. (2013). *Targeting cancer cells with controlled release nanocapsules based on a single aptamer*. Chemical communications, 49(13), 1285-1287.

A final example of a nanoporous material capped with aptamer was the one developed by Martínez-Máñez et al.[89] This novel aptasensor allowed the rapid detection of gliadin (gluten's soluble proteins) with potential use for food control. Celiac disease, an autoimmune condition activated by the consumption of gluten, impacts nearly 1% of the global population. Presently, there is no effective treatment, and managing the condition necessitates the exclusion of gluten from one's diet. A new approach for detecting gluten is developed in this context. Commercially available NAA supports were loaded with rodamine B and then functionalized with 3-(Triethoxysilyl)propyl isocyanate (3-ICPTS), obtaining the S0 support. Subsequently, a modified oligonucleotide with amino (O1) was attached to S0 by urea bonds, forming S1. Finally, the O4 oligonucleotide was used as a cap, remaining closed thanks to the steric interaction with S1. In the presence of the gliadin protein, it is expected to displace the O4 aptamer, releasing the load and increasing the fluorescence emission (Figure 17). This behavior is due to the higher affinity between O4 and gliadin compared to the affinity between O4 and functionalized NAA support. In the absence of gliadin, materials retain the encapsulated load without changes in fluorescence. The LOD (100 $\mu g \cdot kg^{-1}$), and response time (60 min) that were obtained indicate the probe's potential for use in the detection of gluten. Moreover, the detection system was tested in food samples, obtaining a response proportional to the concentration of gliadin in the 100-800 $\mu g \cdot kg^{-1}$ range.

[89] Pla, L., Martínez-Bisbal, M. C., Aznar, E., Sancenón, F., Martínez-Máñez, R., & Santiago-Felipe, S. (2021). *A fluorogenic capped mesoporous aptasensor for gluten detection*. Analytica Chimica Acta, 1147, 178-186.

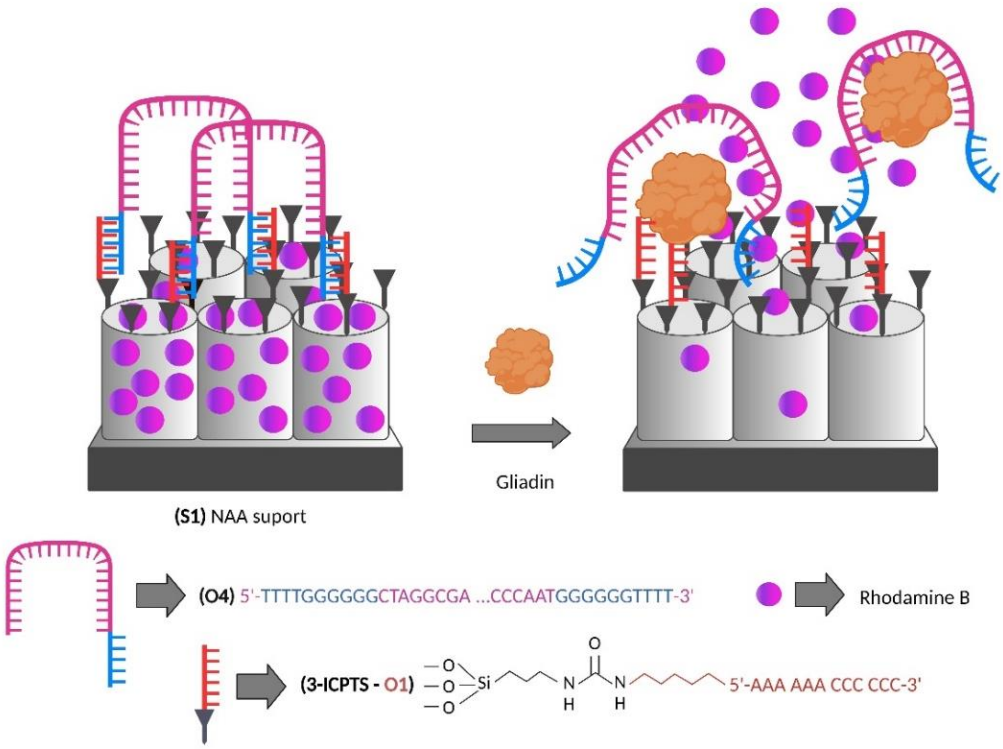

Figure 17. *Diagram of the gated support. When gliadin is present, the nanomaterial capped with the selected oligonucleotide sequence releases encapsulated dye in the pores.*

6. The challenge of pathogen detection

6.1. Generalities

Pathogens are microorganisms or agents that have the ability to cause disease. Unlike microorganisms in the normal flora that harmlessly colonize human organisms, pathogens have specific mechanisms that allow them to infect and cause disease through the following phases: (1) entry through various pathways, such as inhalation from airborne pathogens, ingestion of contaminated food or water, direct contact with infected people or surfaces, or transmission via vectors such as mosquitoes or ticks; (2) adherence via specific molecules, known as adhesins, which allow them to bind to receptors on the

surface of host cells and initiate infection; (3) invasion, employing various strategies to invade host tissues and overcome the body's defense mechanisms; and (4) multiplication and colonization in order to damage host cells, release toxins, or trigger an inflammatory response, all of which contribute to the progression of the infection.[90]

The agents causing these infectious processes can be categorized into 6 groups, each leading to different diseases due to their specific biochemical mechanisms: (1) viruses, which disrupt the host cell's machinery to produce their proteins and replicate their genome; (2) bacteria, with virulence genes promoting host cell replication and spread; (3) fungi and (4) protozoa, evolving during the infection process and complicating the immune system response; (5) helminths (worms), which divert the immune response towards ineffective immunity against them; and (6) prions, non-DNA infectious agents catalyzing protein misfolding in the host cell, converting "normal" proteins into new prions.

Worldwide, infectious diseases caused by pathogens result in large numbers of hospital admissions each year and, in some circumstances, death. Incorrect or late diagnosis also hinders the selection and effectiveness of therapy, leading to difficulties for the patient and a significant increase in healthcare costs. According to the World Health Organization (WHO), adopting a multidisciplinary strategy centered, first, on monitoring via the development of new diagnostic technologies that can enable prevention, is the key to control infectious diseases and reducing the number of deaths.

Detection of pathogens in the human body is carried out through various techniques, such as laboratory tests, immunodiagnosis, PCR, genomic sequencing, microscopy and imaging tests. These tools are essential to identify and diagnose different types of infections, providing essential information for the treatment and control of diseases. However, traditional pathogen detection tests have certain limitations: (1)

[90] Alberts, B., Johnson, A., Lewis, J., Raff, M., Roberts, K., & Walter, P. (2002). *Introduction to pathogens*. In Molecular Biology of the Cell. 4th edition. Garland Science.

limited sensitivity and specificity, resulting in false negatives and false positives; (2) delays in diagnosis and treatment, especially in serious cases of infection, as many detection procedures are time consuming and require sophisticated infraestructures; (3) slow or poor growth of cultures of the pathogens; (4) misidentifications of infections caused by multiple organisms; (5) limitations to detect new strains or variants of emerging pathogens; (6) possible invasiveness and discomfort for the patient; and (7) costs associated with hospitalization.

In recent years, various innovative techniques have been developed to detect infectious pathogens, with the aim of overcoming the limitations of traditional methods. These new techniques include nucleic acid amplification,[91] nanotechnology-based biosensors,[92] mass spectrometry,[93] antigen detection[94] and paper biosensors.[95] All of them have the potential to improve detection capacity, reduce diagnostic times and facilitate the identification of merging infections.

In this scenario, as knowledge about nanotechnology grows, it is offering creative alternatives to overcome limitations of existing technologies. For instance, returning to the use of MSNs, chosen for their low cost, large surface area, adjustable pore size, and excellent biocompatibility, J. Lin et al. recently developed an advance in capping systems

[91] Srivastava, P., & Prasad, D. (2023). *Isothermal nucleic acid amplification and its uses in modern diagnostic technologies.* 3 Biotech, 13(6), 200.

[92] Alafeef, M., Moitra, P., & Pan, D. (2020). *Nano-enabled sensing approaches for pathogenic bacterial detection.* Biosensors and Bioelectronics, 165, 112276.

[93] a) Hernandez, M. M., Banu, R., Shrestha, P., Gonzalez-Reiche, A. S., van de Guchte, A., Farrugia, K., & Paniz-Mondolfi, A. E. (2022). *A robust, highly multiplexed mass spectrometry assay to identify SARS-CoV-2 variants.* Microbiology Spectrum, 10(5), e01736-22; b) Elbehiry, A., Aldubaib, M., Abalkhail, A., Marzouk, E., ALbeloushi, A., Moussa, I., & Rawway, M. (2022). *How MALDI-TOF mass spectrometry technology contributes to microbial infection control in healthcare settings.* Vaccines, 10(11), 1881.

[94] Pavia, C. S., & Plummer, M. M. (2021). *The evolution of rapid antigen detection systems and their application for COVID-19 and other serious respiratory infectious diseases.* Journal of Microbiology, Immunology and Infection, 54(5), 776-786.

[95] a) Batule, B. S., Seok, Y., & Kim, M. G. (2020). *Based nucleic acid testing system for simple and early diagnosis of mosquito-borne RNA viruses from human serum.* Biosensors and Bioelectronics, 151, 111998; b) Yang, Z., Xu, G., Reboud, J., Ali, S. A., Kaur, G., McGiven, J., & Cooper, J. M. (2018). *Rapid veterinary diagnosis of bovine reproductive infectious diseases from semen using paper-origami DNA microfluidics.* ACS sensors, 3(2), 403-409.

for the detection of *Salmonella*.[96] *Salmonella typhimurium* (*S. typhimurium*) has been one of the leading foodborne illnesses worldwide, causing significant public health problems and economic losses. To address the need for accurate and rapid detection, the researchers designed an acid-sensitive microfluidic biosensor using curcumin (CUR) as a signal indicator and ZnO-coated MSNs for signal amplification in colorimetric and fluorescent modes. The process involved several steps: (1) the MSNs were incubated with CUR to obtain MSN@CUR nanoparticles, (2) ZnO nanoparticles were coated onto MSN@CUR to form MSN@CUR@ZnO nanoparticles and thus cap the pores, and (3) the MSN@CUR@ZnO were modified with polyclonal antibodies (pAbs) targeting *S. typhimurium*, developing MSN@CUR@ZnO@pAbs (MCZP NPs) using small molecules 1,2,4,5-tetrazine (Tz) and trans-cyclobutene (TCO). The microfluidic chip, featuring a Koch fractal mixing channel, facilitated the conjugation of immune magnetic nanoparticles (MNPs), *S. typhimurium* cells, and MSN@CUR@ZnO@pAbs to form MNP-bacteria-MSN@CUR@ZnO@pAbs complexes. The final step involved the introduction of acetic acid (HAc) to release CUR from the complexes, enabling measurement of color changes and fluorescence to determine the concentration of *Salmonella* (Figure 18). The incorporation of acid-decomposable ZnO NPs prevented previous release of the CUR signal reporter, leading to signal amplification. The use of HAc for CUR delivery increased stability and enabled bimodal fluorescent and colorimetric detection. Importantly, this biosensor exhibited high sensitivity and specificity (bacterial detection in a range of 10^2 to 10^7 CFU/mL in 1.5 h and detection limits of 63 CFU/mL for colorimetric measurement and 40 CFU/mL for fluorescent measurement), in addition to a high potential for detecting *S. typhimurium* in real samples.

[96] Huang, F., Guo, R., Xue, L., Cai, G., Wang, S., Li, Y., & Lin, J. (2020). *An acid-responsive microfluidic salmonella biosensor using curcumin as signal reporter and ZnO-capped mesoporous silica nanoparticles for signal amplification.* Sensors and Actuators B: Chemical, 312, 127958.

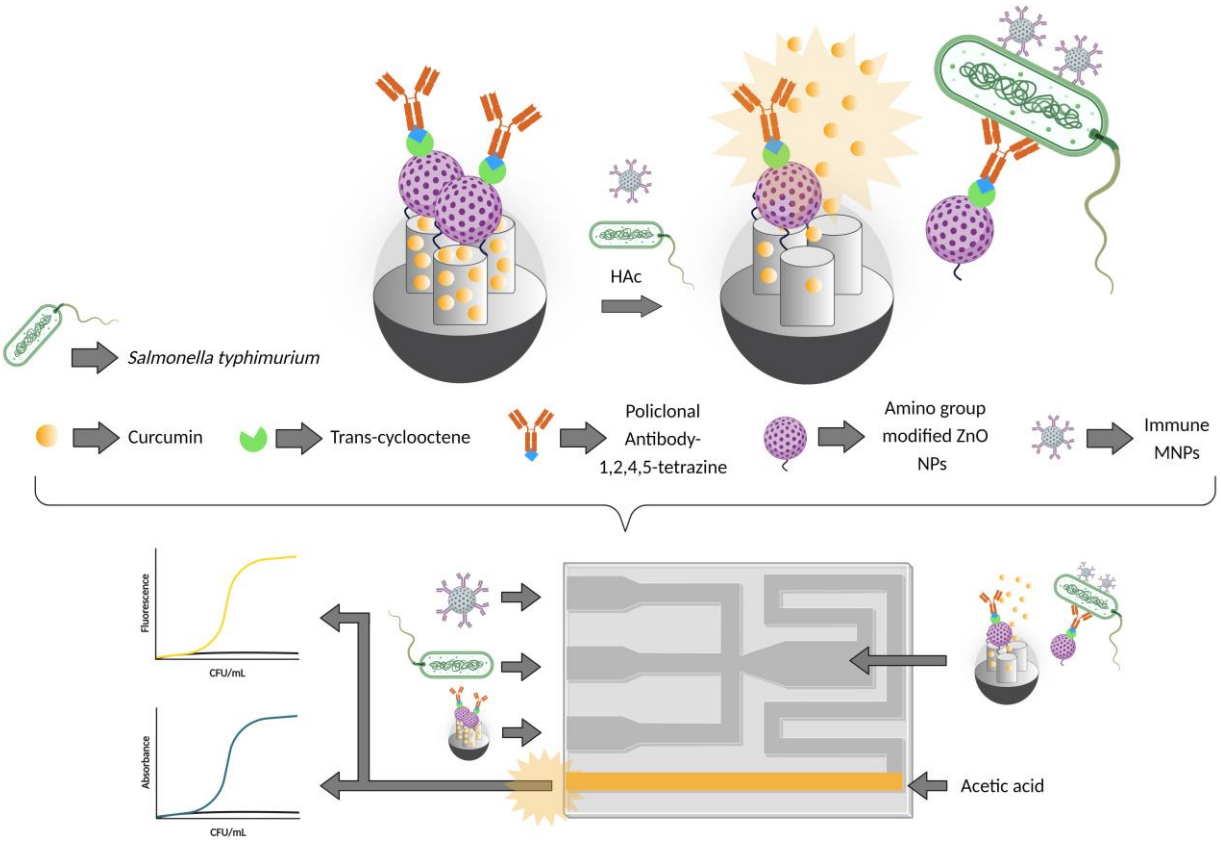

***Figure 18**. Schematic of the proposed microfluidic biosensor for the rapid and precise detection of Salmonella typhimurium.*

In 2020, a study by Aznar and coworkers focused on the use of biosensor technology to detect *Candida auris*, a fungal pathogen associated with serious invasive infections and nosocomial outbreaks reported worldwide since its initial discovery in 2009.[97] Traditional methods to identify this fungus have proven ineffective in clinical laboratories, and molecular approaches often require expensive and specialized

[97] Pla, L., Santiago-Felipe, S., Tormo-Mas, M. Á., Ruiz-Gaitán, A., Pemán, J., Valentin, E., Sancenón, F., Aznar, E., & Martinez-Manez, R. (2021). *Oligonucleotide-capped nanoporous anodic alumina biosensor as diagnostic tool for rapid and accurate detection of Candida auris in clinical samples. Emerging microbes & infections*, 10(1), 407-415.

equipment, making their implementation difficult. In this case, NAA supports were loaded with a rhodamine B followed by functionalization with APTES. Finally, the nanopores were capped with a specific oligonucleotide which contains a sequence corresponding to the unique GPI proteins of the *C. auris* cell wall. In the absence of fungal genomic DNA, the control hybridization buffer showed minimal cargo release due to pore blocking by the oligonucleotide in the NAA support. However, when target *C. auri*s genomic DNA was present, preferential hybridization occurred between the genomic DNA and the oligonucleotide, resulting in unblocking of the pores and subsequent delivery of the cargo (Figure 19). To evaluate the specificity of the developed genomic DNA detection system, tests were performed examining the response in the presence of genomic DNA from other Candida species, including *C. albicans, C. glabrata, C. parapsilopsis, C. tropicalis, C. pseudohaemulonii, C. haemulonii, C. intermedia*, and *C. lusitaniae*. None of these species induced the opening of the nanopores. Furthermore, the controlled material was tested on human blood inoculated with various amounts of *C. auris* cells and demonstrated its ability to successfully identify *C. auris* isolates from eight different countries. This method allowed the accurate identification of *C. auris* in blood cultures from infected patients in 60 minutes, without requiring prior sample preparation or amplification procedures. These results confirmed the high selectivity of the nanodevice and its usefulness as a diagnostic tool to detect *C. auris* in clinical samples.

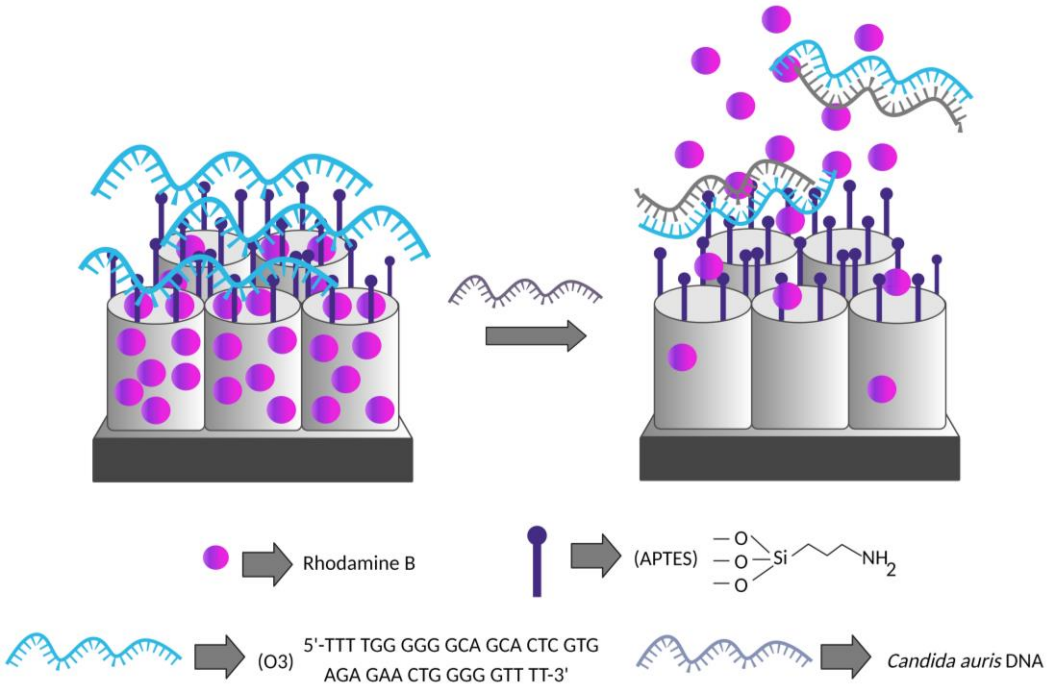

Figure 19. *Schematic representation of the gated NAA support and the selective uncapping and dye delivery in the presence of C. auris genomic DNA.*

The COVID-19 pandemic, which emerged in 2019, has highlighted the vital importance of testing and tracing infected people to stop the transmission of the virus. In this context, the development of rapid and sensitive detection methods for SARS-CoV-2, the virus responsible for COVID-19, was of paramount importance. To address this need, Martínez Máñez et al. focused on the development of a biosensor based on oligonucleotide-capped nanomaterials for the specific detection of the SARS-CoV-2 spike protein (S protein).[98] The detection system employed a NAA scaffold that was loaded with the fluorescent reporter rhodamine B and coated with a DNA aptamer specifically targeting the spike protein (Figure 20). To evaluate its performance, a pseudotype virus

[98] Caballos, I., Aranda, M. N., López-Palacios, A., Pla, L., Santiago-Felipe, S., Hernández-Montoto, A., & Martínez-Máñez, R. (2023*). Aptamer-Capped Nanoporous Anodic Alumina for SARS-CoV-2 Spike Protein Detection*. Advanced Materials Technologies, 2201913.

based on the vesicular stomatitis virus was first used, which contained the S proteins of SARS-CoV-2 on its surface. In the presence of the pseudotype virus, the cap of the nanodevice was selectively displaced, resulting in the release of dye from the pore voids into the medium, reaching pseudotype virus detection at concentrations as low as 7.5 x 10^3 PFU/ml. Additionally, the performance of the nanodevice was also evaluated in COVID-19 inoculated clinical samples with good results.

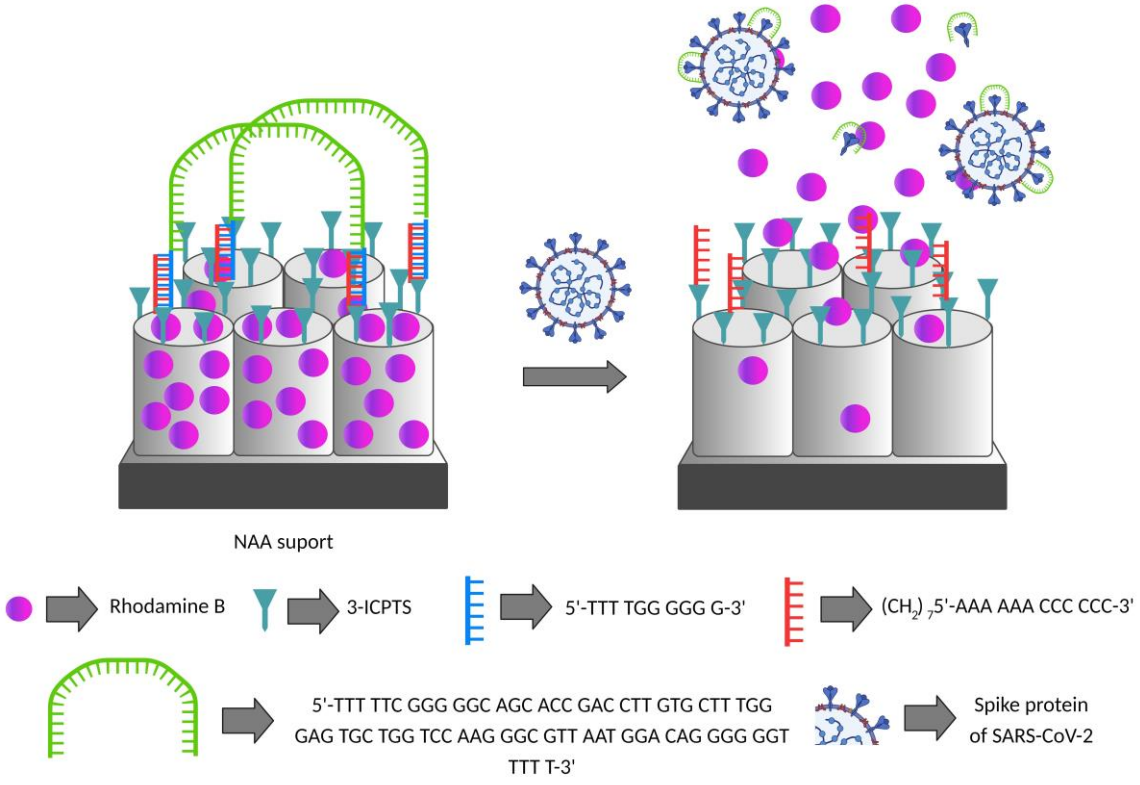

Figure 20. *Diagram showing the gated NAA material's capacity to recognize the SARS-CoV-2 spike protein. The SARS-CoV-2 S protein produced aptamer displacement and the release of the entrapped dye.*

Given the relevance of the gated materials in this thesis, innovative systems for the precise detection of both pathogenic species and biomarkers will be developed. These materials allow specific control of the release of loads, facilitating efficient detection. Design and functionalization strategies will be explored, as well as their ability to differentiate biomarkers, with potential applications in diagnostics and nanomedicine.

6.2. The Human Papiloma Virus case

According to WHO estimates, in 2022 cervical cancer was the fourth leading cause of cancer and death from cancer in women, with approximately 660,000 new cases and nearly 350,000 deaths worldwide.[99] This type of cancer accounts for more than 90% of *Human papillomavirus* (HPV)-related cancers in women. HPVs are a group of small, double-stranded DNA viruses with a preference for the skin, upper respiratory tract, and genital epithelia. There are currently over 150 known HPV types, which are divided into several genera based on their DNA sequences.[100] There are approximately 15 high-risk mucosal HPV strains that are linked to cervical cancer; the most carcinogenic are HPV16 and HPV18, which are thought to be the cause of 50% and 20% of cervical cancers globally, respectively.[101] The connection between these viruses and a subset of other genital cancers, as well as head and neck cancers are shown in Table 1.[102]

[99] Ferlay, J., Laversanne, M., Ervik, M., Lam, F., Colombet, M., Mery, L., & Bray, F. (2024). *Global Cancer Observatory: Cancer Tomorrow (version 1.1).* Lyon, France: International Agency for Research on Cancer Available from: https://gco. iarc. fr/tomorrow. Accessed, 30.

[100] de Villiers, E. M. (2013). *Cross-roads in the classification of papillomaviruses.* Virology, 445(1-2), 2-10.

[101] Smith, J. S., Lindsay, L., Hoots, B., Keys, J., Franceschi, S., Winer, R., & Clifford, G. M. (2007). *Human papillomavirus type distribution in invasive cervical cancer and high-grade cervical lesions: a meta-analysis update.* International journal of cancer, 121(3), 621-632.

[102] Schiffman, M., Herrero, R., DeSalle, R., Hildesheim, A., Wacholder, S., Rodriguez, A. C., & Burk, R. D. (2005*). The carcinogenicity of human papillomavirus types reflects viral evolution*. Virology, 337(1), 76-84.

Table 1. Summary of identified HPV types belonging to the different genera alpha, beta, gamma and mu in the phylogenetic tree of HPV along with the main diseases associated with the various HPV types.

		HPV type	*Disease (% attributed cases)*
Alpha	Mucosal high-risk	HPV16	Cervical squamous cell carcinoma (~50) Cervical adenocarcinoma (~35) Oropharyngeal cancer (~25)
		HPV18	Cervical squamous cell carcinoma (~20) Cervical adenocarcinoma (~35)
		HPV31, 33, 35, 39, 45, 51, 52, 56, 58, 59	Cervical squamous cell carcinoma (~30)
	Mucosal low-risk	HPV6, 11	Benign genital lesions Respiratory papillomatosis
		HPV13, 32	Oral focal epithelial hyperplasia
	Cutaneous benign	HPV2, 3, 27, 57	Skin warts
Mu		HPV1	Skin warts
Beta	Cutaneous	HPV5 and 8	First beta HPV types isolated from SSC of RV individuals
		HPV9, 12, 14, 15, 17, 19-25, 36-38, 47, 49, 75, 76, 80, 92, 93, 96, 98-100, 104, 105, 107, 110, 111, 113, 115, 118, 120, 122, 124, 143, 145, 150-152, 159	Likely associated with SSC in EV patients as well as immuno-compromised and immuno-competent individuals
Gamma		HPV4, 48, 50, 60, 65, 88, 95, 101, 103, 108, 109, 112, 115, 116, 119, 121, 123, 126-142, 144, 146-149, 153-158, 161-170	Unknow

HPV is found in 89% of low-grade squamous intraepithelial lesions and in more than 90% of high-grade squamous intraepithelial lesions and cervical cancer.[103] In low-grade lesions, high- and low-risk genotypes are common, while in high-grade lesions, high-risk genotypes, such as VPH16, predominate. HPV diversity is higher in high-grade lesions

[103] Alarcón-Romero, L. D. C., Organista-Nava, J., Gómez-Gómez, Y., Ortiz-Ortiz, J., Hernández-Sotelo, D., del Moral-Hernández, O., & Illades-Aguiar, B. (2022). *Prevalence and distribution of human papillomavirus genotypes (1997–2019) and their association with cervical cancer and precursor lesions in women from Southern Mexico.* Cancer Control, 29, 10732748221103331.

than in low-grade lesions. VPH16 is the most common genotype in cervical cancer, contributing to 70% of cases, and is also common in other cancers. Its oncogenic potential is associated with persistent infection, high viral load and variants with different cancer capabilities.[104]

Although HPV is a major cause of cervical cancer, a proportion of invasive cervical cancers are negative for this virus. The absence of HPV in these cases can vary significantly between studies, from a minimum of 0.03% to a maximum of 15%. Possible reasons include HPV-independent cancers, misclassification of tumors, HPV types not analyzed, loss of viral genomes, and failure of screening methods.[105] Optimization in virus detection requires minimizing false negatives at all stages, since HPV-negative cervical cancers can represent a subgroup with different biological characteristics, associated with late diagnosis and worse prognosis, which could require different therapeutic strategies.[106]

HPV detection involves several methods, and the choice depends on factors such as sensitivity, specificity, and clinical context:

- **Cervical cytology (Pap smear):** Detects cell changes in the cervix. It is not as sensitive as other tests and requires frequent repetition to prevent cancer.[107]

[104] Shen-Gunther, J., Xia, Q., Cai, H., & Wang, Y. (2021). *HPV DeepSeq: an ultra-fast method of NGS data analysis and visualization using automated workflows and a customized papillomavirus database in CLC genomics workbench*. Pathogens, 10(8), 1026.

[105] a) Tjalma, W. A. A. (2018). *HPV negative cervical cancers and primary HPV screening.* Facts, views & vision in ObGyn, 10(2), 107; b) *Cancer Genome Atlas Research Network. (2017). Integrated genomic and molecular characterization of cervical cancer*. Nature, 543(7645), 378; c) Li, N., Franceschi, S., Howell-Jones, R., Snijders, P. J., & Clifford, G. M. (2011). *Human papillomavirus type distribution in 30,848 invasive cervical cancers worldwide: Variation by geographical region, histological type and year of publication*. International journal of cancer, 128(4), 927-935.

[106] Banister, C. E., Liu, C., Pirisi, L., Creek, K. E., & Buckhaults, P. J. (2017). *Identification and characterization of HPV-independent cervical cancers*. Oncotarget, 8(8), 13375.

[107] Nanda, K., McCrory, D. C., Myers, E. R., Bastian, L. A., Hasselblad, V., Hickey, J. D., & Matchar, D. B. (2000). *Accuracy of the Papanicolaou test in screening for and follow-up of cervical cytologic abnormalities: a systematic review.* Annals of internal medicine, 132(10), 810-819.

- **Primary HPV screening:** Involves collecting cervical or vaginal samples to detect HPV infections. More sensitive than cytology and allows extensions of detection intervals.[108]
- **Joint test (co-testing):** Combines cervical cytology and HPV test. More sensitive than HPV testing alone for certain pre-cancers but may lead to more false-positive results and colposcopy referrals.[109]
- **PCR:** directed at the highly conserved L1 gene in the HPV genome.[110] Although it is efficient and sensitive, it may not detect certain HPVs that do not match designed primers and probes, which could result in undetected infections.[111]

The HPV test exhibits greater sensitivity than cytology in identifying infections and precancerous conditions. This makes it possible to extend detection intervals and improve early detection of adenocarcinomas. In addition, the combination of detection methods could increase the sensitivity in relation to the independent HPV test; however, at the same time it could lead to an increase in false-positive results and subsequent colposcopies. Consequently, for higher specificity and positive predictive values, alternative detection approaches involving the use of nanomaterials have been suggested. In particular, a collection of oligonucleotide-activated NAA materials is proposed here to detect the DNA of different types of HPV quickly and effectively.

---

[108] Arbyn, M., Smith, S. B., Temin, S., Sultana, F., & Castle, P. (2018). *Detecting cervical precancer and reaching underscreened women by using HPV testing on self samples: updated meta-analyses*. Bmj, 363.

[109] Schiffman, M., Kinney, W. K., Cheung, L. C., Gage, J. C., Fetterman, B., Poitras, N. E., & Castle, P. E. (2018*). Relative performance of HPV and cytology components of cotesting in cervical screening.* JNCI: Journal of the National Cancer Institute, 110(5), 501-508.

[110] Abreu, A. L., Souza, R. P., Gimenes, F., & Consolaro, M. E. (2012). *A review of methods for detect human Papillomavirus infection.* Virology journal, 9, 1-9.

[111] a) Mühr, L. S. A., Bzhalava, D., Lagheden, C., Eklund, C., Johansson, H., Forslund, O., & Hultin, E. (2015). *Does human papillomavirus-negative condylomata exist?* Virology, *485*, 283-288; b) Bzhalava, D., Johansson, H., Ekström, J., Faust, H., Möller, B., Eklund, C., & Dillner, J. (2013). *Unbiased approach for virus detection in skin lesions*. PloS one, *8*(6), e65953; c) Arroyo Mühr, L. S., Lagheden, C., Lei, J., Eklund, C., Nordqvist Kleppe, S., Sparén, P., & Dillner, J. (2020). *Deep sequencing detects human papillomavirus (HPV) in cervical cancers negative for HPV by PCR.* British journal of cancer, 123(12), 1790-1795.

6.3. The case of *Vibrio vulnificus*

The evidence supporting climate change is undeniable, and the implications for our planet and its inhabitants are of vital importance. Since the pre-industrial era, the global mean temperature has risen by a total of 1.2 °C.[112] While the primary objective of the Paris Climate Agreement is to limit the global average temperature increase to "well below two degrees,"[113] there is a possibility that we could reach a warming threshold of 1.5 °C by the early 2030s.[114] The rapid melting of ice, the declining biodiversity, the rising sea levels, the increasing rainfall, and the alarming concentrations of carbon dioxide and greenhouse gases in the atmosphere, alongside the growing frequency of extreme weather events, all provide undeniable proof of this reality. These factors impact the proliferation, dissemination, and virulence of pathogens, as well as the routes of transmission, including vectors, food, and water. Changes in human behavior, influenced by climate, can lead to increased contact with pathogens through activities associated with water, especially during periods of prolonged warming. Climate change is also linked to shifts in the geographic range of microbial species, which is a critical factor in the emergence and re-emergence of diseases. Among the affected organisms are *Vibrios*, which are gram-negative bacteria commonly found in marine waters. *Vibrios* thrive in warm and brackish water and are highly influenced by temperature changes.[115] Consequently, they have been identified as a "microbial barometer of climate change" due to their close association with climatic conditions.[116]

[112] World Meteorological Organization. State of the Global Climate 2020. Report No. WMO-No. 1264, (2021).
[113] United Nations. Report of the Conference of the Parties on its twenty-first session, held in Paris from 30 November to 13 December 2015', Paris (2016).
[114] IPCC. Climate Change 2021: The Physical Science Basis. Contribution of Working Group I to the Sixth Assessment Report of the Intergovernmental Panel on Climate Change. (Cambridge University Press, 2021).
[115] Vezzulli, L., Colwell, R. R., & Pruzzo, C. (2013*). Ocean warming and spread of pathogenic vibrios in the aquatic environment.* Microbial ecology, 65, 817-825.
[116] Baker-Austin, C., Trinanes, J., Gonzalez-Escalona, N., & Martinez-Urtaza, J. (2017). *Non-cholera vibrios: the microbial barometer of climate change.* Trends in microbiology, 25(1), 76-84.

Vibrio spp. bacteria thrive in warm water with moderate salinity and are closely associated with various aquatic invertebrates, such as crustaceans, bivalves, and zooplankton[117]. These invertebrates play a significant role in the occurrence and distribution of *Vibrio* bacteria in the environment. Notably, copepods, which are a type of zooplankton and an important component of aquatic fauna, serve as major hosts for *Vibrio* spp., including *Vibrio parahaemolyticus* and *Vibrio vulnificus.*[118] Copepods are also considered vectors for *Vibrio cholerae*, the bacterium responsible for causing cholera. Similarly, *Vibrio* spp. have been observed to concentrate in filter-feeding shellfish, particularly oysters. Oysters have the ability to filter large volumes of water and, in the process, accumulate *Vibrio* bacteria. This is of concern because oysters are often consumed raw or undercooked, which can result in individuals being exposed to high doses of potentially pathogenic *Vibrio* agents.[119]

Within the genus *Vibrio,* the species *vulnificus* is a highly adaptable pathogen capable of infecting humans and aquatic animals, causing vibriosis.[120] First identified in the United States in 1976, [121] it represents a serious threat as an agent of foodborne diseases, with a high mortality rate exceeding 50%.[122] This microorganism is found in water, where it can survive as a mobile cell or form biofilms on various surfaces. [123] Its life

[117] Brumfield, K. D., Usmani, M., Chen, K. M., Gangwar, M., Jutla, A. S., Huq, A., & Colwell, R. R. (2021*). Environmental parameters associated with incidence and transmission of pathogenic Vibrio spp*. Environmental microbiology, 23(12), 7314-7340.

[118] a) Colwell, R. R., Kaper, J., & Joseph, S. W. (1977). *Vibrio cholerae, Vibrio parahaemolyticus, and other vibrios: occurrence and distribution in Chesapeake Bay*. Science, 198(4315), 394-396; b) Colwell, R. R. (1996). Global climate and infectious disease: the cholera paradigm. Science, 274(5295), 2025-2031.

[119] Froelich, B. A., & Noble, R. T. (2016). *Vibrio bacteria in raw oysters: managing risks to human health*. Philosophical Transactions of the Royal Society B: Biological Sciences, 371(1689), 20150209.

[120] a) Ceccarelli, D., Amaro, C., Romalde, J. L., Suffredini, E., & Vezzulli, L. (2019). *Vibrio species*. Food microbiology: fundamentals and frontiers, 347-388; b) Amaro, C., Sanjuán, E., Fouz, B., Pajuelo, D., Lee, C. T., Hor, L. I., & Barrera, R. (2015). *The fish pathogen Vibrio vulnificus biotype 2: epidemiology, phylogeny, and virulence factors involved in warm-water vibriosis.* Microbiology spectrum, 3(3), 3-3.

[121] Hollis, D. G., Weaver, R. E., Baker, C. N., & Thornsberry, C. (1976*). Halophilic Vibrio species isolated from blood cultures.* Journal of Clinical Microbiology, 3(4), 425-431.

[122] Baker-Austin, C., & Oliver, J. D. (2020). *Vibrio vulnificus.* Trends in Microbiology, 28(1), 81-82.

[123] Jones, M. K., & Oliver, J. D. (2009). *Vibrio vulnificus: disease and pathogenesis.* Infection and immunity, 77(5), 1723-1733.

cycle is influenced by temperature and iron concentration, which affects its infection capacity and toxin production. [124] Temperature changes play a role in their transition to an inactive state, known as VBNC (viable but non-culturable), [125] and globally affect the transcription of several genes associated with metabolism, colonization, resistance to innate immunity in fish, as well as the production of key toxins VvhA and RtxA1, and the Vvp protease. Once inside the host, the infection can spread through the circulation. The pathogen capsule protects the microorganism from host immune responses, especially in individuals with excess iron in the body. The release of toxins contributes to sepsis and ultimately death of the host. Mainly, transmission to humans occurs through consumption of raw shellfish or contact with seawater or infected animals, which can cause from gastroenteritis to severe septicaemia, [126] especially dangerous for individuals with weakened immune systems or elevated blood iron levels. [127] Therefore, the presence of this microorganism in fish farms in Europe and the eastern Mediterranean highlights its importance for both human and animal health. [128]

[124] a) Pajuelo, D., Hernández-Cabanyero, C., Sanjuan, E., Lee, C. T., Silva-Hernández, F. X., Hor, L. I., MacKenzie, S., & Amaro, C. (2016*). Iron and Fur in the life cycle of the zoonotic pathogen Vibrio vulnificus*. Environmental Microbiology, 18(11), 4005-4022; b) Hernández-Cabanyero, C., Sanjuán, E., Fouz, B., Pajuelo, D., Vallejos-Vidal, E., Reyes-López, F. E., & Amaro, C. (2020). *The effect of the environmental temperature on the adaptation to host in the zoonotic pathogen Vibrio vulnificus.* Frontiers in microbiology, 11, 489.

[125] a) Oliver, J. D., Hite, F., McDougald, D., Andon, N. L., & Simpson, L. M. (1995). *Entry into, and resuscitation from, the viable but nonculturable state by Vibrio vulnificus in an estuarine environment.* Applied and Environmental Microbiology, 61(7), 2624-2630; b) Smith, B., & Oliver, J. D. (2006*). In situ and in vitro gene expression by Vibrio vulnificus during entry into, persistence within, and resuscitation from the viable but nonculturable state*. Applied and Environmental Microbiology, 72(2), 1445-1451.

[126] a) Coerdt, K. M., & Khachemoune, A. (2021). *Vibrio vulnificus: review of mild to life-threatening skin infections*. Cutis, 107(2), E12-E17; b) Horseman, M. A., & Surani, S. (2011). *A comprehensive review of Vibrio vulnificus: an important cause of severe sepsis and skin and soft-tissue infection.* International Journal of Infectious Diseases, 15(3), e157-e166; c) Baker-Austin, C., & Oliver, J. D. (2018). *Vibrio vulnificus: new insights into a deadly opportunistic pathogen*. Environmental microbiology, 20(2), 423-430.

[127] Hernández-Cabanyero, C., Sanjuán, E., Fouz, B., Pajuelo, D., Vallejos-Vidal, E., Reyes-López, F. E., & Amaro, C. (2020). *The effect of the environmental temperature on the adaptation to host in the zoonotic pathogen Vibrio vulnificus*. Frontiers in microbiology, 11, 489.

[128] a) Brehm, T. T., Berneking, L., Martins, M. S., Dupke, S., Jacob, D., Drechsel, O., Bohnert, J., Becker, K., Kramer, A., Christner, M., Aepfelbacher, M., Schmiedel, S., Rodhe, H., & German Vibrio Study Group. (2021*). Heatwave-associated Vibrio infections in Germany, 2018 and 2019*. Eurosurveillance, 26(41), 2002041; b) Danin-Poleg, Y., Raz, N., Roig, F. J., Amaro, C., & Kashi, Y. (2015). *Draft genome sequence of environmental bacterium Vibrio vulnificus CladeA-yb158*. Genome Announcements, 3(4), 10-1128.

Detection of this pathogen is traditionally done by culture methods,[129] PCR,[130] serological tests,[131] mass spectrometry[132] and next-generation sequencing.[133] While these techniques are effective, biosensor-based methods stand out as the most promising because of their ability to provide rapid in situ detection without the need for complex laboratory equipment or lengthy procedures. Biosensors can quickly identify specific genetic sequences or metabolic products of Vibrio vulnificus, making them especially useful in real-time environmental monitoring, ensuring timely intervention to prevent serious infections.

7. mi-RNA as new biomarkers

7.1. Generalities

miRNAs are small single-stranded RNAs that play a crucial role in controlling the expression of protein-coding genes at the post-transcriptional level,[146] first reported three decades ago in *Caenorhabditis elegans.*[147] It is believed that miRNAs regulate over 60% of

[129] Lee, J. H., Park, S. K., Khan, F., Jo, D. M., Lee, D. H., Kang, M. G., & Kim, Y. M. (2022*). Simultaneous isolation and enumeration of virulent Vibrio cholerae and Vibrio vulnificus using an advanced MPN-PCR method.* Archives of Microbiology, 204(1), 5.

130 Roig, A. P., Carmona-Salido, H., Sanjuán, E., Fouz, B., & Amaro, C. (2022). *A multiplex PCR for the detection of Vibrio vulnificus hazardous to human and/or animal health from seafood.* International Journal of Food Microbiology, 377, 109778.

131 Wangman, P., Surasilp, T., Pengsuk, C., Sithigorngul, P., & Longyant, S. (2021). *Development of a species-specific monoclonal antibody for rapid detection and identification of foodborne pathogen Vibrio vulnificus*. Journal of Food Safety, 41(6), e12939.

132 Boonstra, M., Fouz, B., van Gelderen, B., Dalsgaard, I., Madsen, L., Jansson, E., & Haenen, O. (2023). *Fast and accurate identification by MALDI-TOF of the zoonotic serovar E of Vibrio vulnificus linked to eel culture.* Journal of Fish Diseases, 46(4), 445-452.

133 Wu, Z., Wu, Y., Gao, H., He, X., Yao, Q., Yang, Z.,. & Shao, P. (2022). *Identification and whole-genome sequencing analysis of Vibrio vulnificus strains causing pearl gentian grouper disease in China*. BMC microbiology, 22(1), 200.

[146] Bartel, D. P. (2004). *MicroRNAs: genomics, biogenesis, mechanism, and function*. Cell, 116(2), 281-297.

[147] a) Lee, R. C., Feinbaum, R. L., & Ambros, V. (1993). *The C. elegans heterochronic gene lin-4 encodes small RNAs with antisense complementarity to lin-14.* Cell, 75(5), 843-854; b) Wightman, B., Ha, I., & Ruvkun, G. (1993). *Posttranscriptional regulation of the heterochronic gene lin-14 by lin-4 mediates temporal pattern formation in C. elegans*. Cell, 75(5), 855-862.

protein-coding genes, making them key components in almost all biological activities.[148] Specifically, circulating microRNAs display exceptional stability, making them potential indicators for diagnosis, severity assessment, and therapeutic response in diseases such as cancer, metabolic disorders, and inflammatory conditions.[149]

Despite their intracellular functions, miRNAs are also found in various body fluids, such as blood,[150] saliva,[151] urine,[152] and tears.[153] Extracellular miRNAs can be actively secreted into different entities like exosomes, apoptotic bodies, microvesicles, or bound to RNA-binding proteins or lipoproteins[154]. Alternatively, they can be passively released from necrotic or apoptotic cells. Actively secreted miRNAs are believed to be involved in cell-to-cell communication, whereas the majority of extracellular miRNAs, circulating in a vesicle-free state, do not have any specific function.[155]

Currently, the most common methods for studying microRNAs include quantitative reverse transcription PCR (qRT-PCR),[156] Northern blotting,[157] *in situ*

[148] O'Brien, J., Hayder, H., Zayed, Y., & Peng, C. (2018*). Overview of microRNA biogenesis, mechanisms of actions, and circulation.* Frontiers in endocrinology, 9, 402.

[149] Chen, X., Ba, Y., Ma, L., Cai, X., Yin, Y., Wang, K., Guo, J., Zhang, Y., Chen, J., Guo, X., Li, Q., Li, X., Wang, W., Zhang, Y., Wang, J., Jiang, X., Xiang, Y., Xu, C., Zheng, P., Zhang, J., Li, R., Zhang, H., Shang, X., Gong, T., Ning, G., Wang, J., Zen, K., Zhang, J., & Zhang, C. Y. (2008*). Characterization of microRNAs in serum: a novel class of biomarkers for diagnosis of cancer and other diseases.* Cell research, 18(10), 997-1006.

[150] Mitchell, P. S., Parkin, R. K., Kroh, E. M., Fritz, B. R., Wyman, S. K., Pogosova-Agadjanyan, E. L., Peterson, A., Noteboom, J., O'Briant, K. C., Allen, A., Lin, D. W., Urban, N., Drescher, C. W., Knudsen, B. S., Stirewalk, D. L., Gentleman, R., Vessella, R. L., Nelson, P. S., Martin, D. B., & Tewari, M. (2008). *Circulating microRNAs as stable blood-based markers for cancer detection.* Proceedings of the National Academy of Sciences, 105(30), 10513-10518.

[151] Roi, A., Boia, S., Rusu, L. C., Roi, C. I., Boia, E. R., & Riviș, M. (2023*). Circulating miRNA as a Biomarker in Oral Cancer Liquid Biopsy.* Biomedicines, 11(3), 965.

[152] Kim, J., Park, J., Ki, J., Rho, H. W., Huh, Y. M., Kim, E., Son, H. Y., & Haam, S. (2022). *Simultaneous dual-targeted monitoring of breast cancer circulating miRNA via surface-enhanced Raman spectroscopy.* Biosensors and Bioelectronics, 207, 114143.

[153] Altman, J., Jones, G., Ahmed, S., Sharma, S., & Sharma, A. (2023). *Tear film microRNAs as potential biomarkers: a review.* International journal of molecular sciences, 24(4), 3694.

[154] Cheng, G. (2015). *Circulating miRNAs: roles in cancer diagnosis, prognosis and therapy.* Advanced drug delivery reviews, 81, 75-93.

[155] Bhardwaj, A.; Singh, S.; Singh, A.P. (2010). *MicroRNA-Based Cancer Therapeutics: Big Hope from S-mall RNAs*. Mol. Cell. Pharmacol, 2(5):213–219

[156] Chen, C., Ridzon, D. A., Broomer, A. J., Zhou, Z., Lee, D. H., Nguyen, J. T., & Guegler, K. J. (2005). *Real-time quantification of microRNAs by stem–loop RT–PCR.* Nucleic acids research, 33(20), e179-e179.

[157] Válóczi, A., Hornyik, C., Varga, N., Burgyan, J., Kauppinen, S., & Havelda, Z. (2004). *Sensitive and specific*

hybridization,[158] microarrays, and next-generation sequencing.[159] However, each of these methods has its drawbacks.[160] MicroRNA detection often requires the use of a substantial amount of total RNA, ranging from a single microgram to hundreds of nanograms, for most experiments. Furthermore, many of these techniques require the purification of microRNA and its conversion into complementary DNA (cDNA), which is then amplified using polymerase reactions. Achieving absolute quantification can be challenging, and false positives from contamination is a problem. The amplification process, especially in exponential amplification-based technologies such as qRT-PCR, can magnify errors exponentially, further complicating accurate detection. To address these limitations and improve the detection and validation of microRNAs in complex biological samples, it is crucial to develop analytical systems that preferably do not rely on such kind of amplification. For this, several techniques are currently being developed, including electrochemical techniques,[161] isothermal amplification[162] and probes based on nanoparticles,[163] among others.

Both conventional and nanotechnology-based miRNA quantification methodologies rely on the fundamental molecular recognition event of Watson-Crick base pairing, which involves the hybridization of the target miRNA to a nucleic acid probe.

---

detection of microRNAs by northern blot analysis using LNA-modified oligonucleotide probes. Nucleic acids research, 32(22), e175-e175.

[158] Kloosterman, W. P., Wienholds, E., de Bruijn, E., Kauppinen, S., & Plasterk, R. H. (2006). *In situ detection of miRNAs in animal embryos using LNA-modified oligonucleotide probes.* Nature methods, 3(1), 27-29.

[159] Beckers, M., Mohorianu, I., Stocks, M., Applegate, C., Dalmay, T., & Moulton, V. (2017). *Comprehensive processing of high-throughput small RNA sequencing data including quality checking, normalization, and differential expression analysis using the UEA sRNA Workbench.* RNA, 23(6), 823-835.

[160] a) Koscianska, E., Starega-Roslan, J., Czubala, K., & Krzyzosiak, W. J. (2011). *High-resolution northern blot for a reliable analysis of microRNAs and their precursors.* The Scientific World Journal, 11, 102-117; b) Zhang, X., & Zeng, Y. (2011). *Performing custom microRNA microarray experiments.* JoVE (Journal of Visualized Experiments), (56), e3250.

[161] Li, F., Peng, J., Wang, J., Tang, H., Tan, L., Xie, Q., & Yao, S. (2014). *Carbon nanotube-based label-free electrochemical biosensor for sensitive detection of miRNA-24*. Biosensors and Bioelectronics, 54, 158-164.

[162] Li, C., Li, Z., Jia, H., & Yan, J. (2011). *One-step ultrasensitive detection of microRNAs with loop-mediated isothermal amplification (LAMP).* Chemical Communications, 47(9), 2595-2597.

[163] Hwang, D. W., Song, I. C., Lee, D. S., & Kim, S. (2010). *Smart magnetic fluorescent nanoparticle imaging probes to monitor microRNAs*. Small, 6(1), 81-88.

The key difference between these approaches lies in the subsequent translation of this event into a measurable signal. Nanotechnology-based strategies incorporate elements such as nanomaterials, nanostructuring of a sensing surface, or a combination of both, to facilitate signal transduction and amplification. These nanotechnology elements play a vital role in enhancing the sensitivity and specificity of miRNA quantification, distinguishing them as valuable tools in this field.

Most microRNA studies have focused on the identification of one or a limited set of microRNAs associated with a specific disease. However, it has been observed that some microRNAs may be deregulated in different diseases, which complicates their use as specific biomarkers. To overcome this limitation, it is necessary to perform a global detection of circulating microRNAs in biological samples. This would make it possible to identify a unique set of microRNAs that make up a specific signature for a particular disease or type of cancer[164]. This microRNA signature could offer valuable information for a more precise and personalized diagnosis, as well as for the early detection of diseases. Additionally, other obstacles that need to be addressed include standardization of microRNA detection methods, optimization of assay sensitivity and specificity, and validation in large patient cohorts to ensure reliability and reproducibility of results.[165]

As a result, there are still many opportunities to develop sensitive, trustworthy, robust, and economically advantageous miRNA sensors. The wide range of nanotechnology-based strategies for miRNA quantification that have appeared in the very recent scientific literature is evidence of a growing field of study. Nanotechnology is anticipated to have a major impact in this area.[166]

---

[164] Calin, G. A., & Croce, C. M. (2006). *MicroRNA signatures in human cancers.* Nature reviews cancer, 6(11), 857-866.

[165] Witwer, K. W. (2015). *Circulating microRNA biomarker studies: pitfalls and potential solutions*. Clinical chemistry, 61(1), 56-63.

[166] a)Chandrasekaran, A. R., Punnoose, J. A., Zhou, L., Dey, P., Dey, B. K., & Halvorsen, K. (2019*). DNA nanotechnology approaches for microRNA detection and diagnosis.* Nucleic acids research, 47(20), 10489-10505; b) Degliangeli, F., Pompa, P. P., & Fiammengo, R. (2014). *Nanotechnology-based strategies for the detection and quantification of microRNA.* Chemistry–A European Journal, 20(31), 9476-9492.

7.2. Risk assessment for cardiotoxicity using miRNA detection

Advances in cancer treatments have increased patient survival, but they have also increased mortality due to their side effects. Among these side effects, cardiovascular disease (CVD) is one of the most common, raising concerns about its impact on the long-term health of cancer survivors. Cardiotoxicity, which refers to the direct effects of cancer treatment on the function and structure of the heart, may be one of the causes of this dysfunction, as well as the rapid development of CVD in those patients who already present cardiovascular risk factors[167]. The most thoroughly investigated therapeutic agents related to cardiovascular toxicity are targeted treatments and anthracycline-based therapies[168].

miRNAs are potentially used as diagnostic biomarkers due to their direct correlation with certain diseases,[169] high sensitivity, and biochemical stability.[170] Studies have shown that Cancer Therapy-Related Cardiac Dysfunction (CTRCD) and circulating

[167] Zamorano, J. L., Lancellotti, P., Rodriguez Munoz, D., Aboyans, V., Asteggiano, R., Galderisi, M., Habib, G., Lenihan, D. J., Lip, G. Y. H., Lyon, A. R., Lopez Fernández, T., Mohty, D., Piepoli, M. F., Tamargo, J., Torbick, A., & Suter, T. M. (2016). 2016 *ESC Position Paper on cancer treatments and cardiovascular toxicity developed under the auspices of the ESC Committee for Practice Guidelines: The Task Force for cancer treatments and cardiovascular toxicity of the European Society of Cardiology (ESC).* European heart journal, 37(36), 2768-2801.

[168] a) Cardinale, D., Colombo, A., Bacchiani, G., Tedeschi, I., Meroni, C. A., Veglia, F., Civelli, M., Lamantia, G., Colombo, N., Curigliano, G., Fiorentini, C., & Cipolla, C. M. (2015). *Early detection of anthracycline cardiotoxicity and improvement with heart failure therapy.* Circulation, 131(22), 1981-1988; b) Sawaya, H., Sebag, I. A., Plana, J. C., Januzzi, J. L., Ky, B., Tan, T. C., Cohen, V., Banchs, J., Carver, J. R., Wiegers, S. E., Martin, R. P., Picard, M. H., Gerszten, R. E., Halpern, E. F., Passeri, J., Kuter, I., & Scherrer-Crosbie, M. (2012). *Assessment of echocardiography and biomarkers for the extended prediction of cardiotoxicity in patients treated with anthracyclines, taxanes, and trastuzumab.* Circulation: Cardiovascular Imaging, 5(5), 596-603; c) Martel, S., Maurer, C., Lambertini, M., Pondé, N., & De Azambuja, E. (2017). *Breast cancer treatment-induced cardiotoxicity*. Expert opinion on drug safety, 16(9), 1021-1038; d) Henry, M. L., Niu, J., Zhang, N., Giordano, S. H., & Chavez-MacGregor, M. (2018*). Cardiotoxicity and cardiac monitoring among chemotherapy-treated breast cancer patients.* JACC: Cardiovascular Imaging, 11(8), 1084-1093.

[169] Zhou, S. S., Jin, J. P., Wang, J. Q., Zhang, Z. G., Freedman, J. H., Zheng, Y., & Cai, L. (2018). *miRNAS in cardiovascular diseases: potential biomarkers, therapeutic targets and challenges*. Acta Pharmacologica Sinica, 39(7), 1073-1084.

[170] Glinge, C., Clauss, S., Boddum, K., Jabbari, R., Jabbari, J., Risgaard, B., Tomsits, P., Hildebrand, B., Kääb, S., Wakili, R., Jespersen, T., & Tfelt-Hansen, J. (2017). *Stability of circulating blood-based microRNAs–pre-analytic methodological considerations.* PloS one, 12(2), e0167969.

miRNA levels are linked.[171] A total of 445 miRNAs were found to be differently expressed in breast cancer patients with cardiotoxicity compared to patients without cardiotoxicity in prospective studies published between 2013 and 2023.[172] In connection to cardiotoxicity, it was discovered that 229 miRNAs were downregulated and 216 were upregulated out of the 445 miRNAs. miR-4732-3p, one of the most promising cardioprotective microRNAs, was downregulated in the blood samples of breast cancer patients after anthracycline therapy, according to Sánchez-Sánchez et al. [173] In a prospective observational research, individuals with declining cardiac function during the first year after receiving chemotherapy based on anthracyclines (n = 10 cases) were compared to patients without cardiac dysfunction (n = 10 controls). A second cohort, consisting of 7 cases and 25 controls, confirmed the findings. Although further studies are needed to determine the predictive potential of miR-4732-3p against anthracycline-related myocardial damage, lower levels of this miRNA could indicate early cardiotoxicity in breast cancer patients after anthracycline treatment.

PCR is the standard method for detecting miR-4732-3p because of its high sensitivity,[174] but its high cost, need for specialized personnel and long waiting times make

[171] Brown, C., Mantzaris, M., Nicolaou, E., Karanasiou, G., Papageorgiou, E., Curigliano, G., Cardinale, D., Filipattos, G., Memos, N., Naka, K. K., Papakostantinou, A., Vogazianos, P., Ioulianou, E., Shammas, C., Constantinidou, A., Tozzi, F., Fotiadis, D. I., & Antoniades, A. (2022*). A systematic review of miRNAs as biomarkers for chemotherapy-induced cardiotoxicity in breast cancer patients reveals potentially clinically informative panels as well as key challenges in miRNA research.* Cardio-Oncology, 8(1), 1-18.

[172] Alexandraki, A., Papageorgiou, E., Zacharia, M., Keramida, K., Papakonstantinou, A., Cipolla, C. M., Tsekoura, D., Naka, K., Mazzocco, K., Mauri, D., Tsiknakis, M., Manikis, G. C., Marias, K., Marcou, Y., Kakouri, E., Konstantinou, I., Daniel, M., Galazi, M., Kampouroglou, E., Ribnikar, D., Brown, C., Karanasiou, G., Antoniades, A., Fotiadis, D., Filippatos, G., & Constantinidou, A. (2023). *New Insights in the Era of Clinical Biomarkers as Potential Predictors of Systemic Therapy-Induced Cardiotoxicity in Women with Breast Cancer: A Systematic Review.* Cancers, 15(13), 3290.

[173] Sánchez-Sánchez, R., Reinal, I., Peiró-Molina, E., Buigues, M., Tejedor, S., Hernándiz, A., Selva, M., Hervas, D., Cañada, A. J., Dorronsoro, A., Santaballa, A., Salvador, C., Caiment, F., Kleinjans, J., Martínez Dolz, L., Moscoso, I., Lage, R., González-Juanatey, J. R., Panadero, J., Bernardo, E., & Sepúlveda, P. (2022). *MicroRNA-4732-3p is dysregulated in breast cancer patients with cardiotoxicity, and its therapeutic delivery protects the heart from doxorubicin-induced oxidative stress in rats.* Antioxidants, 11(10), 1955.

[174] Zhuang, W., Liu, C., Hong, Y., Zheng, Y., Huang, M., Tang, H., & Huang, Y. (2024). *Tumor-suppressive miR-4732-3p is sorted into fucosylated exosome by hnRNPK to avoid the inhibition of lung cancer progression.* Journal of Experimental & Clinical Cancer Research, 43(1), 123.

it urgent to find faster and simpler methods. In this context, biosensors are presented as a promising alternative, since they overcome these limitations, allowing the detection of miR-4732-3p with a small amount of sample, which makes them diagnostic tools with great potential for the future.

Objectives

The core idea of this doctoral thesis is the design, development and evaluation of biosensors that combine the unique properties of mesoporous alumina supports with encapsulated dyes and biomolecule capping agents for the following objectives:

- ***Human papilomavirus*** **DNA detection:** To design, prepare and test a collection of rhodamine B-loaded, oligonucleotide-capped NAA films for the sensitive and accurate detection of HPV DNA.
- **Identification of *Vibrio vulnificus* DNA:** To design, prepare and test aptamer-capped NAA films that have been loaded with rhodamine B in order to identify *Vibrio vulnificus*, a pathogenic bacteria, in water samples.
- **Cardiovascular disease prevention:** To design, prepare and test aptamer-capped NAA films loaded with rhodamine B for the detection of miRNA 4732-3p as a valuable diagnostic tool for the evaluation of cardiovascular risk associated with anthracycline treatment.

Human Papilloma Virus DNA detection in clinical samples using fluorogenic probes based on oligonucleotide gated nanoporous anodic alumina films

1. Abstract

In this work, fluorogenic probes based on oligonucleotide capped nanoporous anodic alumina films are developed for specific and sensitive detection of human papilloma virus (HPV) DNA. The probe consists of anodic alumina nanoporous films loaded with the fluorophore rhodamine B and capped with oligonucleotides bearing specific base sequences complementary to genetic material of different high-risk (hr) HPV types. Synthesis protocol is optimized for scale up production of sensors with high reproducibility. Sensor´s surfaces are characterized by scanning electron microscopy (HR-FESEM) and atomic force microscopy (AFM) and their atomic composition is determined by energy dispersive X-ray spectroscopy (EDXS). Oligonucleotide molecules onto nanoporous films block the pores and avoid diffusion of rhodamine to the liquid phase. Pore opening is produced when specific DNA of HPV is present in the medium, resulting in rhodamine B delivery, that is detected by fluorescence measurements. The sensing assay is optimized for reliable fluorescence signal reading. Nine different sensors are synthesized for specific detection of 14 different hr-HPV types in clinical samples with very high sensitivity (100 %) and high selectivity (93-100%), allowing rapid screening of virus infections with very high negative predictive values (100 %). Sensors and sensing assay developed in this work allow multiplexed analysis of clinical samples resulting in faster screening which can be carried out by non-specialized personnel.

2. Introduction

Infectious diseases represent one of the most important health problems causing around 15 million deaths annually worldwide. In this context, the development of new systems for rapid detection of pathogens is of relevance for the advance in early diagnosis, finding appropriate treatments, a much more favourable patients' recovery, a reduction in associated mortality and a significant economic saving. Among infectious diseases, human papilloma virus infection is one of the most important caused by viruses.[1,2,3] Human papilloma virus (HPV) belongs to the Papillomaviridae family, infecting and

replicating in the nucleus of epithelial cells.[4,5] It has a simple structure formed by a protein capsid without envelope and the genetic material (circular double stranded DNA: around 8000 base pairs) that lies in its interior.[6,7,8] Based on their DNA composition (difference of more than 10 % in the nucleotide sequences in the E6, E7 and L1 region) around 77 HPV genotypes have been described. Specific types are considered as high risk (hr) HPV types because they have been identified as causative agents of cervical cancer.[9,10,11] Therefore, screening tools to detect hr-HPV infection allow cervical cancer prevention, management, and treatment.[12,13,14] Moreover, hr-HPV testing on cervical samples appeared to be more sensitive for detection of cervical intraepithelial neoplasia grade 2 or worse (CIN2+) than cytology, though often less specific.[15,16] In this regard, many testing assays have been used for detection of a broad spectrum of hr-HPV types with high reliability, reproducibility, and accuracy.[17,18,19] They include assays that can detect DNA-RNA hybrids without genotyping like the Hybrid Capture 2 (HC2) HPV DNA test, approved by the FDA in 2003, and PCR based assays that can detect HPV DNA with partial genotyping of hr-HPV, like the Cobas 4800 HPV test, approved by the FDA in 2011.[20] These assays have a high sensitivity and negative predictive values. However, they have some drawbacks such as a relatively lower specificity and positive predictive values and the use of expensive, time consuming and complex methods requiring trained personnel. Therefore, alternative rapid diagnostic platforms for detection of different hr-HPV types using smart nanodevice-based biosensors have been designed and developed.[21,22,23] These materials include different types of nanoparticles and electrodes whose surfaces have been modified with different oligonucleotide probes for specific recognition of target DNA.[24,25,26] In these systems, the transduction leading to measurable signal are mainly based on optical and electrochemical processes.[27,28,29] Nevertheless, these reported sensors have been designed only for detection of a few hr-HPV types (mainly 16 and 18) and their capacity for direct HPV detection in clinical samples (detection without any sample treatment) is not usually tested or validated.

Design and development of smart nanodevice-based biosensors bearing gated porous supports for detection of different DNA of pathogens have received increasing

attention during the last years.[30,31,32] These hybrid materials are mainly composed of two subunits: an inorganic porous support in which a fluorogenic molecule can be loaded and a molecular or supramolecular entity grafted onto external surface that can control the fluorophore probe diffusion from inside the pore to the liquid phase.[33,34,35] In these examples, capping molecules on the support's surface act as molecular gates (also known as gatekeepers) blocking the pores and avoiding dye release. Only when specific stimuli are present, as for instance a target analyte to be detected, the structural state of molecular gates changes, unblocking the pores and leading to controlled dye delivery which can be measured by fluorescence spectroscopy.[36] Specifically, in gated biosensors based on this paradigm, a fluorescent signal in the medium is related to the presence of specific genetic material of pathogens, due to the transduction process triggered by the recognition between pathogen's DNA molecules in the medium and a gating oligonucleotides on the porous support's surface, that finally enables the release of the loaded fluorophore.[37] Among inorganic porous supports, mesoporous silica nanoparticles[38,39] and nanoporous anodic alumina (NAA) films[40,41] have been used for sensor development because they have an ordered porous structure composed of tailor-made pores with large specific surface area and pore volume. These supports have high loading capacity and their external surface can be easily modified with alkoxysilane chemistries bearing different functional groups to yield an organic/inorganic interphase, enabling further functionalization of support´s surface with additional molecules or supramolecules through physical interactions or chemical linkages.[42,43] In this regard, nanoporous anodic alumina-based electrochemical biosensors have been used recently for sensitive detection of different analytes including DNA biomolecules.[44,45,46]

Different oligonucleotide-gated porous based sensors have been reported for detection of DNA/RNA or antigens of different pathogens such as: Mycoplasma,[30,31,47] *Candida albicans*,[32] *Candida auris*,[48] *Staphylococcus aureus*,[49] *Pneumocystis jirovecii,*[50] and SARS-CoV-2 virus.[51] These systems are currently demonstrating great potential for the development of sensitive, selective, and low-cost biosensors. However, similar biosensors for detection of hr-HPV types have not been reported yet. In this work sensors for

detection of HPV were developed. Specifically, the platform is configured for the rapid detection of 14 different hr-HPV types associated with the appearance of cervical cancer. For that, a set of 9 biomaterials based on NAA films coated with nucleic acid molecules as gates were designed. The probes consisted of nanoporous anodic alumina supports loaded with rhodamine B (RhB) and whose pores were blocked with diverse oligonucleotide sequences that specifically recognize HPV types (**Figure 1**). Release of the dye from the prepared materials is tested in the presence of the complementary oligonucleotide and validated in clinical samples, demonstrating the potential of this approach for multiplexed screening of HPV infections.

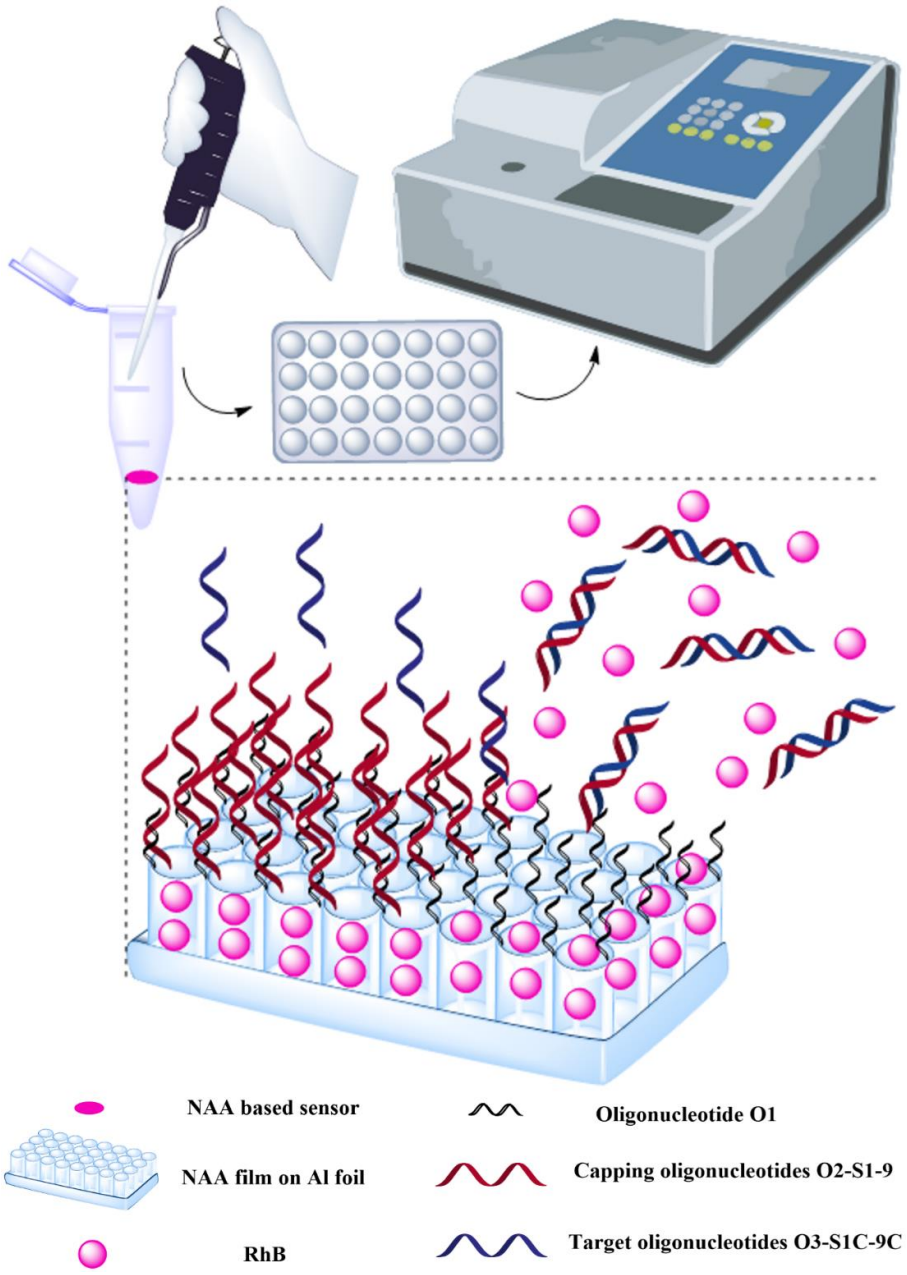

Figure 1. Scheme of fluorogenic sensors for HPV DNA detection based on oligonucleotide gated NAA films loaded with rhodamine B.

3. Results and discussion

Schematic representations of the developed sensors and the steps to prepare them are shown in **Figure 1** and **2**, respectively, whereas the sequences of the oligonucleotides used for the preparation of the sensors are listed in **Table 1**. Capping oligonucleotides **O2-S1-9** have the DNA base sequence of different HPV types overall being able to recognize 14 HPV types, whereas target oligonucleotides **O3-S1C-9C** are the corresponding complementary oligonucleotides used in optimization and testing assays (*vide infra*). The NAA supports are commercially available and have an alumina thickness of 10 ± 0.2 μm, a pore diameter of 5 ± 2 nm and a pore density of $9 \cdot 10^{11}$ cm^{-2}.

Table 1. Nucleotide sequences of 19 oligonucleotides used for sensor preparation and sensing assay.

Oligonucleotide	hr-HPV type	Nucleotide sequence 5'-….-3'
O1	-	NH_2-$(CH_2)_6$-AAA AAA CCC CCC
O2-S1	**S9, 16, 18**	TTTTGGGGGGAGACTGACAAATATCCAATGGTACTTCACTTTTGTTATCCTGCAA CAATTTAAGGGGGGTTTT
O3-S1C	**S9, 16, 18**	TTAAATTGTTGCAGGATAACAAAAGTGAAGTACCATTGGATATTTGTCAGTCT
O2-S2	**45, 18**	TTTTGGGGGGGTTTTGTGCAATCAGTTGCTGTTACCTGTCAAAAGGATACTACA CCTCCAGAAAAGCAGGATCCATATGATAAATTAAAGTGGGGGGTTTT
O3-S2C	**45, 18**	ACTTTAATTTATCATATGGATCCTGCTTTTCTGGAGGTGTAGTATCCTTTTGACA GGTAACAGCAACTGATTGCACAAAAC
O2-S3	**51, 16**	TTTTGGGGGGTAGCTAAAGTAGCTGTTGAACCGGAGCCTTTAATATATAAGTCA GTAGGGACCGATTCACCAACCGTGCCTGAGGGGGGTTTT
O3-S3C	**51, 16**	TCAGGCACGGTTGGTGAATCGGTCCCTACTGACTTATATATTAAAGGCTCCGGT TCAACAGCTACTTTAGCTA
O2-S4	**51**	TTTTGGGGGGCTTGTAGGTGTTGGGGAAGACATTCCTAACGATTATTATATTAA GGGGGGGGTTTT
O3-S4C	**51**	CCTTAATATAATAATCGTTAGGAATGTCTTCCCCAACACCTACAAG
O2-S5	**52**	TTTTGGGGGGCCTTTATTAAACAAGTTTGATGATACTGAAACCAGTAACAAATA TGCTGGTAAACCTGGTATAGATAATAGGGAATGTTGGGGGGTTTT

O3-S5C	**52**	AACATTCCCTATTATCTATACCAGGTTTACCAGCATATTTGTTACTGGTTTCAGTA TCATCAAACTTGTTTAATAAAGG
O2-S6	**33, 58**	TTTTGGGGGGACCCTGATACACAACGATTAGTATGGGCATGTGTAGGCCTTGA AATAGGTAGAGGGCAGCCATTAGGCGTTGGCATAAGTGGTGGGGGGTTTT
O3-S6C	**33, 58**	ACCACTTATGCCAACGCCTAATGGCTGCCCTCTACCTATTTCAAGGCCTACACAT GCCCATACTAATCGTTGTGTATCAGGGT
O2-S7	**35, 33**	TTTTGGGGGGGCCTTAAATATTCCTTAAAATTGTCATTTTTATATGTACTGTCACT AGAAGACACAGCAGAACACACAGACATATTTGTACTACGGGTTGGGGGGTTTT
O3-S7C	**35, 33**	AACCCGTAGTACAAATATGTCTGTGTGTTCTGCTGTGTCTTCTAGTGACAGTACA TATAAAAATGACAATTTTAAGGAATATTTAAGGC
O2-S8	**56, 66**	TTTTGGGGGGGGTACTGATTAATTTTTCGTGCATCATATTTACTTAACTGTTCTG TAGCAGTACTAATAGTCGGGGGGTTTT
O3-S8C	**56, 66**	GACTATTAGTACTGCTACAGAACAGTTAAGTAAATATGATGCACGAAAAATTAA TCAGTACC
O2-S9	**68, 39**	TTTTGGGGGGGGACTGTCACGTATGTCAGTGCCCTTAATATACAATTCAGTAGG TATAGTGTCCCCTACCATGCCGGGGGGTTTT
O3-S9C	**68, 39**	GCATGGTAGGGGACACTATACCTACTGAATTGTATATTAAGGGCACTGACATAC GTGACAGTCC

The starting NAA porous support (**D0**) was easily loaded with the RhB fluorophore by soaking NAA disks in a RhB solution in acetonitrile and gently stirring with an orbital stirrer, yielding **D1**. High loaded dye content was achieved using high concentrated RhB solution in short times of interaction between both phases. RhB encapsulation was evidenced by EDXS analysis. The C, N, and O atomic content in the dye-loaded NAA disk slightly increases respect to the unmodified support. Note that the X-ray emission depth for analysed atoms (<100 nm at 5 kV) is lower than the NAA film thickness (10 µm). (**Figure 3, Table 2, Figure S1, Tables S1-S2 (Supporting Information)**).

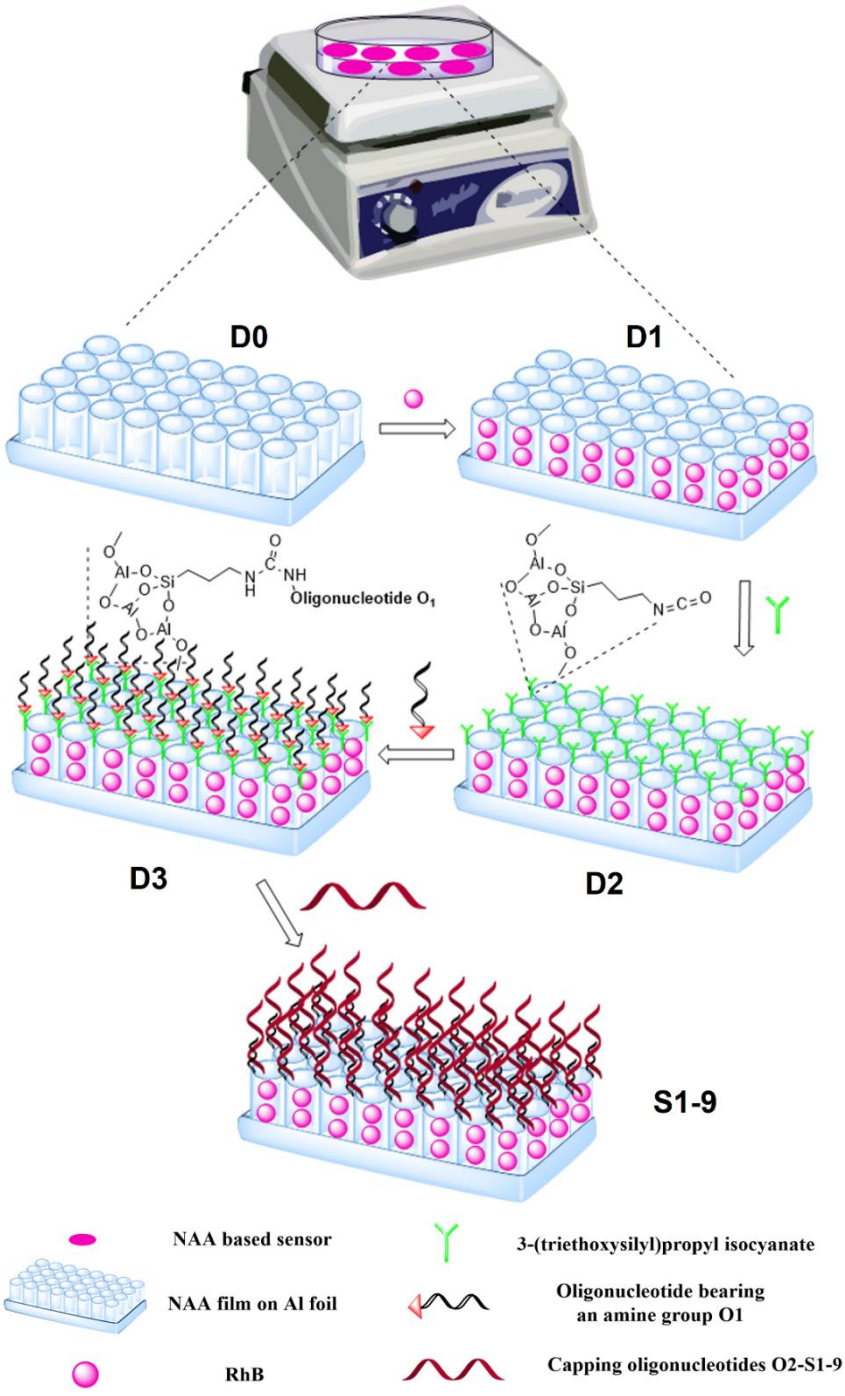

Figure 2. Scheme of the synthesis steps of fluorogenic sensors (**S1-9**) for HPV DNA detection based on oligonucleotide gated NAA films loaded with rhodamine B.

After dye loading, the external surface of the NAA support was functionalized with isocyanate groups to yield **D2** through the reaction between Al-OH groups at the external surface with 3-(triethoxysilyl)propyl isocyanate, resulting in the formation of Al-O-Si bonds (**Figure 2**). In this step, NAA disks were placed on the bottom surface of a closed flask ensuring that NAA films are side up oriented, allowing a better interaction between the alumina surface with the species dissolved in the liquid phase. Also, a gently mixing with an orbital stirrer ensures more homogenous conditions for surface functionalization allowing to obtain sensors in a reproducible manner. Humidity control is also important during these steps to avoid isocyanate hydrolysis and allow a controlled coupling between Al-OH groups at the external surface with 3-(triethoxysilyl)propyl isocyanate, also avoiding uncontrolled alkoxysilane hydrolysis and condensation to form a solid phase on the external surface of the sensors. To avoid humidity, it is important to use freshly prepared RhB solutions for the synthesis and washing steps and use a tightly closed reaction flask. The surface's functionalization with the alkoxysilane was evidenced by electron microscopy and EDXS analysis. Si, C and N atomic content increase after surface modification (**Figure 3, Table 2, Figure S1, Table S3**).

Isocyanate-modified NAA supports (**D2**) were functionalized with oligonucleotide **O1**, bearing and amine group, through urea linkages, to yield **D3**. The oligonucleotide base sequence in **O1** allows the further hybridization of the capping oligonucleotides (**O2-S1-9**) containing the DNA base sequence of different HPV types (*vide infra*) (**Table 1**). After the modification process, P, C, N and O atomic content increases confirming oligonucleotide coupling to the NAA surface (**Table 2**). Lower values of atomic contents were obtained when higher volume of more diluted solution of oligonucleotide **O1** (10 μM, 600 μL) were used in the functionalization process, indicating a lower surface coverage with the oligonucleotide (**Table S4**). We also found that water content in the reaction mixture produces the hydrolysis of isocyanate groups on NAA surface that avoids the covalent coupling of oligonucleotide **O1** on NAA surface.

Finally, NAA disks were coated with oligonucleotides **O2-S1-9** containing the DNA base sequence of 14 different HPV types (part of the L1 region of their genomes coding

the major capsid protein [9]) to yield sensors **S1-9**. These capping oligonucleotides contain in their extremes two sequences complementary to oligonucleotides **O1** (**Table 1**). Elimination of non-hybridized capping oligonucleotides **O2-S1-9** and RhB after the functionalization process, was confirmed by measuring absorbance and fluorescence intensity of supernatants after washing. Both, absorbance at 260 nm corresponding to oligonucleotides **O2-S1-9**, and fluorescence intensity at 585 nm (λ_{ex} = 555 nm) corresponding to RhB, decreased after washing (**Figure S2**). Following this protocol 9 sensors were obtained. All final NAA based sensors were also characterized by electron microscopy and EDXS analysis (**Figure 3, Table 3, Figure S1, Table S5-S13**). Oligonucleotides **O2-S1-9** have a tridimensional structure with nanometric dimensions and adopt a spatial arrangement on the alumina surface that blocked the pores and avoid the diffusion of the fluorophore from the porous structure of the material (*vide infra*). From a macroscopic point of view, oligonucleotide molecules form an organic layer on the inorganic porous support that can be seen in the electron microscopy images. Furthermore, P, C, N and O atomic content increases after surface coating. This inorganic/organic interphase act as a physical barrier that control the diffusion of fluorophore between the porous solid support and the liquid medium. The presence of target complementary oligonucleotides in the medium hybridize to the gating oligonucleotides inducing a displacement, unblocking of the pores and the release of the entrapped fluorophore (*vide infra*). Finally, surface morphology of alumina films during synthesis steps was also characterized by atomic force microscopy (**Figure S3**).

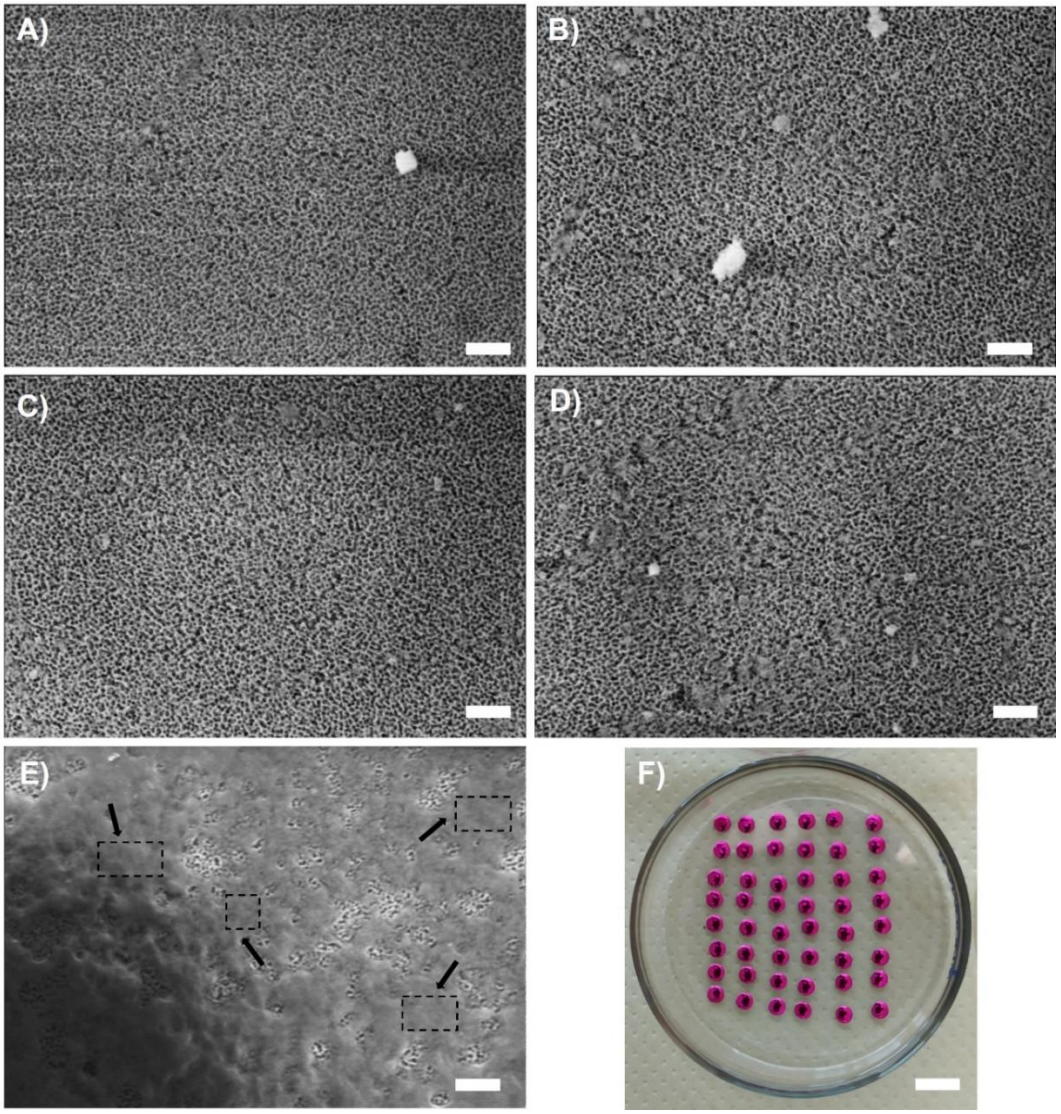

Figure 3. HR-FESEM images of NAA surfaces during synthesis steps (**D0** (A); **D1** (B); **D2** (C); **D3** (D) and final sensors **S1-9** (E), (scale bars: 200 nm) and photographs of the final NAA based sensors (F) (Scale bar: 1 cm). Black arrows indicate some surface areas of porous alumina films coated with a thin layer of gating oligonucleotides.

Table 2. Relative atomic compositions respect to Al atoms of **D0**, **D1**, **D2** and **D3** by EDXS analysis.

Element	D0	D1	D2	D3
C	0 .32 ± 0.01	0.49 ± 0.01	0.51 ± 0.02	0.59 ± 0.02
N	0	0.005 ± 0.002	0.042 ± 0.005	0.056 ± 0.006
O	2.31 ± 0.04	2.43 ± 0.03	2.29 ± 0.06	2.35 ± 0.06
Al	1.00 ± 0.02	1.00 ± 0.01	1.00 ± 0.03	1.00 ± 0.03
Si	0	0	0.037 ± 0.004	0.036 ± 0.004
P	0	0	0	0.006 ± 0.004

Table 3. Relative atomic compositions respect to Al atoms of the sensors **S1-9** by EDXS analysis.

Element	S1	S2	S3	S4	S5	S6	S7	S8	S9
C	0.49 ± 0.01	0.77 ± 0.02	0.83 ± 0.02	0.94 ± 0.02	0.78 ± 0.02	1.18 ± 0.03	0.62 ± 0.02	1.14 ± 0.03	1.06 ± 0.03
N	0.028 ± 0.003	0.117 ± 0.006	0.143 ± 0.006	0.165 ± 0.007	0.145 ± 0.007	0.246 ± 0.009	0.107 ± 0.007	0.210 ± 0.008	0.141 ± 0.007
O	2.46 ± 0.04	2.52 ± 0.05	2.61 ± 0.05	2.64 ± 0.05	2.29 ± 0.05	2.73 ± 0.06	2.19 ± 0.06	2.88 ± 0.06	2.71 ± 0.06
Al	1.00 ± 0.02	1.00 ± 0.02	1.00 ± 0.02	1.00 ± 0.02	1.00 ± 0.02	1.00 ± 0.02	1.00 ± 0.03	1.00 ± 0.02	1.00 ± 0.02
Si	0.015 ± 0.002	0.077 ± 0.004	0.043 ± 0.003	0.032 ± 0.003	0.064 ± 0.004	0.045 ± 0.003	0.018 ± 0.003	0.052 ± 0.004	0.030 ± 0.003
P	0.010 ± 0.002	0.016 ± 0.003	0.036 ± 0.003	0.041 ± 0.004	0.030 ± 0.004	0.062 ± 0.005	0.039 ± 0.005	0.053 ± 0.005	0.038 ± 0.004

After the synthesis and characterization of the 9 sensors, their capacity to selective release RhB in the presence of oligonucleotides complementary to those used for capping was evaluated. Thus, NAA-based sensors were incubated with the corresponding complementary oligonucleotides **O3-S1C-9C** (**Table 3**) in TRIS buffer and released rhodamine B was measured by fluorescence spectroscopy at 585 nm (λ_{ex} = 555 nm) using a plate reader. NAA sensors disks (**S1-9**) non incubated with oligonucleotides were used as negative controls. The release profiles of RhB from the sensors are shown in **Figure 4**. The RhB release profile is plotted as fluorescence intensity variations at different times respect to the initial intensity ($\mathbf{I_t-I_0}$). Results are represented as means and standard deviations of measurements for 3 different nanodevices incubated with Tris

(black squares) and other 3 nanodevices incubated with the corresponding complementary oligonucleotide (red circles). Data of individual nanodevices for all 9 developed sensors, are also shown in **Figure S4 (Supporting Information)**. A negligible release of RhB was produced from sensors used as negative controls even at longer times (60 minutes), confirming the gating capacity of the oligonucleotides on the NNA surface that block the pores and avoid dye diffusion. In contrast, a remarkable dye release was found from NAA disks incubated with corresponding complementary oligonucleotides **O3-S1C-9C**. The complementary oligonucleotides hybridize with the capping oligonucleotides **O2-S1-9** on NAA surface, unblocking the pores, and finally leading to diffusion of RhB (**Figure 1**). Moreover, the calibration curves of the 9 sensors for the detection of the corresponding complementary oligonucleotides **O3-S1C-9C** are shown in **Figure S5**. Limit of detection (**LOD** = 92-265 pM) and sensitivity (**$\Delta(I_{15}-I_0)/\Delta$(log c, M)** = 300-2400) derived from the calibration curves are summarized in **Table S14**. These results confirm the potential capacity of these materials for rapid and sensitive detection of oligonucleotides containing the DNA base sequences of 14 different types of HPV.

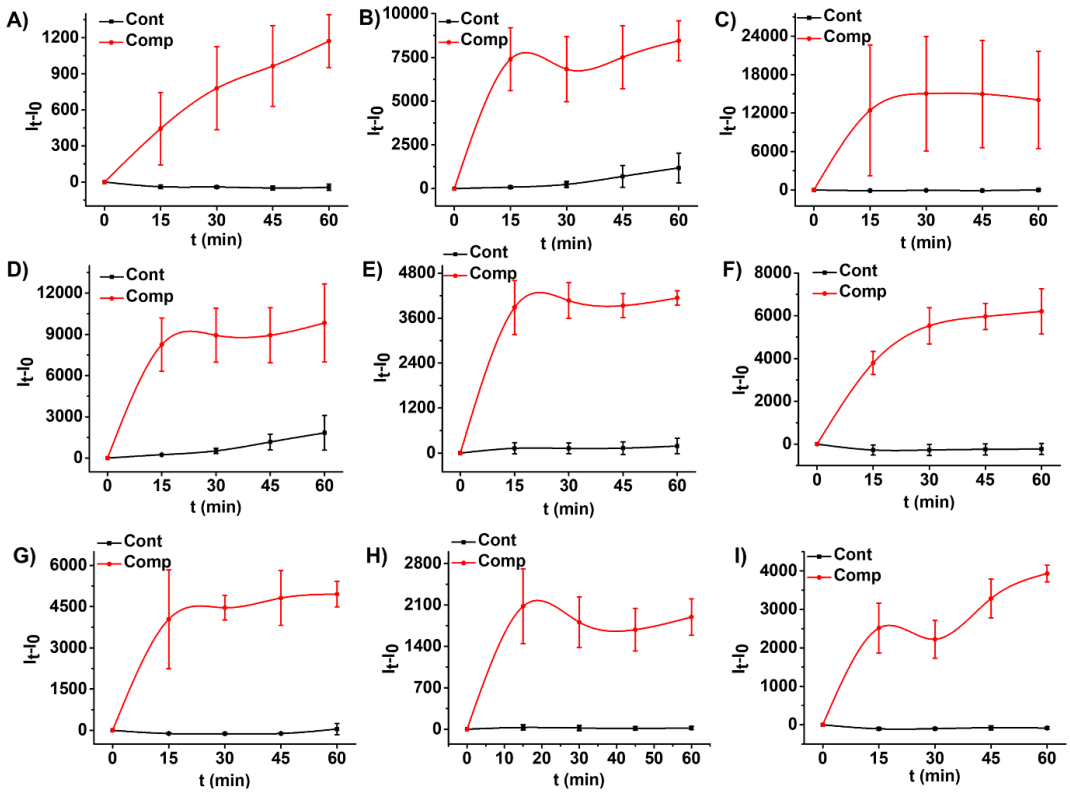

Figure 4. Rhodamine B release profiles from the 9 sensors (**S1** (A); **S2** (B); **S3** (C); **S4** (D); **S5** (E); **S6** (F); **S7** (G); **S8** (H) and **S9** (I)) incubated (Comp) or not (Cont) with the corresponding complementary oligonucleotides **O3-S1C-9C**.

The NAA-based sensor's surfaces after the displacement assays were also analysed by scanning electron microscopy and their atomic composition was determined by EDXS analysis. The results obtained for sensors **S1** are shown in **Figure 5** and **Table 4.** A surface morphology with more opened porous structure can be seen in the image of sensor incubated with the complementary oligonucleotide **O3-S1C**. Moreover, P, C, N and O atomic content is lower than that for the corresponding control sensor, supporting the above-mentioned transduction mechanism involving the displacement of the capping oligonucleotide **O2-S1** in the presence of the complementary **O3-S1C**.

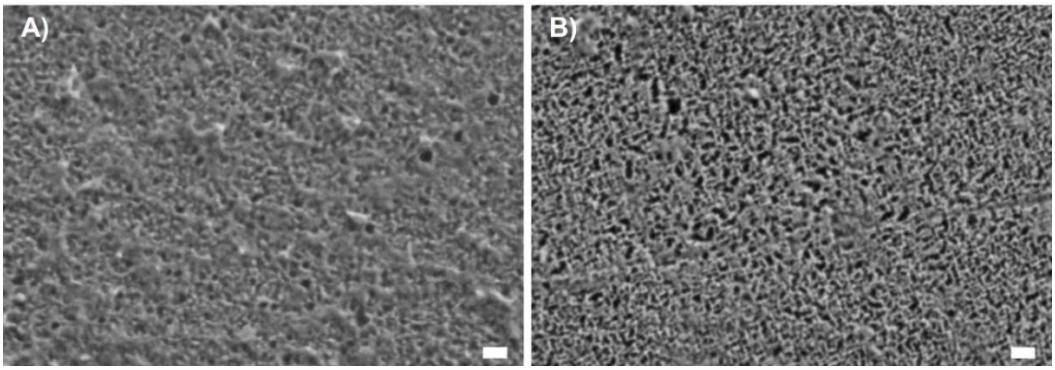

Figure 5. HR-FESEM images of NAA based sensor's surface (**S1**) after incubation with TRIS (A) and complementary oligonucleotides **O3-S1C** (B) (Scale bars: 100 nm).

Table 4. Corresponding atomic composition and atomic ratios respect to Al atoms of NAA surfaces after sensing assay for control (A) and sensor **S1** incubated with complementary oligonucleotides **O3-S1C** (B) by EDXS analysis.

A) Element	Wt%	Atomic%	X/Al
C	11.2 ± 0.2	17.2 ± 0.3	0.68 ± 0.02
N	1.6 ± 0.1	2.1 ± 0.2	0.082 ± 0.007
O	45.5 ± 0.1	52.4 ± 0.5	2.08 ± 0.04
Al	37.0 ± 0.1	25.2 ± 0.3	1.00 ± 0.02
Si	4.33 ± 0.05	2.85 ± 0.05	0.113 ± 0.003
P	0.44± 0.03	0.26 ± 0.02	0.0103 ± 0.0009

B) Element	Wt%	Atomic %	X/Al
C	8.9 ± 0.2	14.0 ± 0.3	0.51 ± 0.02
N	1.4 ± 0.1	1.9 ± 0.2	0.070 ± 0.007
O	45.5 ± 0.1	53.5 ± 0.5	1.95 ± 0.04
Al	39.4 ± 0.1	27.4 ± 0.3	1.00 ± 0.02
Si	4.36 ± 0.05	2.93 ± 0.05	0.107 ± 0.003
P	0.41 ± 0.03	0.25 ± 0.02	0.0091 ± 0.0008

In a further step, the validation of the nine sensors for the detection of 14 different hr-HPV types in 43 clinical samples of patients from Hospital Universitari i Politècnic La Fe, was carried out. Vaginal material was collected from cervical scrapes for both accurate cytological assessment and HPV testing. DNA testing of hr-HPV types was done using multiplex real-time PCR assays (Cobas 4800 HPV test and Seegene ANYPLEX II HPV28 detection kit) for detection and identification of 14 hr-HPV (types 16, 18, 31, 33, 35, 39, 45, 51, 52, 56, 58, 59, 66, and 68). Data of clinical samples were summarized in **Table 5** and **Table S15**. At the same time, detection of HPV in vaginal materials was also carried out using sensors **S1-9**.

Table 5. Data of clinical samples of patients from Hospital Universitari i Politècnic La Fe.

Patient ages (years)	**<30**	**30-39**	**40-49**	**>49**
	6	15	12	9
HPV type	**16**	**18**	**Others**	
	9	10	28	
Cytological Result*	**Negat**	**LSIL**	**HSIL**	**ASCUS**
	26	11	1	5

* Negat: Negative; LSIL: Low grade squamous intraepithelial lesion; HSIL: High grade squamous intraepithelial lesion; ASCUS: Atypical squamous cells of undetermined significance

All **S1-9** NAA sensors were incubated with the 43 vaginal samples collected in PreservCyt medium and released RhB was measured by fluorescence spectroscopy. Data of fluorescence intensity variations at 15 minutes respect to initial intensity ($\mathbf{I_{15}-I_0}$) for each sensor is plotted as scatter dispersion chart, and a box chart representing data distribution is also draw (**Figure 6**). For instance, the obtained results for sensor **S1** (able to detect HPV types 16, 18 and 59) are shown in **Figure 6A**. The signal of the **S1** sensors incubated with samples containing at least one of the 16, 18 and 59 HPV types (as determined by multiplex real-time PCR assays, *vide ante*) were plotted as red squares (labelled as positive, 19 samples). On the other hand, data for **S1** sensors incubated with samples that do not contain 16, 18 and 59 HPV types, were plotted as blue squares (labelled as negative, 24 samples). Note that more than one of those types, and even other types, are present in some of those samples. Signal threshold (horizontal straight line) to decide which samples are positives and negatives using the sensing assay with **S1**, was established at the signal mean plus ten times the standard deviation for 20 **S1** sensors (black squares) incubated with PreservCyt medium and labelled as control sensors. Following this decision criteria, for sensor **S1**, 19 samples were classified as positives (True positives: 19 and False positives: 0) for at least one of the HPV types 16, 18 or 59; whereas 24 samples were classified as negatives (True negatives: 24 and False negatives: 0) (**Table 6**). As it has been described previously the stepwise transduction mechanism in these gated porous support-based sensors implies two spatiotemporally separated events: a recognition step of the target analyte (pathogen´s DNA) by the gatekeeper on the external

surface, and the further signalling event involving the release of high amount of the reporter molecules (RhB) from pores. A signal amplification, instead of analyte amplification using PCR based assays, is an advantage of these gated sensors for highly sensitive DNA detection.[32, 36]

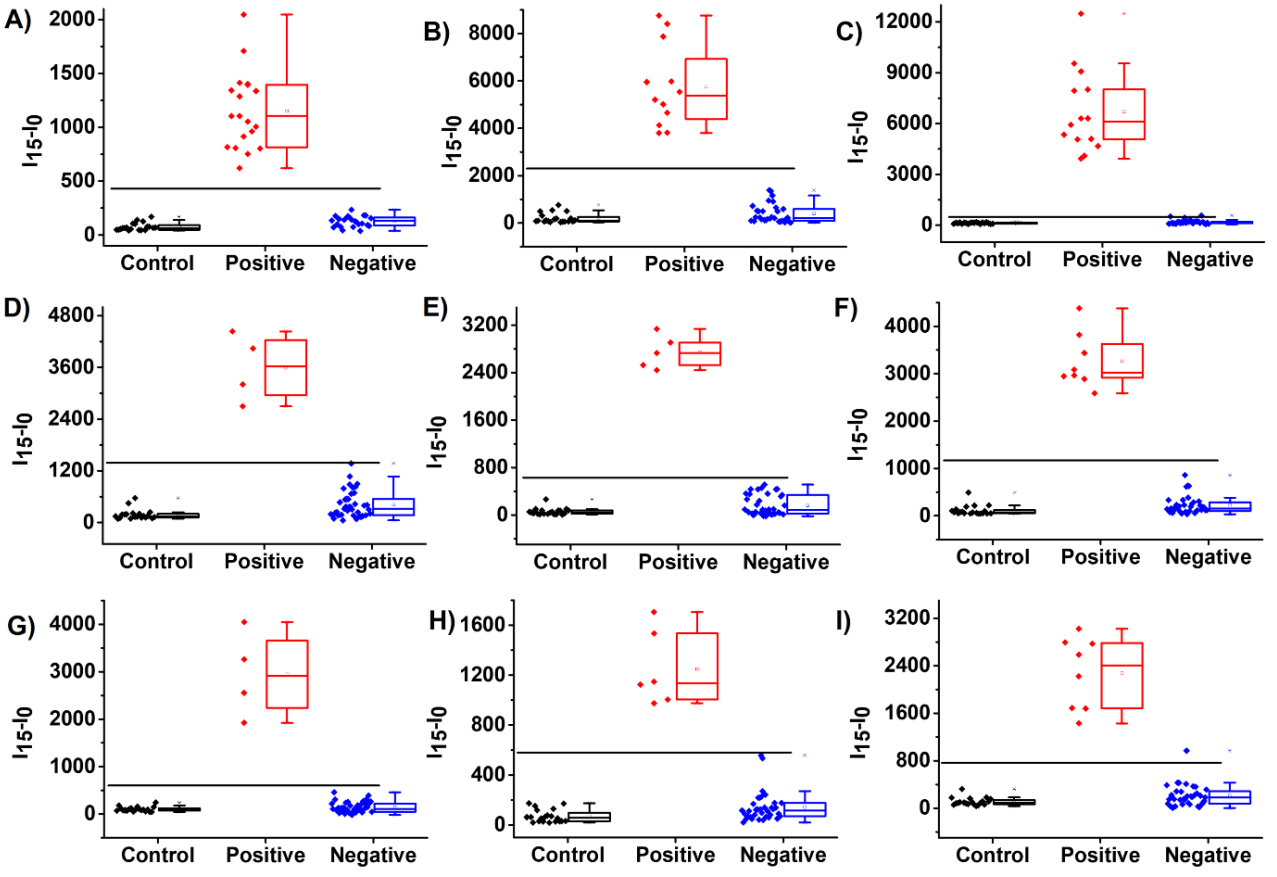

Figure 6. Detection of different hr-HPV types in 43 clinical samples using the 9 sensors developed (**S1** (A); **S2** (B); **S3** (C); **S4** (D); **S5** (E); **S6** (F); **S7** (G); **S8** (H) and **S9** (I)).

Table 6. Validation of the 9 sensors for detection of different hr-HPV types in 43 clinical samples.

Sensor	r-HPV type	Positive sample	Negative sample	True positive	True negative	False positive	False Negative	Sensitivity (%)	Specificity (%)	Positive predictive value (%)	Negative predictive value (%)
S1	**9, 16, 18**	9	24	19	24	0	0	100	100	100	100
S2	**45, 18**	2	31	12	31	0	0	100	100	100	100
S3	**31, 16**	4	29	14	27	2	0	100	93	88	100
S4	**51**	4	39	4	39	0	0	100	100	100	100
S5	**52**	5	38	5	38	0	0	100	100	100	100
S6	**33, 58**	8	35	8	35	0	0	100	100	100	100
S7	**35, 33**	4	39	4	39	0	0	100	100	100	100
S8	**56, 66**	6	37	6	37	0	0	100	100	100	100
S9	**68, 39**	8	35	8	34	1	0	100	97	89	100

Similar studies were also carried out with the remaining **S2-9** sensors and results are plotted in **Figure 6B-I** and in **Table 6**. Very high sensitivity, negative predictive values (100 %), specificities of 93-100 % and positive predictive values in the range 88-100%, were calculated. The lowest values were obtained for sensors **S3** and **S9** for detection of HPV types 16/31 and 39/68, respectively. This behaviour, regarding a relatively lower specificity and positive predictive values compared to sensitivity and negative predictive values, is very common in other standard DNA detection methods for HPV infection screening in clinical samples, due to their very low limit of detection and high sensitivity that generally shows an inverse relationship respect to specificity [20]. Moreover, the receiver-operating characteristic (ROC) analysis was carried out for validation of sensors **S1-9** to discriminate between negative and positive samples (**Figure S4**). An area under curve (AUC) of 1, sensitivity and specificity of 100 % were obtained for all sensors supporting the potential of these gated porous supports as diagnosis tool.

Sensors and sensing assays developed in this work allowed a rapid multiplexed analysis of clinical samples, enabling screening of infections caused by different hr-HPV types with high sensitivity and good specificity. More in detail, the analysis of the 43 samples evaluated with the **S1-9** sensors is summarized in **Table 7**. Samples were

classified as positive (**+**) and negative (-) for the different HPV types detected using the 9 sensors developed. False positive (o) samples were also labelled. As an example, the assays on sample 1 allow to determine that the sample does not contain hr-HPV types **16, 18, 31, 39, 45, 52, 56, 59, 66** and **68**, whereas it contain hr-HPV types **33, 35** and/or **58**, whereas analysis for instance on sample 20 determines that it contain hr-HPV types **39** and/or **68**. Comparing to other biosensors reported for HPV detection, the sensor design and detection protocol described in this work have some advantage regarding the high number of hr-HPV types that can be detected, as recently reported biosensors are designed to only detect hr-HPV types **16** and **18** [22,23,25,28]. Besides, our work demonstrates that a fast and accurate detection of 14 different hr-HPV types in clinical samples can be achieved, whereas for other biosensors previously described HPV detection in clinical samples is usually not reported [24,26,27,29]. The sensing assays reported in this work allow to carry out a multiplexed analysis of clinical samples using an integrated platform for analyte recognition, transduction, and signal reading, allowing faster screening of samples which can be carried out by non-specialized personnel.

Table 7. Multiplexed analysis of 43 clinical samples for screening infections caused by 14 different hr-HPV types using the 9 NAA based sensors developed.

Sample	hr-HPV type*	S1** (59, 16, 18)	S2 (45, 18)	S3 (31, 16)	S4 (51)	S5 (52)	S6 (33, 58)	S7 (35, 33)	S8 (56, 66)	S9 (68, 39)
1	**33**	-	-	-	-	-	+	+	-	-
2	**33**	-	-	-	-	-	+	+	-	-
3	**33**	-	-	-	-	-	+	+	-	o
4	**35, 52**	-	-	-	-	+	-	+	-	-
5	**39**	-	-	-	-	-	-	-	-	+
6	**39, 51**	-	-	-	+	-	-	-	-	+
7	**45**	-	+	-	-	-	-	-	-	-
8	**45, 58**	-	+	-	-	-	+	-	-	-
9	**51**	-	-	-	+	-	-	-	-	-
10	**51, 58**	-	-	-	+	-	+	-	-	-
11	**51, 58**	-	-	-	+	-	+	-	-	-
12	**52**	-	-	-	-	+	-	-	-	-
13	**52, 68**	-	-	-	-	+	-	-	-	+
14	**52, 68**	-	-	-	-	+	-	-	-	+
15	**56**	-	-	-	-	-	-	-	+	-
16	**58**	-	-	-	-	-	+	-	-	-
17	**58**	-	-	-	-	-	+	-	-	-

18	**59**	+	-	-	-	-	-	-	-	-
19	**66**	-	-	o	-	-	-	-	+	-
20	**68**	-	-	-	-	-	-	-	-	+
21	**16**	+	-	+	-	-	-	-	-	-
22	**16**	+	-	+	-	-	-	-	-	-
23	**16**	+	-	+	-	-	-	-	-	-
24	**16**	+	-	+	-	-	-	-	-	-
25	**16**	+	-	+	-	-	-	-	-	-
26	**16, 31, 56**	+	-	+	-	-	-	-	+	-
27	**16, 39**	+	-	+	-	-	-	-	-	+
28	**16, 39, 52, 66**	+	-	+	-	+	-	-	+	+
29	**16, 18**	+	+	+	-	-	-	-	-	-
30	**18**	+	+	-	-	-	-	-	-	-
31	**18**	+	+	-	-	-	-	-	-	-
32	**18**	+	+	-	-	-	-	-	-	-
33	**18**	+	+	-	-	-	-	-	-	-
34	**18**	+	+	-	-	-	-	-	-	-
35	**18**	+	+	o	-	-	-	-	-	-
36	**18**	+	+	-	-	-	-	-	-	-
37	**18**	+	+	-	-	-	-	-	-	-
38	**18**	+	+	-	-	-	-	-	-	-
39	**31**	-	-	+	-	-	-	-	-	-
40	**31**	-	-	+	-	-	-	-	-	-
41	**31**	-	-	+	-	-	-	-	-	-
42	**31, 66, 68**	-	-	+	-	-	-	-	+	+
43	**31, 56**	-	-	+	-	-	-	-	+	-

* HPV types detected using multiplex real-time PCR assays (Cobas 4800 HPV test and Seegene ANYPLEX II HPV28 detection kit)

** HPV types detected using the 9 sensors developed: positive (+); negative (-); false positive (o)

4. Conclusions

Nine sensors based on oligonucleotide gated NAA films loaded with RhB as fluorogenic reporter, are developed for the rapid and sensitive detection of 14 different types of HPV. The preparation protocol is optimized to scale up the production of sensors in a reproducible manner. Key experimental tips are related to using a gently stirring with an orbital stirrer and controlling the humidity during the external surface modification of the nanoporous materials. Sensors are characterized by scanning electron microscopy and the atomic composition of the surfaces was determined after each functionalization step by EDXS. The increase of atomic ratio between C, O, N, Si and P respect to Al confirm the modification of NAA surface with the alkoxysilane, the oligonucleotide **O1** and the

different capping oligonucleotides **O2-S1-9**. The capacity of the sensors for selectively detect the oligonucleotides **O3-S1C-9C** complementary to capping oligonucleotides **O2-S1-9** is confirmed by fluorescence measurements. Only, when the complementary oligonucleotides **O3-S1C-9C** is present in the medium a remarkable RhB release from nanoporous materials is observed. Finally, the sensors are used for the sensitive detection of 14 different types of HPV in 43 clinical samples. High sensitivity and negative predictive values (100 % for both) are observed for all sensors. Also, high specificity and positive predictive values are found.

5. Materials and methods

5.1. Materials

Nanoporous anodic alumina films on Al foils (25 x 75 mm) were purchased from InRedox (Alumina thickness: 10 ± 0.2 μm; pore diameter: 5 ± 2 nm, pore density: $9 \cdot 10^{11}$ cm^{-2}, porosity: 15 ± 2 %). Oligonucleotides were purchased from Integrated DNA Technologies (IDT). Sequences of the 19 oligonucleotides used for sensor synthesis and sensing assay were listed in **Table 1**. Rhodamine B, 3-(triethoxysilyl)propyl isocyanate, triethylamine (TEA), acetonitrile (anhydrous), tris(hydroxymethyl)aminomethane (TRIS), magnesium chloride (anhydrous) and hydrochloric acid were purchased from Sigma Aldrich.

5.2. Characterization techniques

High Resolution Field Emission Scanning Electron Microscopy (HR-FESEM): NAA sensors were placed onto Al disks using carbon cement. Images were acquired using a HR-Field Emission Scanning electron microscope (ZEISS GeminiSEM 500) operating at 5 kV. Atomic composition of analysed surfaces was determined by Energy Dispersive X-ray Spectroscopy (EDXS) using an X-ray detector coupled to microscope. Fluorescence measurements were acquired using a Synergy H1 microplate reader (BioTek, Winooski, VT, USA). Absorption spectra were recorded using a JASCO V-650 UV/vis spectrophotometer.

5.3. Synthesis protocol

NAA films on Al disks (diameter: 2 mm, 24 disks) were soaked in RhB solution in acetonitrile (1.5 mM, 10 mL) at 25 °C during 18 h using an orbital stirrer at 50 rpm. 3-(triethoxysilyl)propyl isocyanate (1 mL) was added dropwise, and the mixture was stirred during 6 h. NAA disks were washed with RhB in acetonitrile (1.5 mM) and dried with paper. NAA disks (48 disks) were soaked in RhB solution in acetonitrile (1.5 mM, 5 mL), then aqueous solution of oligonucleotide **O1** (**Table 1**) bearing an amine group (100 µM, 60 µL) and triethylamine (24 µL) were added subsequently. The mixture was stirred at 25 °C during 3 h using and orbital stirrer at 50 rpm. NAA disks were washed with RhB in acetonitrile (1.5 mM) and dried with paper. Finally, NAA disks (48 disks) were soaked in TRIS buffer (20 mM, $MgCl_2$ 37.5 mM, 5 mL) and then, aqueous solution of capping oligonucleotides **O2-S1-9** (100 µM, 240 µL) was added. The mixture was stirred at 25 °C during 2 h using an orbital stirrer at 50 rpm. NAA disks were washed three times with TRIS buffer and dried with paper. Aliquots of supernatants after capping and washing steps were collected for absorbance and fluorescence measurements.

5.4. Sensing assay

NAA based sensors were soaked in TRIS buffer (1 mL per sensor), then aliquots (200 µL) were taken and added to 96 well plate for initial fluorescence measurements (excitation wavelength (λ_{ex}) = 555 nm, emission wavelength (λ_{em}) = 585 nm) using a plate reader. From the 200 µL, 100 µL was discarded and then, 100 µL of water or aqueous solution of uncapping oligonucleotides **O3-S1C-9C** (1 µM, 100 µL) complementary with capping oligonucleotides **O2-S1-9** used for surface modification of NAA films (**Table 1**), was added. Mixtures were shaken at 25 °C using a thermoshaker at 700 rpm. At schedule times (15, 30, 45 and 60 minutes) aliquots (200 µL) were taken for fluorescence measurements in the same wells than previous ones and mixed again with sensors after measurements. The assay was carried out in triplicate for the 9 different sensors.

5.5. Sample collection and HPV detection using reference methods

Vaginal material was collected from cervical scrapes by clinician ensuring adequate specimen collection (sufficient ectocervical and/or endocervical cells in the cervical transformation zone) for both accurate cytological assessment and HPV testing (**Table 5**). Samples were storage in liquid media using PreservCyt solution from Hologic (Thin Prep 5000).

DNA testing of hr-HPV types was done using multiplex real-time PCR assays (Cobas 4800 HPV test and Seegene ANYPLEX II HPV28 detection kit) for simultaneous detection and identification of 14 hr-HPV (types 16, 18, 31, 33, 35, 39, 45, 51, 52, 56, 58, 59, 66, and 68) allowing to semiquantify the viral load, from low (+; positive within 13 to 17 PCR cycles), to intermediate (++; positive within 8 to 12 cycles), to high (+++; positive within 1 to 7 cycles). (**Table S14**)

5.6. Validation of sensors in clinical samples

Clinical samples (43) of patients from Hospital Universitari i Politècnic La Fe, were collected in PreservCyt medium containing 14 different types of hr-HPV. The validation assay was like above-described sensing assay. Control sensors (20) were soaked in TRIS buffer and after initial fluorescence measurements, 100 µL of PreservCyt medium was added. At the same time 43 sensors were soaked in TRIS buffer and after initial fluorescence measurements, 100 µL of each sample was added. Mixtures were shaken at 25 ^{o}C using a thermoshaker at 700 rpm. Aliquots (200 µL) were taken at 15 minutes for fluorescence measurements in the same wells than initial one. The assay was carried out for validation of the 9 different sensors.

5.7. Ethical committee

Informed written consent was obtained from all subjects included in this work, and the study was approved by the Medicaments Research Ethics Committee – CEIm of Hospital Universitari i Politècnic La Fe (2018/0187).

5.8. Statistical analysis

Statistical analysis was carried out using Origin 9 and GraphPad Prism 8 softwares. Results were considered statistically significant when P-value was <0.05.

6. Supporting Information

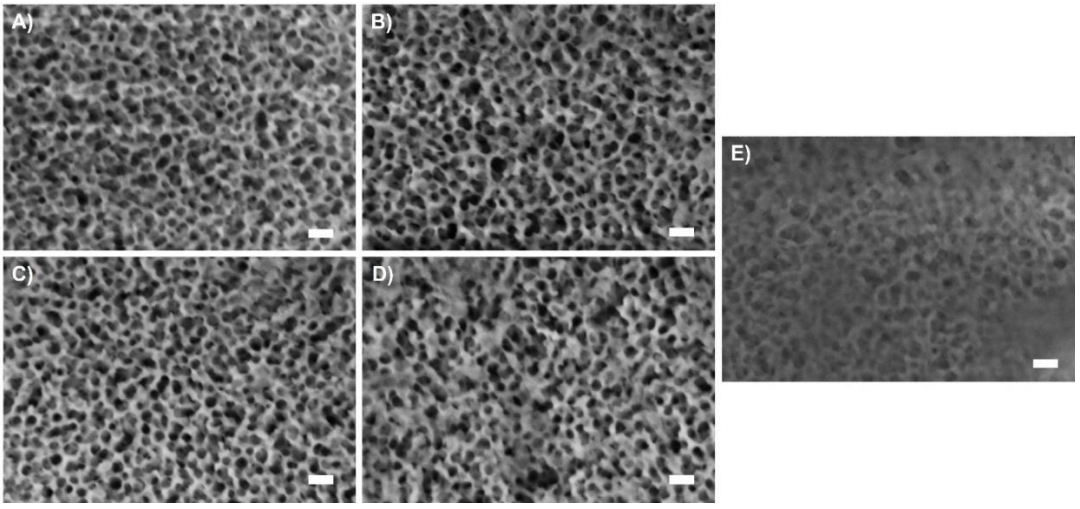

Figure S1. HR-FESEM images of NAA surfaces during synthesis steps (**D0** (A); **D1** (B); **D2** (C); **D3** (D) and final sensors (E)). Scale bars: 40 nm.

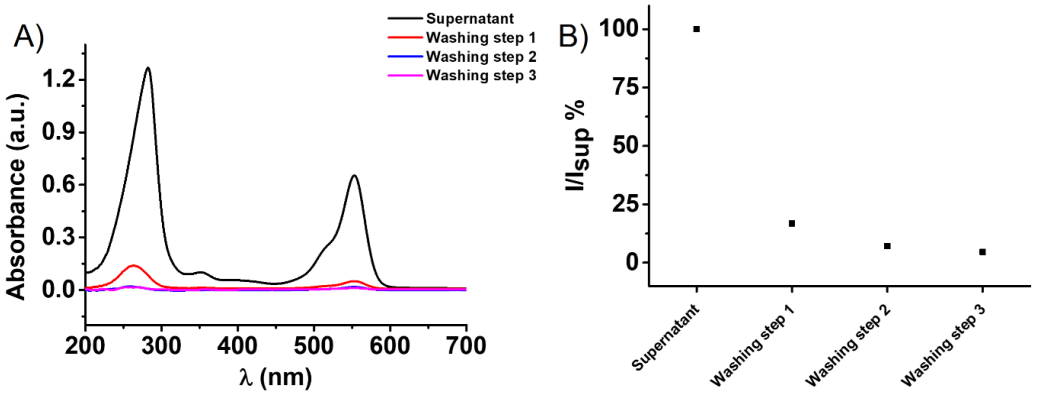

Figure S2. Absorption spectra (A) of supernatants after capping and washing steps and relative fluorescence intensity at 585 nm (λ_{ex} = 555 nm) of supernatants after washing steps respect to fluorescence intensity of supernatant after capping process (B).

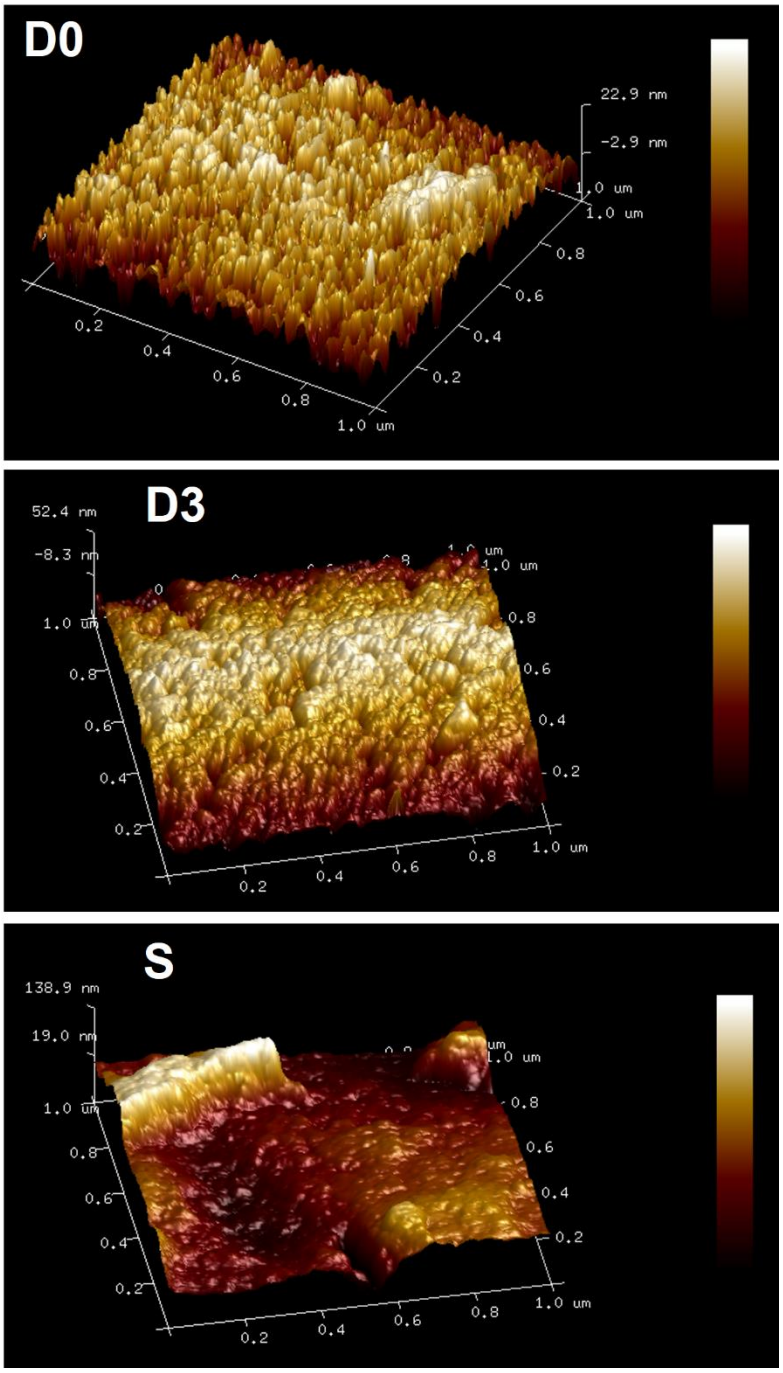

Figure S3. AFM images of NAA surfaces during synthesis steps (**D0**, **D3** and final sensors (**S**)).

Table S1. Atomic composition and atomic ratios respect to Al atoms of NAA surface (**D0**) by EDXS analysis.

Element	Wt%	Atomic %	X/Al
C	5.6 ± 0.1	8.7 ± 0.2	0.32 ± 0.01
N	0	0	0
O	54.5 ± 0.2	63.6 ± 0.5	2.31 ± 0.04
Al	39.9 ± 0.2	27.6 ± 0.3	1.00 ± 0.02
Si	0.08 ± 0.08	0.05 ± 0.05	0.002 ± 0.002
P	0	0	0

Table S2. Atomic composition and atomic ratios respect to Al atoms of NAA surface (**D1**) by EDXS analysis.

Element	Wt%	Atomic %	X/Al
C	8.15 ± 0.09	12.4 ± 0.2	0.49 ± 0.01
N	0.09 ± 0.04	0.12 ± 0.05	0.005 ± 0.002
O	54.2 ± 0.1	62.0 ± 0.4	2.43 ± 0.03
Al	37.6 ± 0.1	25.5 ± 0.2	1.00 ± 0.01
Si	0	0	0
P	0	0	0

Table S3. Atomic composition and atomic ratios respect to Al atoms of NAA surface (**D2**) by EDXS analysis.

Element	Wt%	Atomic %	X/Al
C	8.6 ± 0.2	13.2 ± 0.3	0.51 ± 0.02
N	0.82 ± 0.08	1.1 ± 0.1	0.042 ± 0.005
O	51.3 ± 0.2	59.0 ± 0.7	2.29 ± 0.06
Al	37.8 ± 0.2	25.8 ± 0.3	1.00 ± 0.03
Si	1.4 ± 0.1	0.94 ± 0.08	0.037 ± 0.004
P	0	0	0

Tables S4. Atomic composition and atomic ratios respect to Al atoms of NAA surface (**D3**) by EDXS analysis.

O1 (100 μM, 60 μL)

Element	Wt%	Atomic %	X/Al
C	9.6 ± 0.2	14.5 ± 0.4	0.59 ± 0.02
N	1.07 ± 0.08	1.4 ± 0.1	0.056 ± 0.006
O	51.1 ± 0.2	58.2 ± 0.8	2.35 ± 0.06
Al	36.7 ± 0.2	24.8 ± 0.4	1.00 ± 0.03
Si	1.4 ± 0.1	0.89 ± 0.08	0.036 ± 0.004
P	0.2 ± 0.1	0.14 ± 0.09	0.006 ± 0.004

O1 (10 μM, 600 μL)

Element	Wt%	Atomic %	X/Al
C	7.9 ± 0.1	12.2 ± 0.2	0.48 ± 0.01
N	0.67 ± 0.05	0.88 ± 0.07	0.034 ± 0.003
O	52.5 ± 0.2	60.4 ± 0.5	2.36 ± 0.04
Al	37.5 ± 0.1	25.6 ± 0.2	1.00 ± 0.02
Si	1.23 ± 0.07	0.80 ± 0.05	0.031 ± 0.002
P	0.16 ± 0.09	0.09 ± 0.05	0.004 ± 0.002

Table S5. Atomic composition and atomic ratios respect to Al atoms of NAA based sensor (**S1**) by EDXS analysis.

Element	Wt%	Atomic %	X/Al
C	8.0 ± 0.1	12.2 ± 0.2	0.49 ± 0.01
N	0.54 ± 0.05	0.71 ± 0.07	0.028 ± 0.003
O	53.6 ± 0.1	61.5 ± 0.5	2.46 ± 0.04
Al	36.8 ± 0.1	25.0 ± 0.2	1.00 ± 0.02
Si	0.59 ± 0.06	0.38 ± 0.04	0.015 ± 0.002
P	0.43 ± 0.09	0.26 ± 0.06	0.010 ± 0.002

Table S6. Atomic composition and atomic ratios respect to Al atoms of NAA based sensor (**S2**) by EDXS analysis.

Element	Wt%	Atomic %	X/Al
C	11.4 ± 0.1	17.0 ± 0.3	0.77 ± 0.02
N	2.03 ± 0.06	2.61 ± 0.09	0.117 ± 0.006
O	49.9 ± 0.2	56.1 ± 0.6	2.52 ± 0.05
Al	33.4 ± 0.2	22.2 ± 0.2	1.00 ± 0.02
Si	2.7 ± 0.1	1.72 ± 0.08	0.077 ± 0.004
P	0.6 ± 0.1	0.36 ± 0.07	0.016 ± 0.003

Table S7. Atomic composition and atomic ratios respect to Al atoms of NAA based sensor (**S3**) by EDXS analysis.

Element	Wt%	Atomic %	X/Al
C	12.0 ± 0.1	17.8 ± 0.3	0.83 ± 0.02
N	2.40 ± 0.06	3.06 ± 0.09	0.143 ± 0.006
O	50.3 ± 0.1	56.0 ± 0.5	2.61 ± 0.05
Al	32.5 ± 0.1	21.4 ± 0.2	1.00 ± 0.02
Si	1.46 ± 0.08	0.92 ± 0.06	0.043 ± 0.003
P	1.4 ± 0.1	0.78 ± 0.06	0.036 ± 0.003

Table S8. Atomic composition and atomic ratios respect to Al atoms of NAA based sensor (**S4**) by EDXS analysis.

Element	Wt%	Atomic %	X/Al
C	13.3 ± 0.1	19.5 ± 0.3	0.94 ± 0.02
N	2.71 ± 0.07	3.4 ± 0.1	0.165 ± 0.007
O	49.7 ± 0.2	54.8 ± 0.5	2.64 ± 0.05
Al	31.8 ± 0.1	20.8 ± 0.2	1.00 ± 0.02
Si	1.05 ± 0.07	0.66 ± 0.05	0.032 ± 0.003
P	1.5 ± 0.1	0.85 ± 0.07	0.041 ± 0.004

Table S9. Atomic composition and atomic ratios respect to Al atoms of NAA based sensor (**S5**) by EDXS analysis.

Element	Wt%	Atomic %	X/Al
C	12.0 ± 0.1	18.1 ± 0.3	0.78 ± 0.02
N	2.60 ± 0.07	3.4 ± 0.1	0.145 ± 0.007
O	47.1 ± 0.2	53.2 ± 0.6	2.29 ± 0.05
Al	34.7 ± 0.2	23.2 ± 0.3	1.00 ± 0.02
Si	2.3 ± 0.1	1.49 ± 0.07	0.064 ± 0.004
P	1.2 ± 0.1	0.69 ± 0.08	0.030 ± 0.004

Table S10. Atomic composition and atomic ratios respect to Al atoms of NAA based sensor (**S6**) by EDXS analysis.

Element	Wt%	Atomic %	X/Al
C	15.5 ± 0.1	22.4 ± 0.3	1.18 ± 0.03
N	3.77 ± 0.07	4.7 ± 0.1	0.246 ± 0.009
O	47.8 ± 0.2	51.9 ± 0.5	2.73 ± 0.06
Al	29.5 ± 0.1	19.0 ± 0.2	1.00 ± 0.02
Si	1.40 ± 0.08	0.86 ± 0.05	0.045 ± 0.003
P	2.1 ± 0.1	1.17 ± 0.07	0.062 ± 0.005

Table S11. Atomic composition and atomic ratios respect to Al atoms of NAA based sensor (**S7**) by EDXS analysis.

Element	Wt%	Atomic %	X/Al
C	10.2 ± 0.2	15.5 ± 0.4	0.62 ± 0.02
N	2.05 ± 0.09	2.7 ± 0.1	0.107 ± 0.007
O	48.3 ± 0.2	55.2 ± 0.7	2.19 ± 0.06
Al	37.1 ± 0.2	25.2 ± 0.3	1.00 ± 0.03
Si	0.70 ± 0.08	0.46 ± 0.06	0.018 ± 0.003
P	1.7 ± 0.1	0.98 ± 0.07	0.039 ± 0.005

Table S12. Atomic composition and atomic ratios respect to Al atoms of NAA based sensor (**S8**) by EDXS analysis.

Element	Wt%	Atomic %	X/Al
C	14.7 ± 0.1	21.4 ± 0.3	1.14 ± 0.03
N	3.17 ± 0.07	3.9 ± 0.1	0.210 ± 0.008
O	49.7 ± 0.2	54.0 ± 0.5	2.88 ± 0.06
Al	29.1 ± 0.1	18.8 ± 0.2	1.00 ± 0.02
Si	1.57 ± 0.08	0.97 ± 0.06	0.052 ± 0.004
P	1.8 ± 0.1	0.99 ± 0.07	0.053 ± 0.005

Table S13. Atomic composition and atomic ratios respect to Al atoms of NAA based sensor (**S9**) by EDXS analysis.

Element	Wt%	Atomic %	X/Al
C	14.7 ± 0.1	21.4 ± 0.3	1.06 ± 0.03
N	2.27 ± 0.07	2.8 ± 0.1	0.141 ± 0.007
O	49.8 ± 0.2	54.4 ± 0.4	2.71 ± 0.06
Al	31.0 ± 0.1	20.1 ± 0.2	1.00 ± 0.02
Si	0.97 ± 0.08	0.60 ± 0.05	0.030 ± 0.003
P	1.4 ± 0.1	0.77 ± 0.07	0.038 ± 0.004

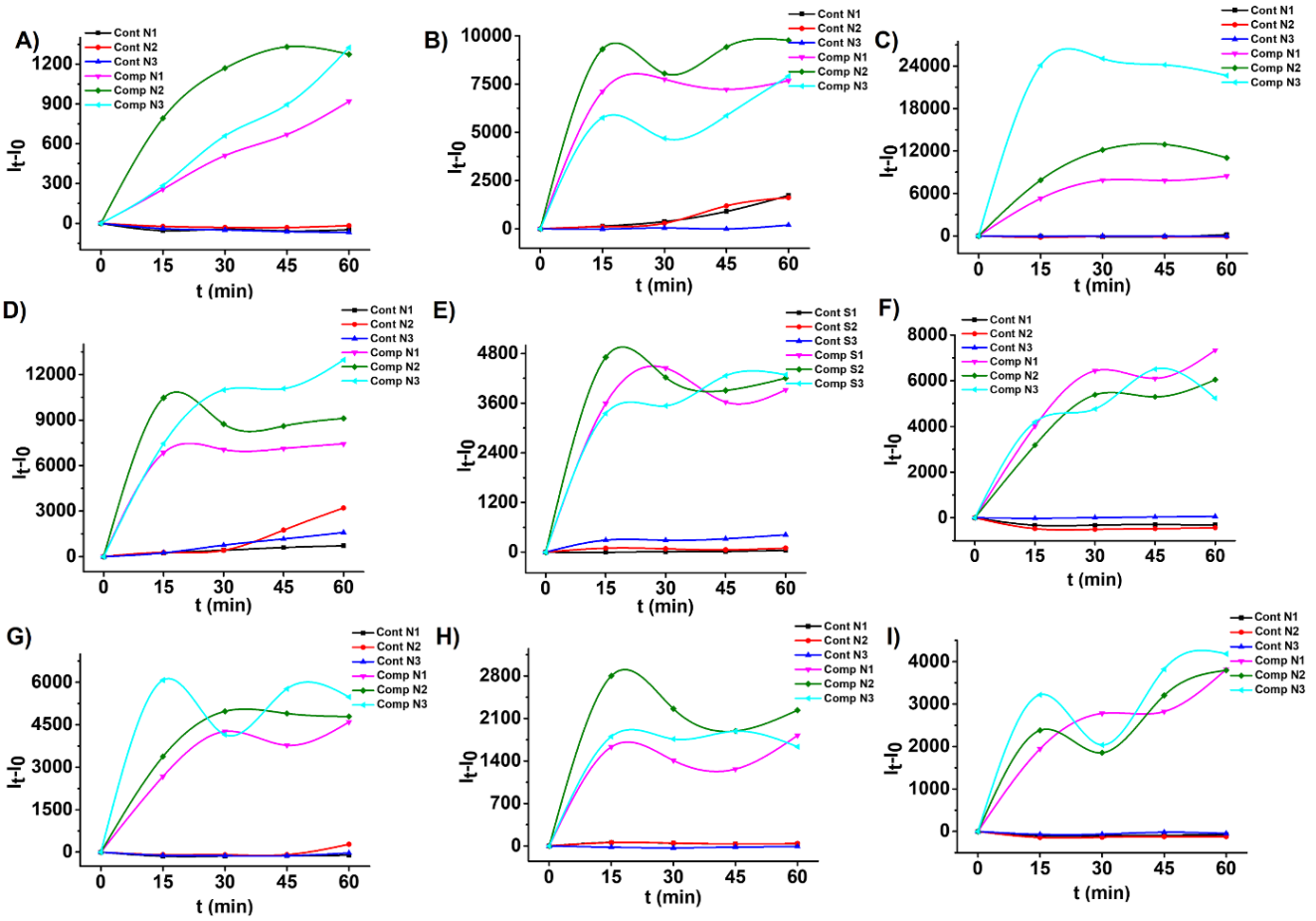

Figure S4. Rhodamine B release profiles from the 9 sensors (**S1** (A); **S2** (B); **S3** (C); **S4** (D); **S5** (E); **S6** (F); **S7** (G); **S8** (H) and **S9** (I)) incubated with the corresponding complementary oligonucleotides **O3-S1C-9C**. Profiles are plotted as fluorescence intensity variations respect to initial intensity ($\mathbf{I_t-I_0}$). Data are represented for 3 individual nanodevices.

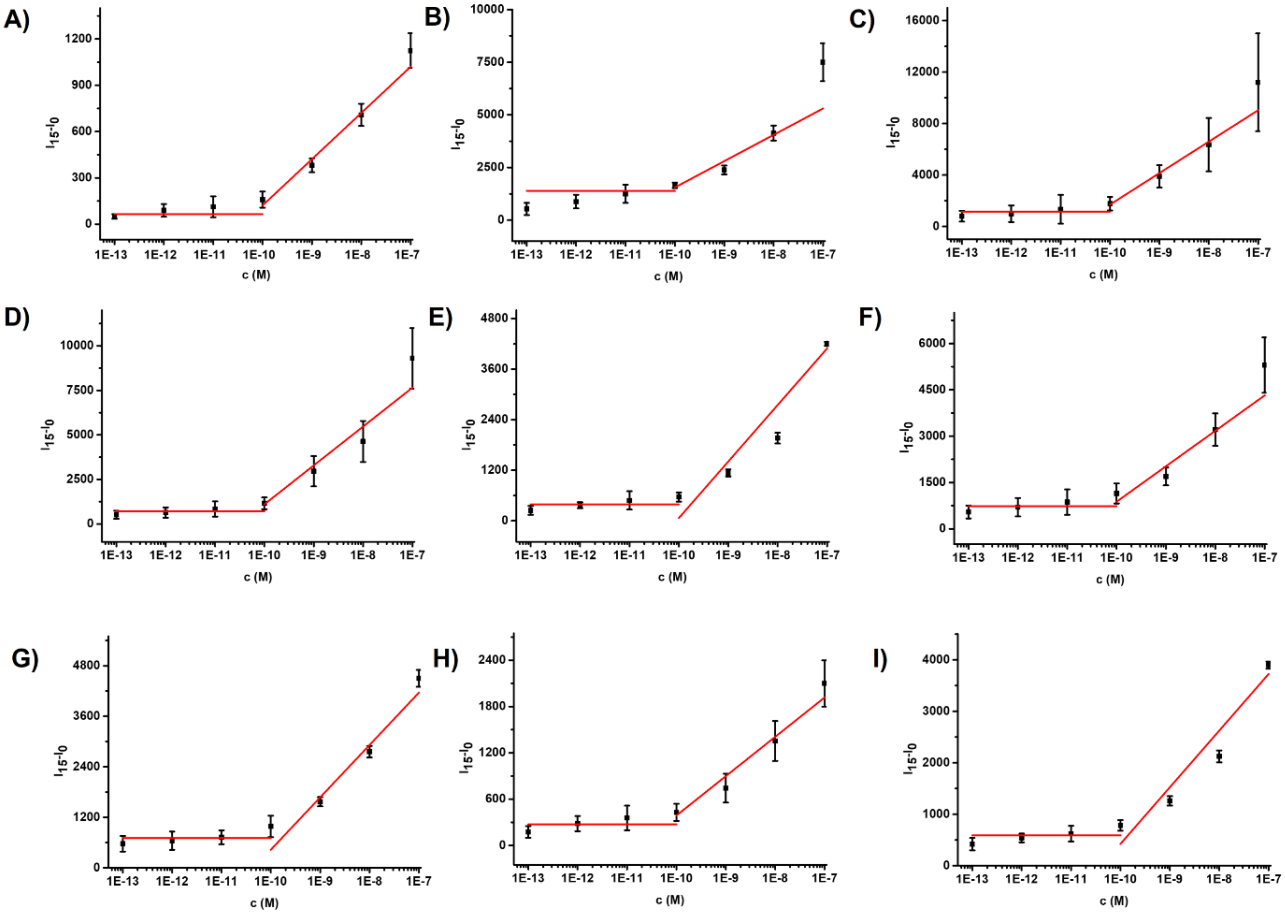

Figure S5. Calibration curves of the 9 sensors (**S1** (A); **S2** (B); **S3** (C); **S4** (D); **S5** (E); **S6** (F); **S7** (G); **S8** (H) and **S9** (I)) for detection of the corresponding complementary oligonucleotides **O3-S1C-9C** at different concentrations. Data are represented as means and standard deviations of measurements for 3 different nanodevices. The limit of detection (LOD) was calculated from the intercept of the horizontal line plus three times the standard deviation. The sensitivity was calculated from the slope of the straight line obtained from the linear fit of data.

Table S14. Limit of detection (LOD) and sensitivity of 9 sensors for detection of complementary oligonucleotides.

Sensor	hr-HPV type	LOD (M)	Sensitivity Δ(I15-I0)/Δ(log c, M)
S1	**59, 16, 18**	$1.02 \cdot 10^{-10}$	300
S2	**45, 18**	$2.23 \cdot 10^{-10}$	1300
S3	**31, 16**	$9.82 \cdot 10^{-11}$	2400
S4	**51**	$9.17 \cdot 10^{-11}$	2200
S5	**52**	$2.41 \cdot 10^{-10}$	1300
S6	**33, 58**	$1.38 \cdot 10^{-10}$	1100
S7	**35, 33**	$2.65 \cdot 10^{-10}$	1200
S8	**56, 66**	$1.43 \cdot 10^{-10}$	510
S9	**68, 39**	$2.34 \cdot 10^{-10}$	1100

LOD and sensitivity were derived from calibration curves in Figure S5.

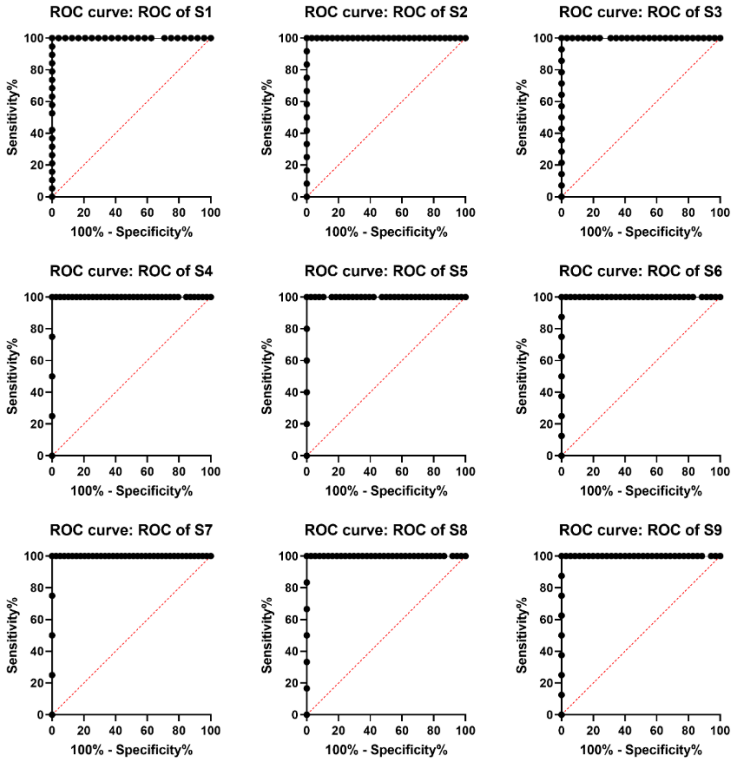

Figure S6. The receiver-operating characteristic (ROC) curves for validation of sensors **S1-9** for detection of 14 different hr-HPV types in 43 clinical samples.

Table S15. Cytological assessment and DNA testing of hr-HPV types in clinical samples using a multiplex real-time PCR assay: Seegene ANYPLEX II HPV28.

Sample	hr-HPV type	Ct (ANYPLEX) *	Cytological results **
1	**33**	++	NEGAT.
2	**33**	++	LSIL
3	**33**	+++	NEGAT.
4	**35, 52**	35 + / 52 +++	NEGAT.
5	**39**	+++	NEGAT.
6	**39, 51**	39 +++ / 51 +	LSIL
7	**45**	++	NEGAT.
8	**45, 58**	45 ++ / 58 ++	NEGAT.
9	**51**	+	NEGAT.
10	**51, 58**	51 ++ / 58 ++	NEGAT.
11	**51, 58**	51 + / 58 +	NEGAT.
12	**52**	++	NEGAT.
13	**52, 68**	52 + / 68 +	NEGAT.
14	**52, 68**	52 ++ / 68 +	NEGAT.
15	**56**	+++	LSIL
16	**58**	++	NEGAT.
17	**58**	++	ASCUS
18	**59**	++	LSIL
19	**66**	+++	LSIL
20	**68**	++	NEGAT.
21	**16**	++	NEGAT.
22	**16**	NA	NEGAT.
23	**16**	NA	HSIL
24	**16**	NA	NEGAT.
25	**16**	NA	NEGAT.
26	**16, 31, 56**	16 ++ / 31 ++ / 56 ++	LSIL
27	**16, 39**	16 ++ / 39 +++	LSIL
28	**16, 39, 52, 66**	16 ++ / 39 + / 52 ++ / 66+	ASCUS
29	**16, 18**	NA	NEGAT.
30	**18**	NA	NEGAT.

31	**18**	NA	LSIL
32	**18**	NA	LSIL
33	**18**	NA	NEGAT.
34	**18**	NA	NEGAT.
35	**18**	NA	NEGAT.
36	**18**	NA	NEGAT.
37	**18**	NA	LSIL
38	**18**	NA	NEGAT.
39	**31**	++	ASCUS
40	**31**	++	ASCUS
41	**31**	++	NEGAT.
42	**31, 66, 68**	31 + / 66 + / 68 ++	LSIL
43	**31, 56**	31 ++ / 56 +	ASCUS

* Semiquantification of viral load:

C_t (PCR cycles): 13-17 (+, low); 8-12 (++, intermediate); 1-7 (+++, high)

NA, not applicable.

** Cytological assessment:

Negat: Negative; LSIL: Low grade squamous intraepithelial lesion; HSIL: High grade squamous intraepithelial lesion; ASCUS: Atypical squamous cells of undetermined significance.

7. Acknowledgements

The authors gratefully acknowledge financial support projects for PID2021-126304OB-C41 and PDI2021-122875OB-100 funded by MCIN/AEI /10.13039/501100011033 / FEDER, UE, project DTS18/00090 from Instituto de Salud Carlos III and FEDER and Generalitat Valenciana (Project PROMETEO CIPROM/2021/007). This work was also supported by CIBER -Consorcio Centro de Investigación Biomédica en Red- (CB06/01/2012), Instituto de Salud Carlos III, Ministerio de Ciencia e Innovación. We thank UPV electron microscopy service for technical support.

8. References

1. Forman, D., de Martel, C., Lacey, C. J., Soerjomataram, I., Lortet-Tieulent, J., Bruni, L., & Franceschi, S. (2012). *Global burden of human papillomavirus and related diseases.* Vaccine, 30, F12-F23.

2. Koutsky, L. (1997). *Epidemiology of genital human papillomavirus infection.* The American journal of medicine, 102(5), 3-8.
3. Crow, J. M. (2012). *HPV: The global burden*. Nature, 488(7413), S2-S3.
4. Tommasino, M. (2014, June). *The human papillomavirus family and its role in carcinogenesis.* In Seminars in cancer biology (Vol. 26, pp. 13-21). Academic Press.
5. Grce, M., & Mravak-Stipetić, M. (2014). *Human papillomavirus–associated diseases.* Clinics in dermatology, 32(2), 253-258.
6. Bernard, H. U., Burk, R. D., Chen, Z., Van Doorslaer, K., Zur Hausen, H., & De Villiers, E. M. (2010). *Classification of papillomaviruses (PVs) based on 189 PV types and proposal of taxonomic amendments.* Virology, 401(1), 70-79.
7. Doorbar, J., Quint, W., Banks, L., Bravo, I. G., Stoler, M., Broker, T. R., & Stanley, M. A. (2012). *The biology and life-cycle of human papillomaviruses.* Vaccine, 30, F55-F70.
8. Ekström, J., Mühr, L. S. A., Bzhalava, D., Söderlund-Strand, A., Hultin, E., Nordin, P., & Dillner, J. (2013). *Diversity of human papillomaviruses in skin lesions.* Virology, *447*(1-2), 300-311.
9. Zur Hausen, H. (1996). *Papillomavirus infections—a major cause of human cancers*. Biochimica et biophysica acta (BBA)-reviews on cancer, 1288(2), F55-F78.
10. Muñoz, N., Bosch, F. X., De Sanjosé, S., Herrero, R., Castellsagué, X., Shah, K. V., & Meijer, C. J. (2003). *Epidemiologic classification of human papillomavirus types associated with cervical cancer.* New England journal of medicine, 348(6), 518-527.
11. Walboomers, J. M., Jacobs, M. V., Manos, M. M., Bosch, F. X., Kummer, J. A., Shah, K. V., & Muñoz, N. (1999). *Human papillomavirus is a necessary cause of invasive cervical cancer worldwide.* The Journal of pathology*, 189*(1), 12-19.
12. Meijer, C. J., Berkhof, J., Castle, P. E., Hesselink, A. T., Franco, E. L., Ronco, G., & Snijders, P. J. (2009). *Guidelines for human papillomavirus DNA test requirements for primary cervical cancer screening in women 30 years and older.* International journal of cancer*, 124*(3), 516-520.
13. Chan, P. K., Picconi, M. A., Cheung, T. H., Giovannelli, L., & Park, J. S. (2012). *Laboratory and clinical aspects of human papillomavirus testing.* Critical reviews in clinical laboratory sciences, 49(4), 117-136.

14. McLaughlin-Drubin, M. E., Meyers, J., & Munger, K. (2012). *Cancer associated human papillomaviruses*. Current opinion in virology, *2*(4), 459-466.
15. Snijders, P. J., Verhoef, V. M., Arbyn, M., Ogilvie, G., Minozzi, S., Banzi, R., & Meijer, C. J. (2013). *High-risk HPV testing on self-sampled versus clinician-collected specimens: a review on the clinical accuracy and impact on population attendance in cervical cancer screening.* International journal of cancer, *132*(10), 2223-2236.
16. Ronco, G., Dillner, J., Elfström, K. M., Tunesi, S., Snijders, P. J., Arbyn, M., ... & Meijer, C. J. (2014). *Efficacy of HPV-based screening for prevention of invasive cervical cancer: follow-up of four European randomised controlled trials.* The lancet, 383(9916), 524-532.
17. Brink, A. A., Snijders, P. J., & Meijer, C. J. (2007). *HPV detection methods.* Disease markers, 23(4), 273-281.
18. Snijders, P. J., Heideman, D. A., & Meijer, C. J. (2010). *Methods for HPV detection in exfoliated cell and tissue specimens.* Apmis, 118(6-7), 520-528.
19. Poljak, M., Cuzick, J., Kocjan, B. J., Iftner, T., Dillner, J., & Arbyn, M. (2012). *Nucleic acid tests for the detection of alpha human papillomaviruses.* Vaccine, 30, F100-F106.
20. Poljak, M., Valenčak, A. O., Domjanič, G. G., Xu, L., & Arbyn, M. (2020). *Commercially available molecular tests for human papillomaviruses: a global overview.* Clinical Microbiology and Infection, 26(9), 1144-1150.
21. Mahmoodi, P., Fani, M., Rezayi, M., Avan, A., Pasdar, Z., Karimi, E., & Ghayour-Mobarhan, M. (2019). *Early detection of cervical cancer based on high-risk HPV DNA-based genosensors: A systematic review.* Biofactors, 45(2), 101-117.
22. Peng, X., Zhang, Y., Lu, D., Guo, Y., & Guo, S. (2019). *Ultrathin Ti3C2 nanosheets based "off-on" fluorescent nanoprobe for rapid and sensitive detection of HPV infection.* Sensors and Actuators B: Chemical, 286, 222-229.
23. Jimenez, A. M. J., Moulick, A., Richtera, L., Krejcova, L., Kalina, L., Datta, R., & Adam, V. (2018). *Dual-color quantum dots-based simultaneous detection of HPV-HIV co-infection.* Sensors and Actuators B: Chemical, 258, 295-303.
24. Shamsipur, M., Nasirian, V., Mansouri, K., Barati, A., Veisi-Raygani, A., & Kashanian, S. (2017). *A highly sensitive quantum dots-DNA nanobiosensor based on fluorescence resonance energy transfer for rapid detection of nanomolar amounts of human papillomavirus 18.* Journal of pharmaceutical and biomedical analysis, 136, 140-147.

25. Jampasa, S., Siangproh, W., Laocharoensuk, R., Yanatatsaneejit, P., Vilaivan, T., & Chailapakul, O. (2018). *A new DNA sensor design for the simultaneous detection of HPV type 16 and 18 DNA.* Sensors and Actuators B: Chemical, 265, 514-521.
26. Teengam, P., Siangproh, W., Tuantranont, A., Henry, C. S., Vilaivan, T., & Chailapakul, O. (2017). *Electrochemical paper-based peptide nucleic acid biosensor for detecting human papillomavirus.* Analytica Chimica Acta, 952, 32-40.
27. Jimenez, A. M. J., Rodrigo, M. A. M., Milosavljevic, V., Krizkova, S., Kopel, P., Heger, Z., & Adam, V. (2017). *Gold nanoparticles-modified nanomaghemite and quantum dots-based hybridization assay for detection of HPV*. Sensors and Actuators B: Chemical, 240, 503-510.
28. Urrego, L. F., Lopez, D. I., Ramirez, K. A., Ramirez, C., & Osma, J. F. (2015). *Biomicrosystem design and fabrication for the human papilloma virus 16 detection.* Sensors and Actuators B: Chemical, 207, 97-104.
29. Chekin, F., Bagga, K., Subramanian, P., Jijie, R., Singh, S. K., Kurungot, S., & Szunerits, S. (2018). *Nucleic aptamer modified porous reduced graphene oxide/MoS2 based electrodes for viral detection: Application to human papillomavirus (HPV).* Sensors and Actuators B: Chemical, 262, 991-1000.
30. Pascual, L., Baroja, I., Aznar, E., Sancenón, F., Marcos, M. D., Murguía, J. R., & Martínez-Máñez, R. (2015). *Oligonucleotide-capped mesoporous silica nanoparticles as DNA-responsive dye delivery systems for genomic DNA detection.* Chemical communications, 51(8), 1414-1416.
31. Pla, L., Xifré-Pérez, E., Ribes, À., Aznar, E., Marcos, M. D., Marsal, L. F., & Sancenon, F. (2017). *A mycoplasma genomic DNA probe using gated nanoporous anodic alumina.* ChemPlusChem, 82(3), 337-341.
32. Ribes, A., Aznar, E., Santiago-Felipe, S., Xifre-Perez, E., Tormo-Mas, M. Á., Peman, J., & Martinez-Manez, R. (2019). *Selective and sensitive probe based in oligonucleotide-capped nanoporous alumina for the rapid screening of infection produced by Candida albicans.* ACS sensors, 4(5), 1291-1298.
33. Aznar, E., Oroval, M., Pascual, L., Murguía, J. R., Martinez-Manez, R., & Sancenon, F. (2016). *Gated materials for on-command release of guest molecules.* Chemical reviews, 116(2), 561-718.

34. García-Fernández, A., Aznar, E., Martínez-Máñez, R., & Sancenon, F. (2020). *New advances in in vivo applications of gated mesoporous silica as drug delivery nanocarriers.* Small, 16(3), 1902242.
35. Llopis-Lorente, A., Lozano-Torres, B., Bernardos, A., Martínez-Máñez, R., & Sancenón, F. (2017). *Mesoporous silica materials for controlled delivery based on enzymes.* Journal of Materials Chemistry B, 5(17), 3069-3083.
36. Sancenón, F., Pascual, L., Oroval, M., Aznar, E., & Martínez-Máñez, R. (2015). Gated silica mesoporous materials in sensing applications. *ChemistryOpen, 4(4), 418-437.*
37. Climent, E., Martínez-Máñez, R., Sancenón, F., Marcos, M. D., Soto, J., Maquieira, A., & Amorós, P. (2010). *Controlled delivery using oligonucleotide-capped mesoporous silica nanoparticles.* Angewandte Chemie, 40(122), 7439-7441.
38. Castillo, R. R., Baeza, A., & Vallet-Regí, M. (2017). *Recent applications of the combination of mesoporous silica nanoparticles with nucleic acids: development of bioresponsive devices, carriers and sensors.* Biomaterials science, 5(3), 353-377.
39. Pla, L., Lozano-Torres, B., Martínez-Máñez, R., Sancenón, F., & Ros-Lis, J. V. (2019). *Overview of the evolution of silica-based chromo-fluorogenic nanosensors.* Sensors, 19(23), 5138.
40. Santos, A., Kumeria, T., & Losic, D. (2014). *Nanoporous anodic alumina: a versatile platform for optical biosensors.* Materials, 7(6), 4297-4320.
41. Rajeev, G., Prieto Simon, B., Marsal, L. F., & Voelcker, N. H. (2018). A*dvances in nanoporous anodic alumina-based biosensors to detect biomarkers of clinical significance: a review.* Advanced Healthcare Materials, 7(5), 1700904.
42. Alberti, S., Soler-Illia, G. J., & Azzaroni, O. (2015). *Gated supramolecular chemistry in hybrid mesoporous silica nanoarchitectures: controlled delivery and molecular transport in response to chemical, physical and biological stimuli.* Chemical Communications, 51(28), 6050-6075.
43. Lee, W., & Park, S. J. (2014). *Porous anodic aluminum oxide: anodization and templated synthesis of functional nanostructures.* Chemical reviews, 114(15), 7487-7556.
44. Ye, W. W., Shi, J. Y., Chan, C. Y., Zhang, Y., & Yang, M. (2014). *A nanoporous membrane based impedance sensing platform for DNA sensing with gold nanoparticle amplification.* Sensors and Actuators B: Chemical, 193, 877-882.

45. Ye, W., Xu, Y., Zheng, L., Zhang, Y., Yang, M., & Sun, P. (2016). *A nanoporous alumina membrane based electrochemical biosensor for histamine determination with biofunctionalized magnetic nanoparticles concentration and signal amplification.* Sensors, 16(10), 1767.
46. Tian, F., Lyu, J., Shi, J., Tan, F., & Yang, M. (2016). *A polymeric microfluidic device integrated with nanoporous alumina membranes for simultaneous detection of multiple foodborne pathogens.* Sensors and Actuators B: Chemical, 225, 312-318.
47. Climent, E., Mondragon, L., Martínez-Máñez, R., Sancenon, F., Marcos, M. D., Murguía, J. R., & Pérez-Payá, E. (2013). *Selective, highly sensitive, and rapid detection of genomic DNA by using gated materials: Mycoplasma detection.* Angewandte Chemie International Edition, 52(34).
48. Pla, L., Santiago-Felipe, S., Tormo-Mas, M. Á., Ruiz-Gaitán, A., Pemán, J., Valentín, E., & Martínez-Máñez, R. (2021). *Oligonucleotide-capped nanoporous anodic alumina biosensor as diagnostic tool for rapid and accurate detection of Candida auris in clinical samples.* Emerging microbes & infections, 10(1), 407-415.
49. Pla, L., Santiago-Felipe, S., Tormo-Mas, M. Á., Pemán, J., Sancenon, F., Aznar, E., & Martinez-Manez, R. (2020). *Aptamer-capped nanoporous anodic alumina for Staphylococcus aureus detection.* Sensors and Actuators B: Chemical, 320, 128281.
50. Pla, L., Aviñó, A., Eritja, R., Ruiz-Gaitán, A., Pemán, J., Friaza, V., & Santiago-Felipe, S. (2020). *Triplex hybridization-based nanosystem for the rapid screening of Pneumocystis pneumonia in clinical samples.* Journal of Fungi, 6(4), 292.
51. Caballos, I., Aranda, M. N., López-Palacios, A., Pla, L., Santiago-Felipe, S., Hernández-Montoto, A., ... & Martínez-Máñez, R. (2023). *Aptamer-capped nanoporous anodic alumina for SARS-CoV-2 spike protein detection.* Advanced Materials Technologies, 8(11), 2201913.

Development of an Innovative Fluorogenic Biosensor for Direct Detection of *Vibrio vulnificus*, a Climate Change Biomarker

1. Abstract

Vibrio vulnificus, a marine pathogen an climate change biomarker, poses significant risks to human health through consumption of contaminated seafood or exposure to seawater. Rapid, precise detection techniques are crucial for diagnosing vibriosis and monitoring *V. vulnificus* in environmental samples. We report herein a novel fluorogenic biosensor for the efficient detection of *V. vulnificus*. The biosensor is based on nanoporous alumina loaded with rhodamine B and capped with a specific oligonucleotide probe. The interaction between the probe and *V. vulnificus* DNA triggers pore opening and release of the fluorophore that is detected via fluorescence measurements. The biosensor can effectively detect *V. vulnificus* across different laboratory-contaminated natural samples (including fish mucus and serum, human serum and sterilized brackish water) and is further validated using samples from lake and seawater, notably without requiring DNA extraction or amplification. The biosensor offers a dual-purpose tool for coastal warming surveillance and swift vibriosis diagnosis in humans and animals.

2. Introduction

Climate change is intensifying the spread of marine pathogens such as *Vibrio vulnificus,* which thrives in brackish water ecosystems across temperate, tropical, and subtropical regions.[1,2,3] The warming of ocean waters and the resultant decrease in salinity, direct outcomes of global warming, are causing an expansion in both the population and geographic distribution of *V. vulnificus,* moving into areas previously cooler.[1,2,3] This pathogen causes vibriosis in humans and fish, a condition that in humans ranges from gastroenteritis to deadly fulminant septicemia within 24-48 hours of infection.[4,5] Human vibriosis transmission occurs through the consumption of raw or undercooked seafood and contact with seawater or diseased animals (zoonosis).[6,7,8] It should be noted that primary sepsis caused by ingestion of this bacterium is the leading cause of mortality due to foodborne pathogens.[9]

Multiple immunological and genetic methods have been developed for the detection and identification of this species.[10,11,12,13,14,15,16] However, the detection of *V. vulnificus* from environmental samples usually require the prior collection of pure cultures, which considerably lengthens the detection process. Among different methods, real-time PCR (or qPCR) and LAMP (loop-mediated isothermal amplification) stand out because, being the most sensitive (limit of detection around 10^2 bacteria mL^{-1}) the previous step of obtaining pure cultures could in some cases be obviated.[14,15,16] However, the former requires technical skills that might influence the efficiency of reaction amplification and the quality of standard curves, which affects the accuracy of detection, and the latter is sensitive to the external environment and may cause false positives.[14,15,16] In addition, these methods are expensive and complex as they require pregenomic DNA extraction performed by qualified personnel using specialized equipment. Summarizing qPCR and LAMP techniques, while sensitive, face challenges in cost, complexity, and the risk of false positives.

From another point of view, the advent of biosensor technology has shown considerable promise in pathogen detection, including *V. vulnificus*.[17,18,19,20,21] Among the biosensors developed, a fluorogenic biosensor based on DNAzyme,[18] a sensor that uses a specific functionalized oligonucleotide probe and measures impedance changes,[19] a sensor that combines recombinase-assisted amplification (RAA) and the CRISPR/Cas12a system[20] and a biosensor based on RAA and lateral flow strip,[21] stand out for their sensitivity and specificity. Although the limits of detection of these systems are usually below that of conventional PCR, they are not below that of qPCR.

Another line of work that may lead to improved sensors is based on the use of nanomaterials combined with biomolecules to give bioorganic-inorganic hybrid systems.[22] Among different nanomaterials, nanoporous anodic alumina (NAA) has become one of the most widely used for sensor development due to its exceptional qualities such as biocompatibility, easily tunable surfaces and high loading capacity. NAA becomes powerful detection and diagnostic tools when loaded with indicators and capped with specific biomolecules.[23,24] This is generally carried out using alkoxysilane

chemistry that allows different (bio)molecules to be easily attached to the outer surface of NAA.[25,26,27] Following this approach, different nucleic acids such as DNA, RNA and aptamers, have been widely used as gatekeepers on mesoporous supports and have demonstrated outstanding applications.[28,29,30] For instance, some works reported the use of DNA and mesoporous materials to develop gated-nanodevices for the identification of different microorganisms, including virus.[31,32,3334]

Based on the above, we report herein a gated nanostructured hybrid biosensor for the optical detection of *V. vulnificus.* The biosensor is based on the NAA scaffold that is loaded with Rhodamine B (RhB) and capped with a specific oligonucleotide containing the base sequency of the *V. vulnificus* cytolysin structural gene (*vvhA*). The oligonucleotide inhibits fluorophore release by blocking the pores. In the presence of *V. vulnificus* DNA the capping oligonucleotide is displaced, allowing the pore opening and RhB delivery. The sensitivity and specificity of the biosensor was tested with different types of laboratory-contaminated natural samples (fish mucus and serum; human serum; and sterilized natural brackish water) and was validated in natural lake and seawater samples. Remarkably, *V. vulnificus* detection from natural water was successful without the need for prior DNA extraction or amplification steps. Consequently, this novel design enables direct and specific detection of *V. vulnificus* representing a step forward towards environmental monitoring and diagnosis of vibriosis in humans and animals.

3. Results and discussion

3.1. Development and characterization of the sensing system

A two-step process was used to obtain the **S1** support from NAA films. In a first step, the outer surface of NAA supports (**S0**) was functionalized with APTES in toluene and subsequently, supports were loaded with RhB using a RhB solution in acetonitrile. When we attempted to carry out dye loading and surface functionalization in the same reaction mixture in acetonitrile, a change of the optical properties of RhB and uncontrolled hydrolysis of APTES were observed, that resulted in the formation of a solid phase on the

NAA surface. This was avoided when the two-step procedure described above was performed.

In the next step, oligonucleotide **O1**, containing a partial base sequence of *V. vulnificus* cytolysin *vvhA* gene, was linked to the external surface through electrostatic interaction between the positively charged amino moieties on the support's surface and the negatively charged oligonucleotide backbone, resulting in the final sensor material **S2**. As shown in **Figure 1**, the oligonucleotide probe on the sensor surface is expected to block the pores preventing dye release while hybridization of the pathogen complementary ssDNA to the oligonucleotide probe on the sensor surface is expected to cause pore opening when *V. vulnificus* is present, allowing the release of the entrapped RhB.

HR-FESEM and EDXS analysis were performed on the initial NAA scaffold and on **S1** and **S2**. As described by the provider, the NAA support (InRedox®) is composed of anodic aluminum oxide films grown on 0.1 mm thick aluminum layers with a pore density $9 \cdot 10^{11}$ cm^{-2}. In the upper part of the funnel, the pores are 20-30 nm in size that decrease to ca. 5 nm in the lower part. It was calculated that 4 ng of RhB per g of NAA can be loaded and released with this pore morphology. HR-FESEM images of the NAA scaffold (**Figure 2A**) and **S2** sensor (**Figure 2B**) confirmed the porous structure of the NAA starting support, while the final **S2** biosensor shows the outer surface coated with an organic phase corresponding to the capping oligonucleotides.

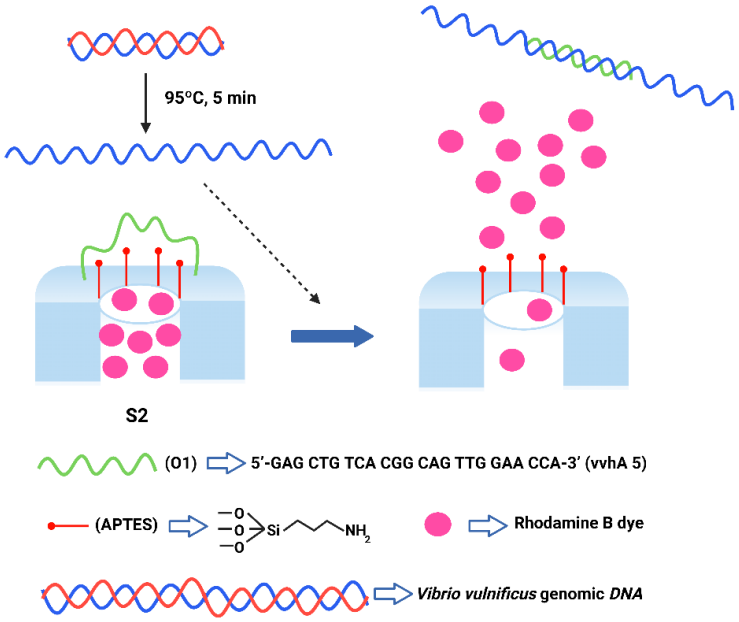

Figure 1. Scheme of fluorogenic biosensor **S2** based on oligonucleotide gated NAA films for *V. vulnificus* DNA detection. NAA films were loaded with rhodamine B and the external surface was functionalized with an oligonucleotide probe containing the base sequency of *V. vulnificus vvhA* gene, that blocks the pores and avoids dye release. In the presence of the bacterial DNA, selective delivery of entrapped RhB is achieved.

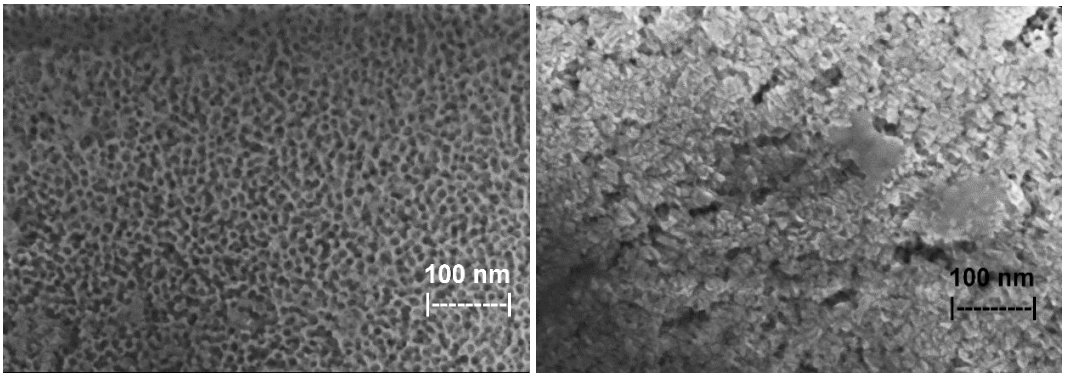

Figure 2. HR-FESEM images of (A) the starting NAA support and (B) the final **S2** biosensor.

To determine the atomic content of the prepared materials (**S0**, **S1** and **S2**), energy dispersive X-ray spectroscopy (EDXS) was carried out (**Table 2**). The **S1** support has a high C/Al content after dye loading and surface functionalization with aminopropyl moieties, which decreased in **S2** due to partial dye leakage during the **O1** coating process and incomplete pore blocking of some of the pores in the material by **O1**. Additionally, the presence of aminopropylsilyl groups is supported by the presence of N and Si on **S1** and **S2** supports. Finally, P was present in the final material **S2**, indicating the presence of the **O1** coating oligonucleotide, which was not detected in the NAA and **S1** supports.

Table 2. Analysis of the atomic element ratios in the different supports by energy dispersive X-ray spectroscopy (EDXS).

	C/Al	N/Al	Si/Al	P/Al
S0	0.12±0.02	-	-	-
S1	1.98±0.05	0.42±0.01	0.15±0.02	-
S2	0.67±0.03	0.51±0.02	0.11±0.01	0.02±0.01

3.2. Dye relese kinetics

The ability of the **S2** biosensor to detect the *V. vulnificus* DNA region of interest was first studied using an oligonucleotide complementary to the **O1** oligonucleotide probe that covers the surface of the support. **Figure 3A** shows the release profile of RhB from **S2** in the presence and absence of the complementary oligonucleotide **O1c**. When the target oligonucleotide **O1c** was present, a remarkable release of dye from the pores was observed due to hybridization with the capping oligonucleotide **O1** followed by pore opening. In contrast, when the complementary oligonucleotide was absent, a very low level of dye was released, indicating that the probes electrostatically attached to the scaffold surface effectively blocked the pores preventing dye delivery (**Figure 1**). This transduction mechanism differs substantially from classical "binding site-signaling subunit" probes. Sensors based on gated materials perform their signaling by releasing a

large number of trapped dyes independently of the stoichiometry of the host-guest interaction on their surface. This protocol allows the development of detection systems with high sensitivity due to signal amplification (*vide infra*).

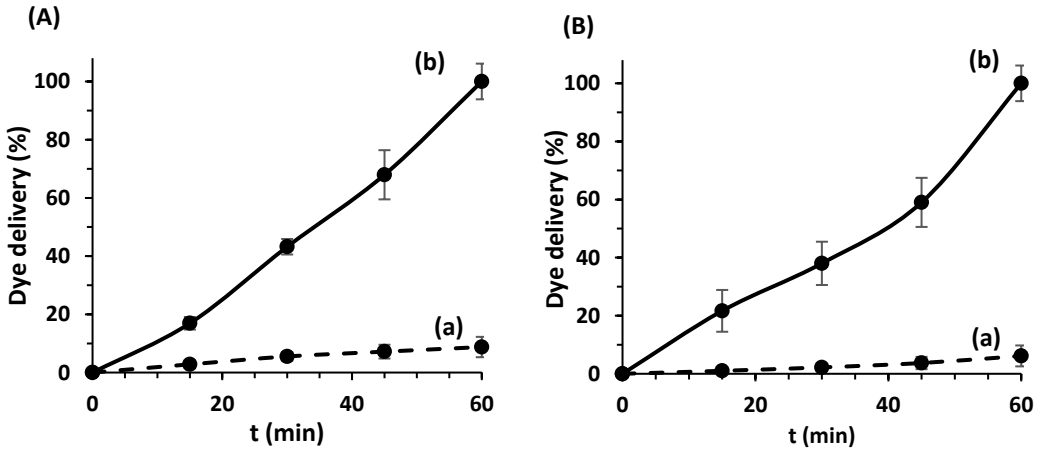

Figure 3. (A) Rhodamine B delivery from **S2** in (a) the absence and (b) the presence of 1 µM complementary **O1c** target oligonucleotide in hybridization buffer. **(B)** Rhodamine B release from sensor **S2** in (a) the absence and (b) the presence of *V. vulnificus* bacteria at 10^3 CFU mL^{-1}.

In a second step, the **S2** sensor was evaluated to detect *V. vulnificus* in a bacterial suspension. RhB release was negligible without bacteria, as shown in curve (a) of **Figure 3B**, suggesting that the **O1** oligonucleotide anchored to the scaffold surface effectively closed the pores. In contrast, diffusion of the dye into the aqueous solution was remarkable when *V. vulnificus* cells were present (curve (b)). Specific recognition of the bacterial DNA by the gated biosensor caused hybridization with the oligonucleotide probe on the surface of the support, displacement of the dsDNA, unblocking the pores and allowing the delivery of the dye. Of note is the high performance of the sensor for direct detection of cellular DNA without sample pre-treatment for DNA extraction and amplification due to the enhanced permeability of the cell membrane in the TRIS buffer that can lead to cell lysis and DNA release.

3.3. Analytical performance: sensitivity and specificity studies

The limit of detection (LOD) of biosensor was calculated by determining the amount of dye released by **S2** after 60 min of incubation at different cell concentrations in the range between 10^{-3} to 10^{4} CFU mL^{-1}. A LOD of 10^{2} CFU mL^{-1} was calculated based on the intersection point of the two slopes of the plotted curve (**Figure 4**). These results showed that the dye delivered was directly related to the concentration of *V. vulnificus*, supporting the transduction mechanism detailed above. Furthermore, the LOD obtained is within the range of the previously reported most sensitive methods for the detection of *V. vulnificus*. Multiple studies using qPCR, reported LODs of 50–200 copies L^{-1}, which correspond to a DNA concentration range of around 1 nM.[16] Besides, our proposed method has a lower LOD than a DNAzyme-based biosensor that detects *V. vulnificus* at about 10^{3} CFU mL^{-1}.[18]

According to the suggested detection mechanism, the amount of dye released depends on the amount of target DNA that would cause displacement of the coating oligonucleotide and pore opening. Recent studies have shown that the number of dye molecules released per DNA molecule in similar gated sensors is in the 10^{4}-10^{11} range.[31,32] To determine the amplification capacity of the biosensor, the **S2** support was incubated with a known amount of denaturalized genomic DNA from *V. vulnificus* (1.16×10^{-3} µg mL^{-1}). Released RhB amount from porous support was quantified by fluorescence measurements using a calibration curve at different dye concentrations. The quantity of RhB released form sensor was then directly associated with the amount of DNA detected. The amplification capacity of the gated porous sensor was determined resulting in $1.3 \cdot 10^{5}$ molecules of RhB released per genomic DNA molecule.

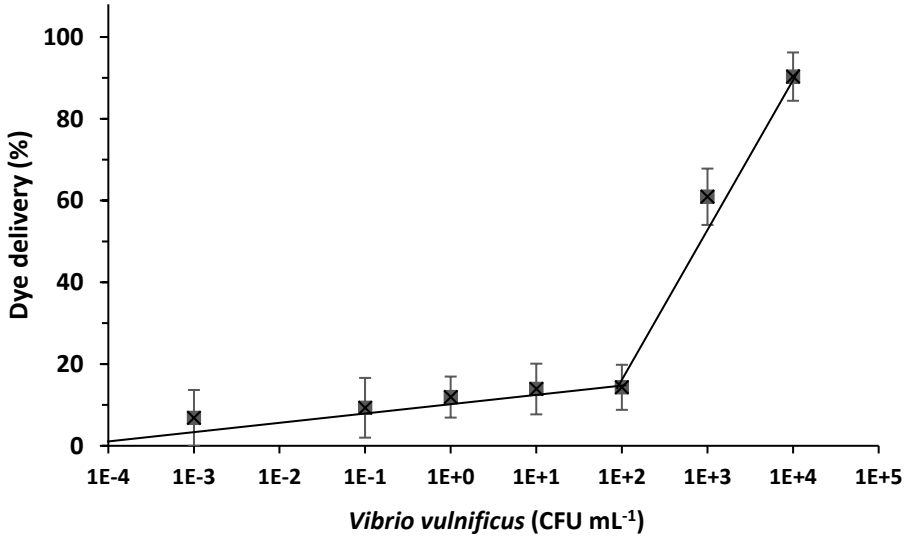

Figure 4. Dye release from sensor **S2** in the presence of *V. vulnificus* at different concentrations.

A second assay was conducted to determine the specificity of the biosensors by evaluating the response of **S2** to different *Vibrio* species (*V. harveyi, V. parahaemolyticus, V. cholerae*) as well as mixtures of them (*V. vulnificus + V. harveyi, V. vulnificus + V. parahaemolyticus, V. vulnificus + cholerae, V. vulnificus + V. harveyi + V. parahaemolyticus + V. cholerae*). Dye release from 9 independent **S2** supports was monitored at values of 10^3 CFU mL^{-1} of each *Vibrio* species in the medium after 60 min of incubation. The dye release measurement from the **S2** support in the absence of stimulus (blank) serves as a baseline for system release during sample measurement. The presence of other *Vibrio* species resulted in a slightly higher RhB release compared to the blank, while a significant release of dye was only observed when *V. vulnificus* was present (**Figure 5**). Furthermore, similar fluorescence signal enhancement was produced when *V. vulnificus* was alone or in combination with other *Vibrio* species. These results demonstrate the ability of the **S2** sensors to selectively detect *V. vulnificus*.

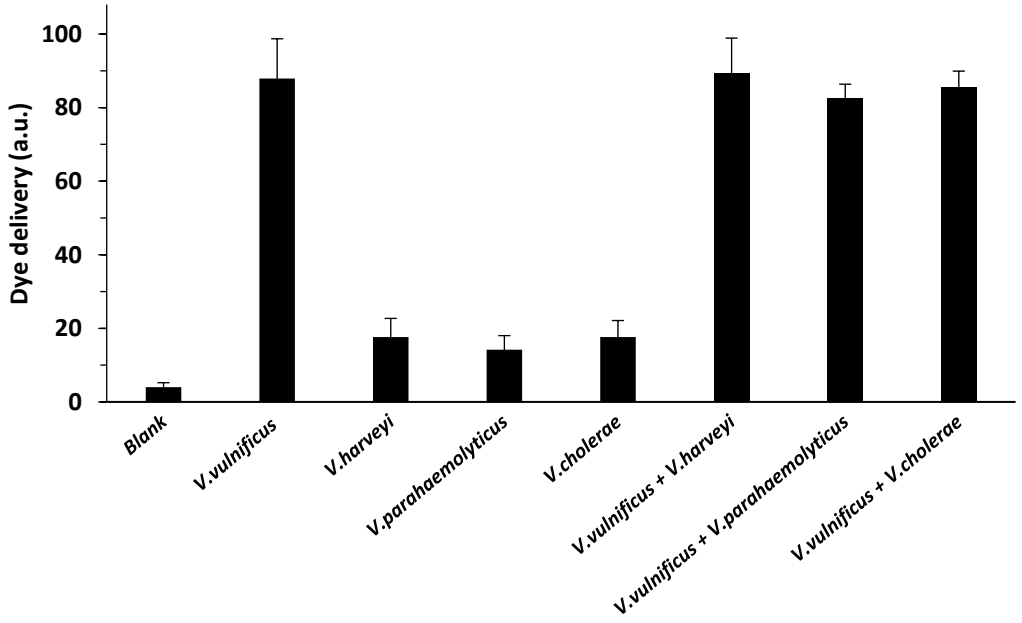

Figure 5. Released dye from sensor **S2** in presence of 10^3 CFU mL^{-1} of *V. vulnificus*, *V. harveyi, V. parahaemolyticus, V. cholerae* a mixture of *V. vulnificus + V. harveyi,* a mixture of *V. vulnificus + V. parahaemolyticus* and a mixture of *V. vulnificus + cholerae.*

3.4. *V. vulnificus* detection in artificially inoculated natural samples

The robustness of the system was evaluated by determining the capacity of the **S2** to detect *V. vulnificus* in different media simulating either environmental or clinical samples. To this end, *V. vulnificus* cells were inoculated at 10^3 CFU mL^{-1} into previously sterilized brackish water from natural ecosystems, fresh eel mucus, and human and eel serum. In all media, *V. vulnificus* caused a displacement of the gating oligonucleotide and dye delivery (**Figure 6**).

Finally, the LOD of **S2** was also calculated in sterilized natural brackish water inoculated with different *V. vulnificus* cell concentrations (10^{-3} to 10^{5} CFU mL^{-1}). The amount of dye released was proportional to the *V. vulnificus* cell concentration, resulting in a LOD of 500 CFU mL^{-1}. Despite the absence of previous culture, sample treatment, or amplification steps, the LOD obtained with this probe is comparable to that previously found in buffer media (**Figure 4**) and to that found by Yang et al.[16] using qPCR. This result demonstrates the potential of the sensor to analyze containing-*V. vulnificus* samples quickly and efficiently. It was also demonstrated that the **S2** sensors can be stored for weeks and used without any change in the sensing properties of supports, paving the way for potential *in situ* applications.[38]

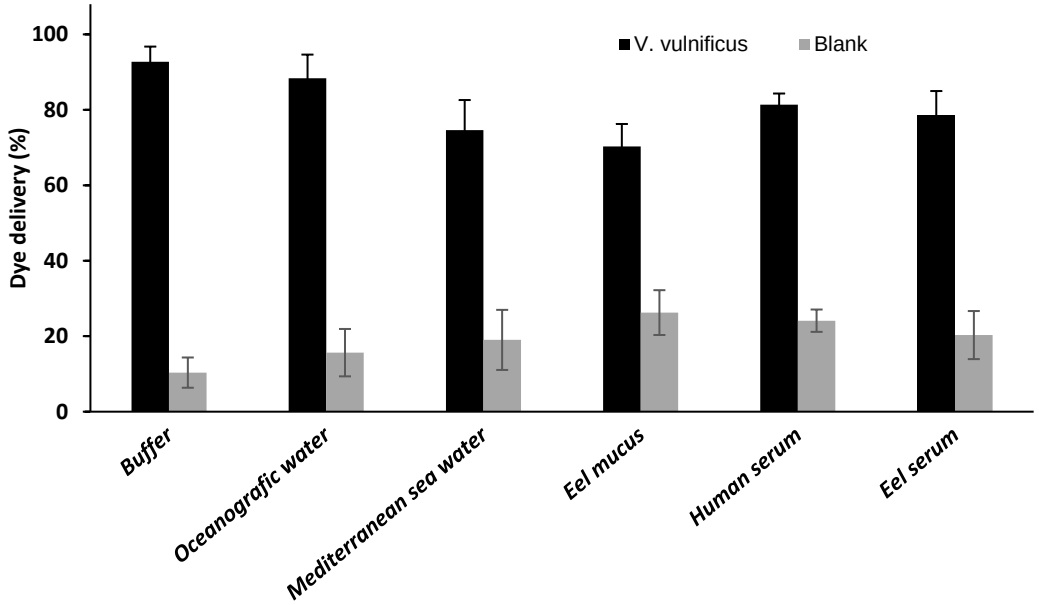

Figure 6. Released dye from sensor **S2** incubated with *V. vulnificus* (10^{3} CFU mL^{-1}) in different media.

3.5. *V. vulnificus* detection in natural samples

Currently, the method of identification of *V. vulnificus* varies depending on whether the sample to be tested contains only *V. vulnificus* (clinical sample of vibriosis case) or not (environmental sample). In the former case, direct identification is feasible

by any of the mentioned methods (PCR, qPCR, biosensors, etc) while in the latter, *V. vulnificus* DNA must first be amplified by microbiological (enrichment in specific media) or genetic (different types of PCR) methods. Direct identification of *V. vulnificus* from environmental samples has not been evaluated due to *V. vulnificus* is outcompeted by other bacterial species.[39,40,41]

Table 3. Main physicochemical properties of the water samples in different sampling locations.

Sampling point	Temperature (°C)	Conductivity (µS/cm)
Perellonet	18	1692
Natural park: Albufera Lake	18	1627
Natural park: Albufera Lake	9	1741
Mediterranean sea (Perellonet beach)	13	51700
Perellonet	8	1765
Perellonet	8	1794
Perellonet	8	1821
Natural park: Albufera Lake (Puchol's Gola)	8	1615
Natural park: Albufera Lake	20	1606
Mediterranean sea (Perellonet beach)	19.5	4890
Perellonet	20.5	1680
Perellonet	20.5	1721
Natural park: Albufera Lake (Puchol's Gola)	20	1947

To find out whether our **S2** biosensor would be able to detect *V. vulnificus* from natural waters, we performed a series of sampling in ecosystems near Valencia (Spain) (**Table 3**) and proceeded to the analysis and detection of this pathogen using **S2** directly with the water samples and, in parallel, using the protocol reported by Pérez-Roig et al.[37] involving prior enrichment in alkaline peptone water for 8 h followed by DNA isolation and PCR detection. The assays were performed in triplicate. As shown in **Table 4**, all samples in which *V. vulnificus* was detected directly using the **S2** biosensor without prior enrichment step were also positives when using the reference method by PCR detection from the enrichment broth. This gives to the method reported herein a sensitivity and specificity of 100 %, together with positive and negative predictive values of 100 %. Significantly, our method outperforms conventional reference methods in terms of accuracy (no sample pretreatment required), ease of use (can be used by untrained personnel), speed (provides reliable results in less than one hour) and cost-effectiveness (eliminates the need for expensive equipment and allows miniaturization).

Table 4. Analysis of water samples using the biosensor **S2** and the reference *V. vulnificus* detection method.[37]

# Sample	Reference method (Enrichment plus PCR detection)[a]	S2[b]
1	+	**+**
2	+	**+**
3	-	**-**
4	-	**-**
5	-	**-**
6	-	**-**
7	-	**-**
8	-	**-**
9	+	**+**

10	**+**	**+**
11	**+**	**+**
12	**+**	**+**
13	**+**	**+**

[a] (+) positive identification by PCR after enrichment.

[b] (+) positive indicates fluorescence intensity equals or exceeds 3-fold the standard deviation for three negative controls at 575 nm (λ_{exc} = 555 nm).

4. Conclusion

In summary, we have developed and rigorously tested a highly selective and sensitive fluorogenic biosensor for detecting *V. vulnificus*, utilizing nanoporous materials combined with short DNA sequences tailored specifically for this purpose. The biosensor is based on the use of NAA scaffolds loaded with RhB and coated with an oligonucleotide targeting a sequence unique to *V. vulnificus*. The interaction with the target bacteria DNA triggers the opening of the pores and the subsequent release of RhB, allowing for the detection of the pathogen. This biosensor demonstrated exceptional selectivity for *V. vulnificus*, showing no cross-reactivity with other Vibrio species, and exhibited limits of detection (LOD) in natural water samples comparable to those achieved by other state-of-the-art *V. vulnificus* detection methods. Its effectiveness was proven in detecting *V. vulnificus* directly from simulated-natural and -clinical samples as well as natural environmental samples, demonstrating its potential for monitoring coastal water quality and for the rapid diagnosis of vibriosis in humans and animals. Furthermore, by employing various reporters and capping sequences, this sensor design could be easily adapted for the multiplexed detection of the four most clinically significant *Vibrio* species, *V. vulnificus, V. parahaemolyticus, V. alginolyticus,* and *V. cholerae*, highlighting its versatility and broad applicability in public health and environmental monitoring.

5. Materials and methods

5.1. General Techniques and chemicals used in Sensor Assays

Techniques: NAA surfaces were characterized by High Resolution Field Emission Scanning Electron Microscopy (HR-FESEM). NAA systems were placed onto Al disks using carbon cement. Images were acquired using a HR-Field Emission Scanning electron microscope (ZEISS GeminiSEM 500) operating at 5 kV. The atomic composition of analysed surfaces was determined by Energy Dispersive X-ray Spectroscopy (EDXS) using an X-ray detector coupled to the microscope.

Chemicals: 3-aminopropyltriethoxysilane (APTES), hydrochloric acid, RhB, magnesium chloride (anhydrous), acetonitrile (anhydrous), toluene (anhydrous) and tris(hydroxymethyl)aminomethane (TRIS) were acquired from Sigma-Aldrich (Spain). InRedox Company, Longmont, CO, provided NAA supports (Anodized aluminum oxide (AAO) film on Al substrate size 25 mm x 75 mm, AAO pore diameter 5±2 nm, AAO thickness 10±0.5 µm.). Oligonucleotide (5'-GAG CTG TCA CGG CAG TTG GAA CCA-3') (**O1**) and its complementary (5'-TGG TTC CAA CTG CCG TGA CAG CTC-3') (**O1c**) were obtained from Thermo Fisher Scientific (Madrid, Spain).

5.2. Synthesis of materials S1 and S2

The **S1** supports were prepared by immersing 24 NAA scaffolds (2 mm in diameter) in 8 mL of (3-aminopropyl)triethoxysilane (0.22 mmol) solution in toluene for 6 h using an orbital stirrer at 50 rpm. In the next step, the functionalized supports were washed three times with 8 mL of toluene, 8 mL of acetone, and dried overnight at 60 °C. Afterwards, dried supports were stirred with 8 mL of RhB solution in acetonitrile (1 mM) during 18 h to obtain **S1** supports.

To prepare the final sensors, **S2**, **S1** supports were immersed in a capping solution of oligonucleotide **O1** in hybridization buffer (20 mM TRIS-HCl, 37.5 mM $MgCl_2$, pH 7.5). An optimized capping solution of 5 µL **O1** (100 µM) in a final volume of 250 µL TRIS was placed under shaking at 37 °C overnight for functionalization of two **S1** supports. Finally, gated

supports were washed three times with 1 mL of TRIS buffer to remove the excess of unbounded **O1** on support´s surface.

5.3. Quantification of the loaded dye

To calculate the amount of the RhB that can be loaded in the porous structure of NAA films, a pair of independent **S2** supports were soaked in 1 mL of TRIS buffer. A control support was stirred at 37 °C while the other one was stirred at 90 °C for 60 min to force the pore opening and dye release. The media fluorescence was measured at 575 nm (λ_{exc} = 555 nm) using a Synergy H1 microplate reader (BioTek, Winooski, Vermont, USA). The concentration of released RhB was calculated using a calibration curve at different dye concentrations. The experiment was done by triplicate.

5.4. Bacterial culture and DNA extraction

V. vulnificus strains representative of the main phylogenetic lineages as well as strains of other vibrio species (*V. harveyi, V. parahaemolyticus* and *V. cholerae*) co-existing in the same habitats were selected for the study (**Table 1**). The strains were routinely cultured in LB (Luria-Bertani medium) and on LB agar, both supplemented with 0.5 % NaCl (LB-1, LB-1 agar) at 28 °C for 24 h and were kept frozen at -80 ºC in LB-1 plus 20 % glycerol. DNA was extracted from overnight bacteria LB-1 cultures using the GenElute™ Bacterial Genomic DNA (Sigma, Spain) kit according to the manufacturer's instructions.

Table 1. *V. vulnificus* strains used in the study and their characteristics.

Strain*	**Isolation data**			**Subtyping****		
	Source	**Geographic location/year of isolation**	**Phylogenetic linage-clade**	**pv. *piscis***	***pilF* PCR**	***fpcrp* PCR**
CECT 4999	Diseased eel	Spain, 1999	L2-clade E	+	+	+
YJ016	Human blood	Taiwan, 1993	L1	−	+	−

A14	Diseased eel	Spain, 2002	L2-clade A	+	−	+
12	Health tilapia	Israel, 2002	L3	+	+	+

* Additional strains belonging to *V. cholerae*, *V. harveyi* and *V. parahaemolyticus* from the private collection of prof. Amaro's lab were also used in some experiments.

** Pathovar *piscis* subtyping based on the character virulent for fish of the isolate.[35] *pilF* typing detects a polymormism in *pilF* related to public health concern[36]; *fpcrp* typing detects a gene essential for fish virulence that encodes a fish-phagocytosis-and-complement-resistance protein[37]

5.5. Detection protocol

The release of RhB to the solution in the presence of the target complementary DNA was determined to evaluate the capacity of the **S2** sensors for *V. vulnificus* detection. Two independent **S2** supports were submerged in 900 µL of hybridization buffer in a typical experiment. Then, 100 µL of the complementary DNA oligonucleotide (10 µM) and 100 µL of the hybridization buffer were added to each support, respectively. Mixtures were stirred at 37 °C and aliquots of both solutions were taken at scheduled intervals. The fluorescence of the solution was measured at 575 nm (λ_{exc} = 555 nm) to assess dye release. Three replicates were performed in the experiment.

Furthermore, suspensions of *V. vulnificus* live cells in phosphate buffer saline (PBS) were used to evaluate sensor response. Each **S2** sensor was immersed in 900 µL of TRIS buffer plus either 100 µL of bacterial suspension (10^4 CFU (Colony Forming Units) mL^{-1}) or 100 µL of TRIS buffer (negative control). Aliquots of each solution were obtained at scheduled intervals while shaking at 37 °C. In both assays, the amount of dye released was detected monitoring the fluorescence of the solutions (λ_{exc} = 555 nm, λ_{em} = 575 nm) using a plate reader.

5.6. Signal Amplification Assay

Two **S2** supports were submerged in 990 µL of hybridization buffer. Additionally, genomic DNA from *V. vulnificus* (1.16×10^{-3} µg mL^{-1}) was denaturalized at 95 °C for 5 minutes, then cooled immediately in an ice bath (3 min). 10 µL of denaturalized genomic DNA was then added to one support and 10 µL of water was added to the control one. Both supports were incubated for 60 minutes at 37 °C with shaking. After incubation, aliquots (100 µL) were taken to measure the fluorescence. Released RhB amount was quantified using a calibration curve at different dye concentrations performed at the same time. The quantity of DNA detected in the experiment was then directly associated with the amount of RhB released.

5.7. Sensitivity and Selectivity Assessment

For sensitivity and selectivity assessment, suspensions of *V. vulnificus* live cells in phosphate buffer saline (PBS) were used. To calculate the limit of detection (LOD) of the gated sensor, ten **S2** sensors were immersed in 1 mL of ten-fold bacterial dilutions (from 10^{-5} to 10^{4} CFU mL^{-1}) in hybridization buffer (20 mM TRIS-HCl, 37.5 mM $MgCl_2$, pH 7.5). After 60 minutes incubation at 37 ºC, released RhB was detected monitoring the fluorescence of the solutions (λ_{exc} = 555 nm, λ_{em} = 575 nm) using a plate reader.

To evaluate sensor´s selectivity, different **S2** sensors were suspended in 1 mL of TRIS buffer (20 mM TRIS-HCl, 37.5 mM $MgCl_2$, pH 7.5) with cell cultures from *V. vulnificus, V. cholerae, V. harveyi*, and *V. parahaemolyticus* and a combination of them at a final concentration of 10^3 CFU mL^{-1}. A control support was mixed with hybridization buffer without added cells, and the mixtures were stirred for 60 minutes at 37 °C. Finally, solution fluorescence at 575 nm (λ_{exc} = 555 nm) was measured to determine the amount of rhodamine B delivered.

5.8. Sensor Assessment with Natural Samples

The ability of **S2** sensor to detect *V. vulnificus* was evaluated using fish and human serum, to simulate clinical sampling, as well as fish mucus and natural brackish water, to simulate environmental monitoring. Fish serum and fish mucus were obtained from farmed eels according to Marco-Noales et al.[38] Human serum was purchased from SIGMA (Spain) and water samples were taken from natural ecosystems (Albufera lake and neighboring beaches) near the city of Valencia. All samples (except human serum and part of the brackish water samples) were sterilized by filtration (0.22 mm filters (Millipore)). The **S2** sensors were immersed in 800 µL of hybridization buffer mixed with 100 µL of each sample and then a suspension of *V. vulnificus* (100 µL, 10^3-10^5 CFU mL^{-1}) was added. A mixture of 800 µL of hybridization buffer with 200 µL of the sample without adding the bacteria was used as a negative control.

Unsterilized brackish water samples were processed for the presence of *V. vulnificus* using the selected sensor and conventional microbiological methods as a control. The **S2** sensors were immersed in 850 µL of hybridization buffer and 150 µL of unsterilized brackish water was added. Another **S2** sensor was immersed in 1000 µL of hybridization buffer as a secondary control in both types of analysis. The solutions containing the sensors were then shaken for 60 min at 37 °C and fluorescence was measured at 575 nm with an excitation wavelength of 555 nm to determine the amount of RhB released from the porous supports.

Microbiological controls of the unsterilized brackish water were performed according to Pérez-Roig et al.[37] Briefly, the procedure consists of enrichment in alkaline peptone water (pH 8.6) for 6-8 h followed by identification with a *V. vulnificus*-specific PCR using as target the same gene as the one selected for the sensor, *vvhA*.

6. Acknowledgements

This research was supported by project PID2021-126304OB-C41 funded by MCIN/ AEI /10.13039/501100011033/ and by European Regional Development Fund - A way of doing Europe. This work has received funding from the European Union's Horizon 2020

research and innovation programme under grant agreement No 899708. This research was supported by CIBER -Consorcio Centro de Investigación Biomédica en Red- (CB06/01/2012), Instituto de Salud Carlos III, Ministerio de Ciencia e Innovación. This study is part of the ThinkInAzul programme and was supported by the grant THINKINAZUL/2021/027 from MCIN (Spanish Ministry of Science and Innovation), with funding from the European Union NextGeneration EU (PRTR-C17. I1) and the Generalitat Valenciana, Spain (GV). The study was also supported by the grants PID 2020-120619RBI00 funded by MCIN/AEI/10.13039/501100011033 and CIAICO/2021/293 funded by "Conselleria de Educación, Universidades y Empleo" (Generalitat Valenciana, Spain). The authors want to thank the Electron Microscopy Service at the UPV for support. I. C. thanks the Instituto de Salud Carlos III for her predoctoral fellowship (IFI21/00008). A.L. thanks to the Ministerio de Universidades for her predoctoral grant (FPU20/05297). **Figure 1** was done with BioRender (ww.biorender.com).

7. References

1. Baker-Austin, C., Trinanes, J. A., Taylor, N. G., Hartnell, R., Siitonen, A., Martinez-Urtaza, J. (2013). *Emerging Vibrio risk at high latitudes in response to ocean warming.* Nature climate change, 3(1), 73-77.
2. Baker-Austin, C., Oliver, J. D. (2018). *Vibrio vulnificus: new insights into a deadly opportunistic pathogen.* Environmental microbiology, 20(2), 423-430.
3. Fleischmann, S., Herrig, I., Wesp, J., Stiedl, J., Reifferscheid, G., Strauch, E., Alter, T., Brennholt, N. (2022). *Prevalence and Distribution of Potentially Human Pathogenic Vibrio spp. on German North and Baltic Sea Coasts.* Front. Cell. Infect. Microbiol., 12, 846819.
4. Amaro, C., Fouz, B., Sanjuán, E., & Romalde, J. L. (2020). *Vibriosis.* In *Climate change and infectious fish diseases* (pp. 182-210). Wallingford UK: CABI.
5. Ceccarelli, D., Amaro, C., Romalde, J. L., Suffredini, E., & Vezzulli, L. (2019). *Vibrio species.* Food microbiology: fundamentals and frontiers, 347-388.
6. Oliver, J. D. (2015). *The biology of Vibrio vulnificus.* Microbiology spectrum, 3(3), 1-10.

7. Dalsgaard, A., Frimodt-Møller, N., Bruun, B., Høi, L., Larsen, J. L. (1996). *Clinical manifestations and molecular epidemiology of Vibrio vulnificus infections in Denmark*. European Journal of Clinical Microbiology and Infectious Diseases, 15, 227-232.
8. Veenstra, J., Rietra, P. J., Stoutenbeek, C. P., Coster, J. M., de Gier, H. H., Dirks-Go, S. (1992). *Infection by an indole-negative variant of Vibrio vulnificus transmitted by eels.* Journal of Infectious Diseases, 166(1), 209-210.
9. Baker-Austin, C., McArthur, J. V., Lindell, A. H., Wright, M. S., Tuckfield, R. C., Gooch, J., Stepanauskas, R. (2009). *Multi-site analysis reveals widespread antibiotic resistance in the marine pathogen Vibrio vulnificus*. Microbial ecology, 57, 151-159.
10. Kassim, N., Mtenga, A. B., Lee, W. G., Kim, J. S., Shim, W. B., & Chung, D. H. (2011). *Production of Coturnix quail immunoglobulins Y (IgYs) against Vibrio parahaemolyticus and Vibrio vulnificus.* Food Science and Biotechnology, 20, 1577-1583.
11. Cantet, F., Hervio-Heath, D., Caro, A., Le Mennec, C., Monteil, C., Quéméré, C., Monfort, P. (2013). *Quantification of Vibrio parahaemolyticus, Vibrio vulnificus and Vibrio cholerae in French Mediterranean coastal lagoons*. Research in microbiology, 164(8), 867-874.
12. Cañigral, I., Moreno, Y., Alonso, J. L., González, A., Ferrús, M. A. (2010*). Detection of Vibrio vulnificus in seafood, seawater and wastewater samples from a Mediterranean coastal area.* Microbiological research, 165(8), 657-664.
13. Harwood, V. J., Gandhi, J. P., Wright, A. C. (2004*). Methods for isolation and confirmation of Vibrio vulnificus from oysters and environmental sources: a review.* Journal of Microbiological Methods, 59(3), 301-316.
14. Surasilp, T., Longyant, S., Rukpratanporn, S., Sridulyakul, P., Sithigorngul, P., Chaivisuthangkura, P. (2011). *Rapid and sensitive detection of Vibrio vulnificus by loop-mediated isothermal amplification combined with lateral flow dipstick targeted to rpoS gene.* Molecular and cellular probes, 25(4), 158-163.
15. Han, F., Wang, F., Ge, B. (2011). *Detecting potentially virulent Vibrio vulnificus strains in raw oysters by quantitative loop-mediated isothermal amplification.* Applied and environmental microbiology, 77(8), 2589-2595.
16. Yang, X., Zhang, X., Wang, Y., Shen, H., Jiang, G., Dong, J., Gao, S. (2020). *A real-time recombinase polymerase amplification method for rapid detection of Vibrio vulnificus in seafood.* Frontiers in microbiology, 11, 586981.

17. Dicle Y, Karamese M. (2024) *Biosensors for the detection of pathogenic bacteria: current status and future perspectives.* Future Microbiol, 19(3). doi: 10.2217/fmb-2023-0182.
18. Fan, S., Ma, C., Tian, X., Ma, X., Qin, M., Wu, H., Wang, S. (2021). *Detection of Vibrio vulnificus in seafood with a DNAzyme-based biosensor.* Frontiers in Microbiology, 12, 655845.
19. Pérez-Roig, A., Ibarlucea, B., Amaro, C., Cuniberti, G. (2024) *Vibrio vulnificus marine pathogen detection with thin-film impedance biosensors.* Biosensors and Bioelectronics: X, 17, 100454.
20. Xiao, X., Lin, Z., Huang, X., Lu, J., Zhou, Y., Zheng, L., Lou, Y. (2021) *Rapid and sensitive detection of Vibrio vulnificus using CRISPR/Cas12a combined with a Recombinase-Aided Amplification Assay*. Frontiers in Microbiology, 12, 767315.
21. Wang, P., Liao, L., Ma, C., Zhang, X., Yu, J., Yi, L., Liu, X., Shen, H., Gao, S., Lu, Q. (2021) *Duplex on-site detection of Vibrio cholerae and Vibrio vulnificus by Recombinase Polymerase Amplification and three-segment lateral flow strips.* Biosensors, 11, 151
22. Pla, L., Lozano-Torres, B., Martínez-Máñez, R., Sancenón, F., Ros-Lis, J. V. (2019). *Overview of the evolution of silica-based chromo-fluorogenic nanosensors.* Sensors, 19(23), 5138.
23. Aznar, E., Oroval, M., Pascual, L., Murguía, J. R., Martinez-Manez, R., Sancenon, F. (2016). *Gated materials for on-command release of guest molecules.* Chemical reviews, 116(2), 561-718.
24. Sancenón, F., Pascual, L., Oroval, M., Aznar, E., Martínez-Máñez, R. (2015). *Gated silica mesoporous materials in sensing applications.* ChemistryOpen, 4(4), 418-437.
25. Baranowska, M., Slota, A. J., Eravuchira, P. J., Macias, G., Xifré-Pérez, E., Pallares, J., Marsal, L. F. (2014*). Protein attachment to nanoporous anodic alumina for biotechnological applications: influence of pore size, protein size and functionalization path.* Colloids and Surfaces B: Biointerfaces, 122, 375-383.
26. Llopis-Lorente, A., Lozano-Torres, B., Bernardos, A., Martínez-Máñez, R., Sancenón, F. (2017*). Mesoporous silica materials for controlled delivery based on enzymes.* Journal of Materials Chemistry B, 5(17), 3069-3083.
27. Pla, L., Xifré-Pérez, E., Ribes, À., Aznar, E., Marcos, M. D., Marsal, L. F., Sancenón, F. (2017). *A mycoplasma genomic DNA probe using gated nanoporous anodic alumina.* ChemPlusChem, 82(3), 337-341.

28. Ribes, A., Santiago-Felipe, S., Avino, A., Candela-Noguera, V., Eritja, R., Sancenon, F., Aznar, E. (2018). *Design of oligonucleotide-capped mesoporous silica nanoparticles for the detection of miRNA-145 by duplex and triplex formation.* Sensors and Actuators B: Chemical, 277, 598-603.
29. Garrido-Cano, I., Pla, L., Santiago-Felipe, S., Simon, S., Ortega, B., Bermejo, B., Martinez-Manez, R. (2021). *Nanoporous anodic alumina-based sensor for miR-99a-5p detection as an effective early breast cancer diagnostic tool.* ACS sensors, 6(3), 1022-1029.
30. Ribes, A., Aznar, E., Santiago-Felipe, S., Xifre-Perez, E., Tormo-Mas, M. Á., Peman, J., Martinez-Manez, R. (2019). *Selective and sensitive probe based in oligonucleotide-capped nanoporous alumina for the rapid screening of infection produced by Candida albicans.* ACS sensors, 4(5), 1291-1298.
31. Pla, L., Santiago-Felipe, S., Tormo-Mas, M. Á., Ruiz-Gaitán, A., Pemán, J., Valentín, E., Martínez-Máñez, R. (2021). *Oligonucleotide-capped nanoporous anodic alumina biosensor as diagnostic tool for rapid and accurate detection of Candida auris in clinical samples.* Emerging microbes & infections, 10(1), 407-415.
32. Pla, L., Santiago-Felipe, S., Tormo-Mas, M. Á., Pemán, J., Sancenon, F., Aznar, E., Martinez-Manez, R. (2020). *Aptamer-capped nanoporous anodic alumina for Staphylococcus aureus detection.* Sensors and Actuators B: Chemical, 320, 128281.
33. Caballos, I., Aranda, M. N., López-Palacios, A., Pla, L., Santiago-Felipe, S., Hernández-Montoto, A., Tormo-Mas, M. A., Pemán, J., Gómez-Ruiz, M. D., Calabuig, E., Sánchez-Sendra, B., Francés-Gómez, C., Geller, R., Aznar, E., Martínez-Máñez, R. (2023) *Aptamer-Capped Nanoporous Anodic Alumina for SARS-CoV-2 Spike Protein Detection.* Adv. Mater. Technol. 8, 2201913
34. Hernández-Montoto, A., Aranda, M. A., Caballos, I., López-Palacios, A., Tormo-Mas, M. A., Pemán, J., Prieto Rodríguez, M., Picornell, C., Aznar, E., Martínez-Máñez, R. (2023) *Human papilloma virus DNA detection in clinical samples using fluorogenic probes based on oligonucleotide gated nanoporous anodic alumina films.* Adv. Healthcare Mater. 12, 2203326
35. Roig, F.J., González-Candelas, F., Sanjuán, E., Fouz, B., Feil, E.J., Llorens, C., Baker-Austin, C., Oliver, J.D., Danin-Poleg, Y., Gibas, C.J., Kashi, Y., Gulig, P.A., Morrison, S.S., Amaro, C. (2018) *Phylogeny of Vibrio vulnificus from the Analysis of the Core-Genome: Implications*

for Intra-Species Taxonomy. Front Microbiol. 8, 2613. doi: 10.3389/fmicb.2017.02613. eCollection 2017. PMID: 29358930

36. Roig, F.J., Sanjuán, E., Llorens, A., Amaro, C. (2010) *pilF Polymorphism-based PCR to distinguish vibrio vulnificus strains potentially dangerous to public health.* Appl Environ Microbiol. 76(5), 1328-33.
37. Pérez-Roig, A., Carmona-Salido, H., Sanjuán, E., Fouz, B., Amaro, C. (2022). *A multiplex PCR for the detection of Vibrio vulnificus hazardous to human and/or animal health from seafood.* International Journal of Food Microbiology, 377, 109778.
38. Ribes, À., Santiago-Felipe, S., Bernardos, A., Marcos, M. D., Pardo, T., Sancenón, F., Aznar, E. (2017). *Two new fluorogenic aptasensors based on capped mesoporous silica nanoparticles to detect ochratoxin A.* ChemistryOpen, 6(5), 653-659.
39. Liang, J. H., Liang, W. H., Deng, Y. Q., Fu, Z. G., Deng, J. L., Chen, Y. H. (2021*). Vibrio vulnificus infection attributed to bee sting: a case report.* Emerging Microbes & Infections, 10(1), 1890-1895.
40. Lee, J. H., Park, S. K., Khan, F., Jo, D. M., Lee, D. H., Kang, M. G., Kim, Y. M. (2022). *Simultaneous isolation and enumeration of virulent Vibrio cholerae and Vibrio vulnificus using an advanced MPN-PCR method*. Archives of Microbiology, 204(1), 5.
41. Bonny, S. Q., Hossain, M. M., Uddin, S. M. K., Pulingam, T., Sagadevan, S., Johan, M. R. (2022). *Current trends in polymerase chain reaction-based detection of three major human pathogenic vibrios.* Critical reviews in food science and nutrition, 62(5), 1317-1335

Nanoporous Oligonucleotide-Capped Alumina Sensors for Rapid Screening of miR-4732-3p

1. Abstract

MicroRNAs (miRNAs) have recently gained interest due to their potential use as diagnostic biomarkers. Many diseases have been associated with its deregulation, such as miR-4732-3p, a molecule associated with cardiovascular stress and cardioprotection. We present herein the development a highly sensitive and selective nanoporous anodic alumina (NAA) biosensor for the detection of this specific biomarker in human serum samples. The NAA pores are capped by oligonucleotides yet the cargo (rhodamine B) is released in the presence of miR-4732-3p. This procedure allows for the detection of miR-4732-3p at low concentration in patient serum samples and a shorter detection time compared to classical methods like qPCR. This sensor holds significant promise for the early detection of cardiovascular stressors, including myocardial ischemia and cardiotoxicity.

2. Introduction

miRNAs, non-coding RNAs, play a crucial role in post-transcriptional gene regulation by fine-tuning gene expression. These miRNAs bind to their mRNA targets, negatively affecting the expression of specific proteins by degrading mRNA or inhibiting its translation. These proteins are related to various pathological processes, such as cardiovascular disease[1] and cancer,[2] and are found in numerous human fluids, including serum and plasma. Given their high level of stability, miRNAs and other non-coding RNAs are emerging as potential biomarkers of cardiotoxicity[3] and therapeutic targets.[4,5]

A recent prospective study evaluated the cardiac function of women who received anthracyclines for the treatment of breast cancer, analyzing postchemotherapy serum samples by sequencing miRNA (miRNA-seq) to determine miR-4732-3p regulation. Anthracycline-induced cardiotoxicity, a serious side effect of chemotherapy caused by oxidative stress in cardiomyocytes, was studied in patients with breast cancer, identifying 25 microRNAs with differentially expressed serum levels among those who developed

cardiotoxicity and those who did not. miR-4732-3p was found to be reduced in patients with cardiotoxicity and showed cardioprotective effects in experimental models.[6]

Traditional methods for detection of miRNAs include real-time PCR (qPCR), which amplifies and quantifies specific miRNAs, yet is laborious, costly and requires sophisticated equipment; hybridization in microarrays, which has lower sensitivity and specificity and may undergo non-specific hybridization;[7] and RNA sequencing (RNA-seq), which while providing detailed information, is costly, complex and requires intensive analysis.[8] Moroever miRNA detection methods face additional problems such as the low abundance of miRNAs, their instability and degradation, and the need for large sample volumes.[9,10] Innovative designs based on nanomaterials, such as colloidal gold biosensors, quantum dots (QDs)[11] and nanopore anodic alumina (NAA) with dyes,[12] offer high sensitivity, specificity and speed, overcoming several limitations of traditional methods and providing more efficient and effective solutions for the detection of miRNAs.

In recent years, nanomaterials have played a crucial role in detection applications due to their ability to provide simple, sensitive, and fast responses to target analytes.[13-17] These materials are notable for their biocompatibility, high internal surface area, high load capacity, and ease of surface modification.[18-21] Specifically, nanoporous alumina (NAA) supports can be functionalized with various organic molecules, acting as "molecular gates" to create stimulus-sensitive systems.[22-25] These materials can serve as probes when loaded with dyes, with their capping mechanism activated only in the presence of the target analyte, thereby offering high sensitivity and rapid results with minimal sample preparation. Recent studies have demonstrated the effectiveness of these molecular gate-based biosensors for miRNA detection. For instance, we have recently developed a nanomaterial for detecting miRNA-145 for diagnostic purposes.[26] Similarly, we developed a system for detecting downregulated miR-99a-5p in plasma, capable of distinguishing healthy controls from breast cancer patients with high efficiency and accuracy, even in the early stages of the disease.[27] To utilize circulating miRNAs for diagnosis effectively, it is essential to develop methods that are simple, rapid, effective, and low-cost, taking advantage of the signal amplification effect of these nanomaterials.

The use of gated-NAA materials with oligonucleotides has been consolidated as an option in the development of biosensors, standing out for its ability to achieve significant signal amplification by releasing multiple signaling molecules trapped by a few analyte molecules.[28-30] In this scenario, we report herein an innovative strategy for the detection of miRNA-4732-3p based on these principles. By designing a specific oligonucleotide that hybridizes selectively with miR-4732-3p sequences, we have developed a system where NAA nanopores, loaded with rodamine B, are capped, thus preventing the release of the dye. However, the presence of miR-4732-3p induces the release of the dye, generating an observable fluorescent signal. Our system has demonstrated high selectivity and sensitivity to detect miR-4732-3p in 60 minutes, and the biosensor has been validated in plasma samples from both healthy adults and cancer patients. This promising approach offers early and accurate detection of biomarkers relevant to human health, overcoming the limitations of traditional methods such as PCR by providing rapid results, sensitive and specific with reduced processing time and minimal sample handling.

3. Results and discussion

3.1. General techniques

High-resolution field emission scanning electron microscopy (HR-FESEM) was used to characterize NAA surfaces. NAA systems were fixed to aluminum disks using carbon cement. The images were captured with a high-resolution field emission scanning electron microscope (ZEISS GeminiSEM 500) operating at 5 kV. The atomic composition of the surfaces was analyzed using energy dispersion X-ray spectroscopy (EDXS), using an X-ray detector attached to the microscope.

3.2. Chemicals

The following reactiveswere obtained from Sigma-Aldrich Quimica (Madrid, Spain): tris(hydroxymethyl)aminomethane (TRIS), hydrochloric acid, (3-aminopropyl) triethoxysilane (APTES), and rhodamine B. InRedox NAA scaffolds were obtained from

Longmont, Colorado, USA. Thermo Fisher Scientific (Waltham, MA) provided the 5' -TTT TGG GGG GCA GAA CAG GAC AGG TCA GGG CGG GGG GTT TT -3' sequence for miR-4732-3p (obtained from mirbase.org) and MiRvana mimic of miR-16-5p.

3.3. Synthesis of materials S1 and S2

To develop **S1**, 24 NAA scaffolds (2 mm in diameter) were immersed in a toluene solution of (3-aminopropyl)triethoxysilane (0.22 mmol). Afterwards, the supports were washed with eight mL of toluene followed by eight mL of pure acetone, and dried overnight at 60°C. In the following step, **S1** nanomaterials were immersed in a solution of rhodamine B in anhydrous acetonitrile (1 mM) and then treated with TRIS hybridization buffer (20 mM Tris-HCl, 37.5 mM MgCl2, pH 7.5) containing capping oligonucleotide **O1** for 1 hour under agitation at 37°C. Finally TRIS hybridization buffer was used to wash the final **S2** biosensors.

3.4. Cargo Quantification

The amount of loaded rhodamine B in the pores was determined by immersing two S2 supports in 1 mL of TRIS buffer. To induce maximum cargo delivery, one of the supports was stirred at 90 °C for 1 h. In the control experiment, another support was stirred at 25 °C for 1 h. A calibration curve was used to determine the fluorophore released (λ_{exc} = 555 nm, λ_{em} = 575 nm). Triplicates were carried out in this experiment.

3.5. Assay protocol

Typical assays involved submerging two separate **S2** solids in separate solutions containing 900 µL of TRIS. Following this, 100 µL of miRNA-4732-3p (1µM) or hybridization buffer (control) were added to the solids and agitated for 1 hour at 37°C taking aliquots every 15 minutes. A fluorescence measurement at 575 nm was used to monitor the release of rhodamine B (λ_{exc} = 555 nm). Exteriments were performed in triplicate.

S2 was also evaluated in human serum media in response to increasing miRNA-4732-3p concentrations. For this, eight prepared **S2** materials were submerged separately in 250 µL of serum from healthy controls plus 750 uL of TRIS buffer, to which 100 uL of

different concentrations of miRNA-4732-3p (between 0 and 1000 nM) were added. Following 60 minutes of stirring at room temperature, aliquots were obtained at 0 and 60 minutes. Lastly, fluorescence emission at 575 nm (λ_{exc} = 555 nm) was used to determine the released rhodamine B. A total of 24 **S2** supports were used in triplicate in the experiment.

3.6. Amplification assay

In order to measure the signal amplification, two **S2** solids were soaked in 900 µL of hybridization buffer. Afterwards, 100 µL of miRNA-4732-3p (1 µM) were added to one support. On the second support, 100 µL of TRIS buffer was added as a control. Incubation of solids at 37 °C for one hour was followed by measurement of the fluorescence (λ_{exc} = 555 nm, λ_{em} = 585 nm). Calibration curves were used to determine the amount of dye released.

3.7. Selectivity

For the evaluation of the selectivity of the nanosensor, **S2** supports were exposed to target miRNA-4732-3p as well as miRNAs such as miR-99a-5p, miR-30b-5p, and miR-16-5p (final concentration of 10^{-1} µM), which were each mixed in a final volume of 1 mL of TRIS hybridization buffer, and tested under constant stirring for 1 h at 37 °C. As a negative control, 1 mL of TRIS hybridization buffer was tested. Rhodamine B delivery was determined by fluorescence at 575 nm (λ_{exc} = 555 nm). An average of 12 **S2** support were used in triplicate for the experiment.

3.8. Patients

The observational study was conducted in a prospective cohort of 26 patients with breast cancer at Hospital Universitari i Politècnic La Fe. All patients were >18 years of age and were enrolled after informed consent. Serum samples were obtained af different timepoints from the beginning of treatment and were stored at -80ºC at the HUiPLaFe Biobank.

3.9. Analysis of clinical samples

Expression of miR-4732-3p was carried out using real-time quantitative PCR (qPCR) and nanoporous oligonucleotide coated alumina sensors. Blood tubes containing ethylenediaminettraacetic acid (EDTA) were centrifuged at 2000 rpm for 10 minutes at 4°C. The plasma upper phase was stored at -80 °C until later use.

- The miRNA isolation was performed from 250µl of serum using the miRNeasy mini kit (Qiagen), reverse transcription was performed using the miRCURY LNA™ Universal RT miRNA PCR Kit, and quantification was performed using the miRCURY LNA™ Universal RT miRNA PCR Kit (both from Exiqon A/S, Vedbaek, Denmark). Real-time qPCR was performed using the ViiA TM 7 Real-Time PCR System, and analyzed with the QuantStudio Real-Time PCR Software and DataAssist v3.01 (both from Applied Biosystems, Carlsbad, CA).
- The validation analysis was performed by adding 100 µL of serum to a support **S2** and diluting it in 300 µL of hybridization buffer (final test volume 400 µL). At 37°C, the supports were agitated for an hour. Delivery of rodamine B was determined by fluorescence (λ_{exc} = 555 nm, λ_{em} = 585 nm). Negative control was TRIS buffer.

3.10. Ethical committee

The clinical study was approved by the Ethics Committee of the Instituto de Investigación Sanitaria La Fe (2012/0452) according to the principles of the Declaration of Helsinki.

4. Conclusion

In the clinical field, it is increasingly important to develop new strategies for sensitive and label-free detection of miRNAs. Here we present a DNA-gated mesoporous biosensor to detect miR-4732-3p, a biomarker of cardiotoxicity and heart failure. An oligonucleotide that specifically hybridizes to miR-4732-3p is used to cap the pores of NAA previously loaded with rhodamine B and functionalised with amino groups. We demonstrate that the system is caped (no dye is released), however the cargo is released in the presenc of the target miRNA (i.e. miR-4732-3p). A high level of selectivity and sensitivity was achieved with a LOD as low as 1 nM. We demonstrate that our method can be used directly with serum to detect miR-4732-3p without the need for miRNA isolation or retrotranscription, making it faster than conventional techniques, in addition to being more cost-effective and using low-cost equipment. Our results highlight the potential of our biosensor for early detection of anthracycline-associated cardiotoxicity by identifying circulating miR-4732-3p, which could improve prognosis and reduce costs associated with more radical treatments. This strategy can be extrapolated to develop nanostructured devices to detect other circulating target miRNAs.

5. Results and discussion

5.1. Development and characterization of sensing system

In this study, we developed a rapid, reliable, and easy-to-use tool for detecting circulating miR-4732-3p in clinical samples. This was accomplished by loading rhodamine B into pores of NAA support. **S1** was obtained by functionalizing the external surface with APTES and **S2** was obtained by capping the pores in **S1** with oligonucleotide **O1** via the formation of strong electrostatic interactions between the the positively charged amines in the support and the negatively charged oligonucleotide. The system was developed to allow the delivery of entrapped rhodamine B in the presence of miR-4732-3p (**Figure 1**).

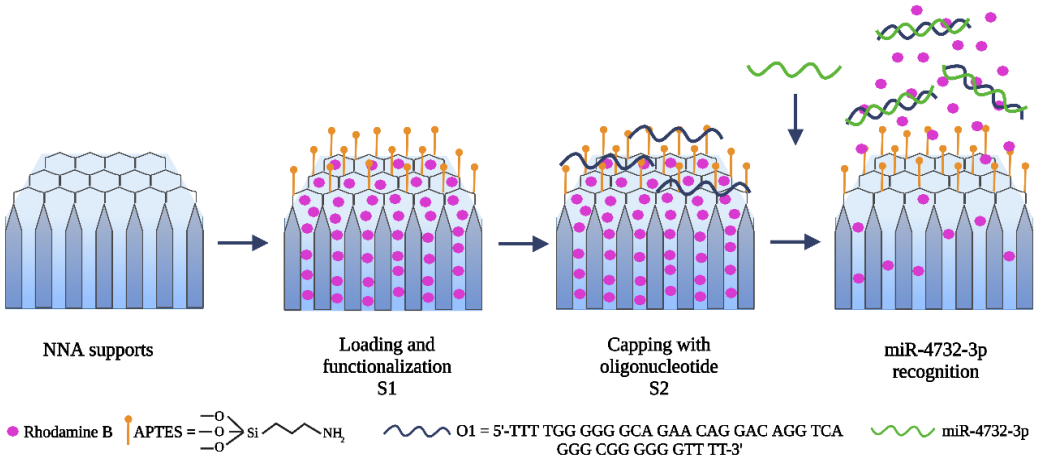

Figure 1. Representation of **S2** material preparation and sensing. Solid **S1** was obtained by loading rhodamine B onto nanoporous anodic alumina (NAA) and functionalization with APTES. **S2** was obtained by the interaction of **S1** with a miR-4732-3p-binding oligonucleotide. MiRNA recognition induces rhodamine B delivery.

EDX and FESEM analysis were carried out on NAA raw materials **S1**, and **S2**. NAA supports available commercially are composed of anodic aluminum oxide films overlaid with 0.1 mm thick aluminum layers with pore densities of $9x10^{11}$ cm^{-2}. In the funnel-shaped pores, the size of the pores gradually decreases from the top to the bottom, starting at 20-30 nm and ending at 5 nm. Under this depth, the pore configuration becomes uniform along 10 µm, reaching a profundity of 15 nm. **Figure 2** shows the porous structure of the NAA scaffold and **S2** containing an external layer attributed to the presence of the capping **O1** oligonucleotide.

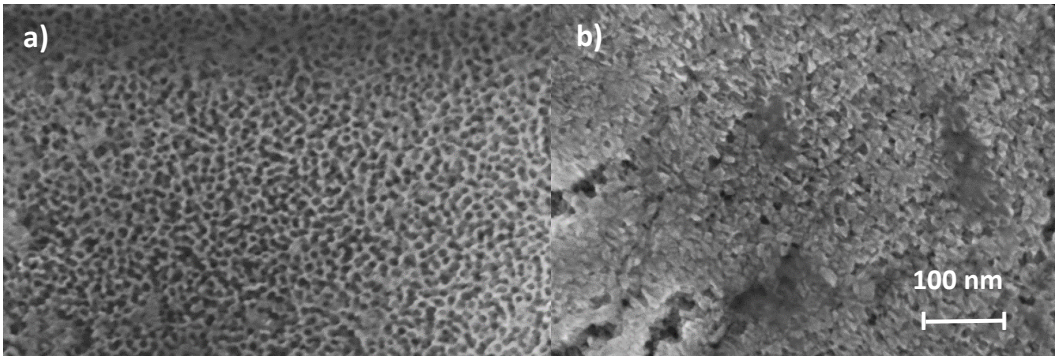

Figure 2. The NAA support (a) and solid **S2** (b) in FESEM. Photographs of the solids are included as insets.

X-ray energy-dispersive spectroscopy was used to determine the organic content of successively prepared materials (**S1**, and **S2**). As a result of APTES functionalization and the loading of Rhodamine B dye, **S1** has high carbon (C/Al) and nitrogen (N/Al) contents. The amounts decreased for **S2** due to dye leakage during the capping process with **O1** and to incomplete blockage of some of the pores. Phosphorus was detected in the final material **S2** (P/Al) as opposed to NAA or **S1** and evidence the presence of the capping oligonucleotide **O1** (**Table 1**).

Table 1. Study of EDX data on the atomic element ratios in various prepared solids.

	C/Al	N/Al	P/Al
S1	2.33	0.37	
S2	0.76	0.40	0.02

5.2. Delivery kinetics

A preliminary in vitro study was conducted to detect miR-4732-3p. For this, **S2** was immersed in a solution containing 10^{-1} µM of miR-4732-3p in TRIS buffer ir in a control TRIS buffer solution. Incubation for 1 h was followed by fluorescence measurement to determine rhodamine B release. The delivery profiles of rhodamine B from **S2** in the presence and the absence of miR-4732-3p are shown in **Figure 3**. Dye delivery from **S2** in hybridization buffer is remarkably low (about 10% of the maximum amount of released

fluorophore, as illustrated in curve a). In contrast, miR-4732-3p causes much higher levels of rhodamine B delivery (10-fold at 60 min, curve b).

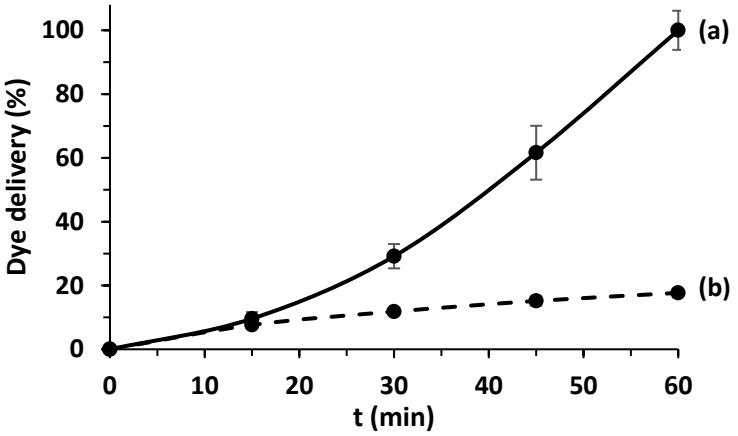

Figure 3. Rhodamine B release from solid **S2** (a) in the absence or (b) in the presence of miR-4732-3p (10^{-1} μM). Mean ± standard deviation (SD).

Recent research has shown that in similar gated matrials a unique DNA molecule can deliver about 10^4–10^{11} dye molecules upon pore opening.[24,29] Also, other studies have shown that miRNA detection can induce an average release of 2×10^{11} rhodamine B molecules.[26] In this work, miR-4732-3p at 1 nM induces the release of 1×10^{10} molecules of rhodamine B from **S2** highlighting the efficiency of signal amplification.

5.3. Analytical performance: sensitivity, specificity and robustness studies

In order to assess the method's sensitivity, we measured **S2**'s response to different concentrations of miRNA-4732-3p at 60 minutes. The results show (**Figure 4**) that the rhodamine B released is proportional to the concentration of miR-4732-3p, which confirms the uncapping protocol shown in **Figure 1**. A linear response was observed at 10^{-3}-10^4 nM concentrations, and 1 nM was determined as the limit of detection (LOD). This LOD is below the range of the circulating miRNA concentration in human plasma, which usually ranges from femtomolar to nanomolar. This suggests the possible use of the proposed system for the detection of miRNA in clinical samples.[31]

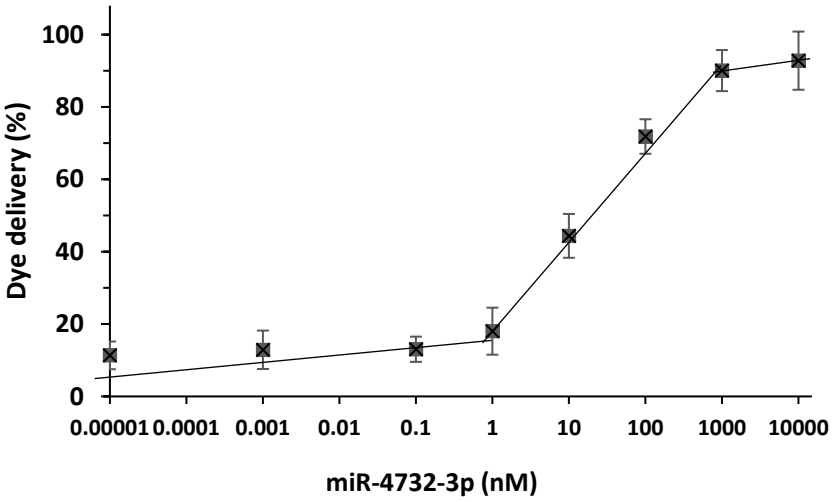

Figure 4. Rhodamine B release from **S2** support in TRIS buffer (pH 7.4) at different concentrations of miR-4732-3p. Mean ± SD.

Further selectivity experiments confirmed the detection of miR-4732-3p using **S2** in contrast to the inability of the biosensor to detect other miRNAs such as miR-16-5p, miR-991-5p or miR-30b-5p (**Figure 5**).

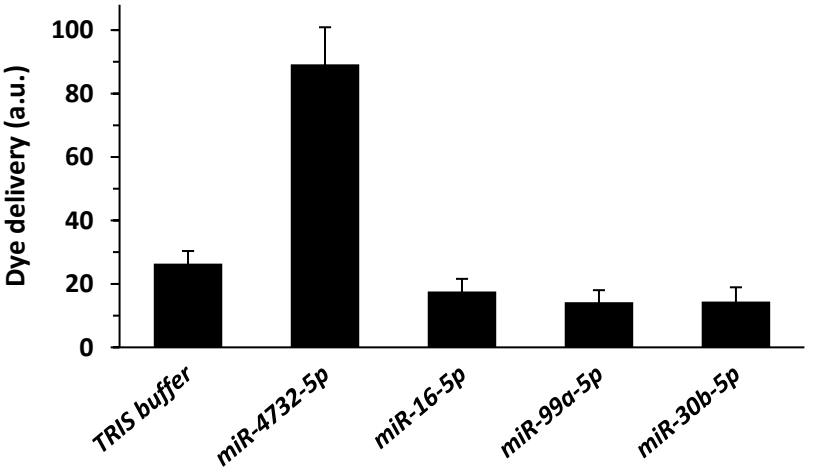

Figure 5. Proposed method's selectivity. Fluorescence of rhodamine B released from **S2** supports in the presence of 10^{-1} μM miR-4732-3p, miR-16-5p, miR-99a-5p, miR-30b-5p, and TRIS buffer. Mean ± SD.

5.4. Validation in clinical samples

Driven by earlier encouraging results, we went on to validate the suitability of nanodevices in real clinical samples. In this sense, miR-4723-3p was detected in the serum of 26 patients using the biosensor **S2** and qRT-PCR. The miR-4723-3p signal observed (in a.u.) was compared for both methods (**Figure 6**). Our findings revealed a coincidence between the rodamine B release pattern and circulating levels of miR-4723-3p in the patients' serum, as obtained by qRT-PCR.

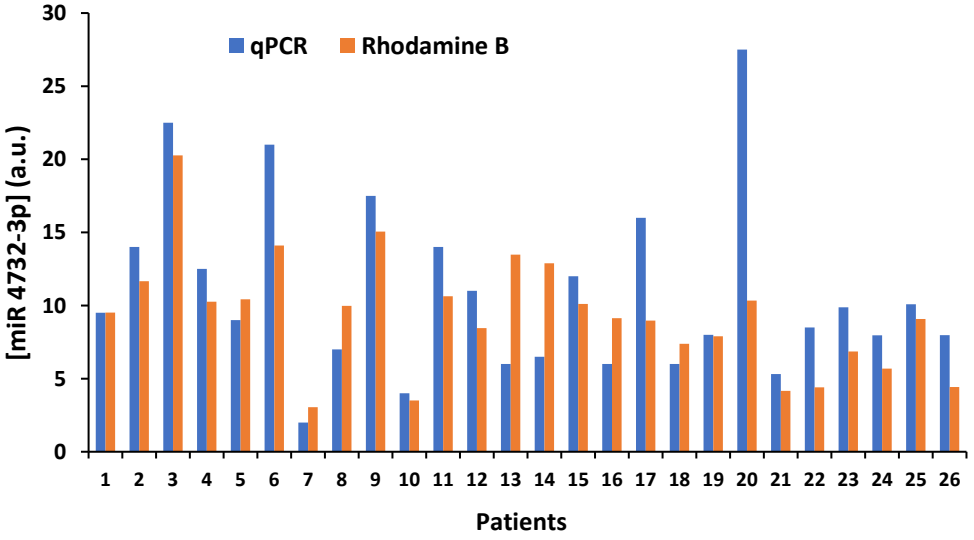

Figure 6. The trend of miR-4732-3p concentration levels in arbitrary units is shown by qPCR and release of rhodamine B by **S2** biosensors in serum from 26 patients.

The line graph in **Figure 6** compares the results of the qPCR method (blue line) with the molecular gate method that releases rodamine B (orange line) in terms of concentration [miR 4732-3p] in different patient sera (1 to 26). Both lines exhibit similar patterns in most of the samples, suggesting that both methods detect comparable trends in concentrations. Although qPCR shows higher values in several samples in absolute terms, in some, such as 12 and 14, the values are practically identical, indicating a close agreement between the two methods.

By contrasting the molecular gate method that releases rodamine B with qPCR in terms of miR 4732-3p concentration, it is concluded that the former has significant advantages in terms of detection speed, lower cost and ease of handling samples. The graph illustrates that the gated material detects miR 4732-3p concentrations in a significantly shorter time than qPCR (30 minutes in front of 5-7 hours), which makes it especially useful in hospital settings that demand rapid responses for clinical decisions. In addition, by requiring fewer resources and being less costly, this method could be more accessible to hospitals with limited budgets. Finally, the reduced sample handling required for method using **S2** makes it ideal for any laboratory staff, increasing its practicality and usefulness in clinical environments.

Other researchers have also developed fluorescence biosensors to detect miRNA. For example, Aw et al. designed a conformation-induced fluorescence method with a detection limit (LOD) close to 1 μM,[32] while Chen et al. developed a 100 nM switch-conversion ratiometric fluorescence biosensor.[33] In addition, new miRNA detection strategies have also been tested in serum patients, such as the Hizir team, who used nanographene oxide to detect miR-21 and miR-141 in serum (LOD 1.2 nM),[34] and Li's group, who employed rolling circle amplification with a fork probe to detect miR-486-5p in lung cancer samples.[35] However, our DNA-controlled mesoporous biosensor for the detection of miR-4732-3p reaches an LOD as low as 1 nM directly in serum, which introduces a new technology that could boost the next generation of minimally invasive diagnostic and complementary tests.

6. Acknowledgements

This research was supported by project PID2021-126304OB-C41 funded by MCIN/ AEI /10.13039/501100011033/ and by European Regional Development Fund - A way of doing Europe. This work has received funding from the European Union's Horizon 2020 research and innovation programme under grant agreement No 899708. This research was supported by CIBER -Consorcio Centro de Investigación Biomédica en Red- (CB06/01/2012), Instituto de Salud Carlos III, Ministerio de Ciencia e Innovación. This

study forms part of the Advanced Materials programme (MFA/2022/049) and was supported by MCIN with funding from European Union NextGenerationEU (PRTR-C17.I1) and by Generalitat Valenciana. The study was also supported by the grants PID 2020-120619RBI00 funded by MCIN/AEI/10.13039/501100011033 and CIAICO/2021/293 funded by "Conselleria de Educación, Universidades y Empleo" (Generalitat Valenciana, Spain). The authors want to thank the Electron Microscopy Service at the UPV for support. I. C. thanks the Instituto de Salud Carlos III for her predoctoral fellowship (IFI21/00008). A.L. thanks to the Ministerio de Universidades for her predoctoral grant (FPU20/05297). **Figure 1** was done with BioRender (ww.biorender.com).

7. References

1. Van Rooij, E., Sutherland, L. B., Liu, N., Williams, A. H., McAnally, J., Gerard, R. D., & Olson, E. N. (2006). *A signature pattern of stress-responsive microRNAs that can evoke cardiac hypertrophy and heart failure.* Proceedings of the National Academy of Sciences, 103(48), 18255-18260.
2. Allegra, A., Alonci, A., Campo, S., Penna, G., Petrungaro, A., Gerace, D., & Musolino, C. (2012). *Circulating microRNAs: new biomarkers in diagnosis, prognosis and treatment of cancer.* International journal of oncology, 41(6), 1897-1912.
3. Leger, K. J., Leonard, D., Nielson, D., de Lemos, J. A., Mammen, P. P., & Winick, N. J. (2017). *Circulating micro RNA s: Potential Markers of Cardiotoxicity in Children and Young Adults Treated With Anthracycline Chemotherapy.* Journal of the American Heart Association, 6(4), e004653.
4. Han, D., Wang, Y., Wang, Y., Dai, X., Zhou, T., Chen, J., & Cao, F. (2020). *The tumor-suppressive human circular RNA CircITCH sponges miR-330-5p to ameliorate doxorubicin-induced cardiotoxicity through upregulating SIRT6, survivin, and SERCA2a.* Circulation research, 127(4), e108-e125.
5. Tong, Z., Jiang, B., Wu, Y., Liu, Y., Li, Y., Gao, M., & Xiao, X. (2015). *MiR-21 protected cardiomyocytes against doxorubicin-induced apoptosis by targeting BTG2.* International journal of molecular sciences, 16(7), 14511-14525.
6. Sánchez-Sánchez, R., Reinal, I., Peiró-Molina, E., Buigues, M., Tejedor, S., Hernándiz, A., & Sepúlveda, P. (2022). *MicroRNA-4732-3p is dysregulated in breast cancer patients with*

cardiotoxicity, and its therapeutic delivery protects the heart from doxorubicin-induced oxidative stress in rats. Antioxidants, 11(10), 1955.

7. Mohammadi-Yeganeh, S., Paryan, M., Mirab Samiee, S., Soleimani, M., Arefian, E., Azadmanesh, K., & Karimipoor, M. (2013). *Development of a robust, low cost stem-loop real-time quantification PCR technique for miRNA expression analysis.* Molecular biology reports, 40, 3665-3674.
8. Motorin, Y. y Helm, M. (2023). *General principles and limitations for the detection of RNA modifications by sequencing.* Chemical Research Accounts, 9950-9964.
9. Tian, T., Wang, J., & Zhou, X. (2015). *A review: microRNA detection methods.* Organic & biomolecular chemistry, 13(8), 2226-2238.
10. Al-Hawary, S. I. S., Saleh, R. O., Mansouri, S., Noraldeen, S. A. M., Alawadi, A. H., Kareem, A. H., & Mustafa, Y. F. (2024). *Isothermal amplification methods in cancer-related miRNA detection; a new paradigm in study of cancer pathology.* Pathology-Research and Practice, 254, 155072.
11. Harshita, Wu, H. F., & Kailasa, S. K. (2023). *Recent advances in nanomaterials-based optical sensors for detection of various biomarkers (inorganic species, organic and biomolecules).* Luminescence, 38(7), 954-998.
12. Rajeev, G., Prieto Simon, B., Marsal, L. F., & Voelcker, N. H. (2018). *Advances in nanoporous anodic alumina-based biosensors to detect biomarkers of clinical significance: a review.* Advanced Healthcare Materials, 7(5), 1700904.
13. El Sayed, S., Giménez, C., Aznar, E., Martínez-Máñez, R., Sancenón, F., & Licchelli, M. (2015). *Highly selective and sensitive detection of glutathione using mesoporous silica nanoparticles capped with disulfide-containing oligo (ethylene glycol) chains.* Organic & biomolecular chemistry, 13(4), 1017-1021.
14. Garrido, E., Climent, E., Marcos, M. D., Sancenón, F., Rurack, K., & Martínez-Máñez, R. (2022). *Dualplex lateral flow assay for simultaneous scopolamine and "cannibal drug" detection based on receptor-gated mesoporous nanoparticles.* Nanoscale, 14(37), 13505-13513.
15. de Luis, B., Morellá-Aucejo, Á., Llopis-Lorente, A., Martínez-Latorre, J., Sancenón, F., López, C., & Martínez-Máñez, R. (2022). *Nanoprogrammed Cross-Kingdom Communication Between Living Microorganisms.* Nano Letters, 22(5), 1836-1844.

16. Otri, I., Medaglia, S., Aznar, E., Sancenón, F., & Martínez-Máñez, R. (2022). *Fluorogenic Detection of Human Serum Albumin Using Curcumin-Capped Mesoporous Silica Nanoparticles.* Molecules, 27(3), 1133.
17. de Luis, B., Llopis-Lorente, A., Rincón, P., Gadea, J., Sancenón, F., Aznar, E., & Martínez-Máñez, R. (2019). *An interactive model of communication between abiotic nanodevices and microorganisms.* Angewandte Chemie International Edition, 58(42), 14986-14990.
18. Ribes, À., Aznar, E., Bernardos, A., Marcos, M. D., Amorós, P., Martínez-Máñez, R., & Sancenón, F. (2017). *Fluorogenic sensing of carcinogenic bisphenol A using aptamer-capped mesoporous silica nanoparticles.* Chemistry–A European Journal, 23(36), 8581-8584.
19. García-Acosta, B., Comes, M., Bricks, J. L., Kudinova, M. A., Kurdyukov, V. V., Tolmachev, A. I., & Amorós, P. (2006). S*ensory hybrid host materials for the selective chromo-fluorogenic detection of biogenic amines.* Chemical communications, (21), 2239-2241.
20. Butt, M. A. (2024). *Racetrack Ring Resonator-Based on Hybrid Plasmonic Waveguide for Refractive Index Sensing.* Micromachines, 15(5), 610.
21. Ribes, A., Santiago-Felipe, S., Avino, A., Candela-Noguera, V., Eritja, R., Sancenon, F., & Aznar, E. (2018). *Design of oligonucleotide-capped mesoporous silica nanoparticles for the detection of miRNA-145 by duplex and triplex formation.* Sensors and Actuators B: Chemical, 277, 598-603.
22. Pla, L., Aviñó, A., Eritja, R., Ruiz-Gaitán, A., Pemán, J., Friaza, V., & Santiago-Felipe, S. (2020). *Triplex hybridization-based nanosystem for the rapid screening of Pneumocystis pneumonia in clinical samples.* Journal of Fungi, 6(4), 292.
23. Caballos, I., Aranda, M. N., López-Palacios, A., Pla, L., Santiago-Felipe, S., Hernández-Montoto, A., & Martínez-Máñez, R. (2023). *Aptamer-Capped Nanoporous Anodic Alumina for SARS-CoV-2 Spike Protein Detection.* Advanced Materials Technologies, 8(11), 2201913.
24. Pla, L., Santiago-Felipe, S., Tormo-Mas, M. Á., Peman, J., Sancenon, F., Aznar, E., & Martinez-Manez, R. (2020). *Aptamer-capped nanoporous anodic alumina for Staphylococcus aureus detection.* Sensors and Actuators B: Chemical, 320, 128281.
25. Pla, L., Xifré-Pérez, E., Ribes, À., Aznar, E., Marcos, M. D., Marsal, L. F., & Sancenón, F. (2017). *A mycoplasma genomic DNA probe using gated nanoporous anodic alumina.* ChemPlusChem, 82(3), 337-341.

26. Garrido-Cano, I., Pla, L., Santiago-Felipe, S., Simon, S., Ortega, B., Bermejo, B., & Martinez-Manez, R. (2021). *Nanoporous anodic alumina-based sensor for miR-99a-5p detection as an effective early breast cancer diagnostic tool.* ACS sensors, 6(3), 1022-1029.
27. Ribes, À., Xifré-Pérez, E., Aznar, E., Sancenón, F., Pardo, T., Marsal, L. F., & Martínez-Máñez, R. (2016). *Molecular gated nanoporous anodic alumina for the detection of cocaine.* Scientific Reports, 6(1), 38649.
28. Xifre-Perez, E., Ferre-Borrull, J., & Marsal, L. F. (2022). *Oligonucleotic probes and immunosensors based on nanoporous anodic alumina for screening of diseases.* Advanced Materials Technologies, 7(9), 2101591.
29. Pla, L., Santiago-Felipe, S., Tormo-Mas, M. Á., Ruiz-Gaitán, A., Pemán, J., Valentín, E., & Martínez-Máñez, R. (2021). *Oligonucleotide-capped nanoporous anodic alumina biosensor as diagnostic tool for rapid and accurate detection of Candida auris in clinical samples.* Emerging microbes & infections, 10(1), 407-415.
30. Pla, L., Martínez-Bisbal, M. C., Aznar, E., Sancenón, F., Martínez-Máñez, R., & Santiago-Felipe, S. (2021). *A fluorogenic capped mesoporous aptasensor for gluten detection.* Analytica Chimica Acta, 1147, 178-186.
31. Ragan, C., Zuker, M., & Ragan, M. A. (2011). *Quantitative prediction of miRNA-mRNA interaction based on equilibrium concentrations.* PLoS computational biology, 7(2), e1001090.
32. Aw, S. S., Tang, M. X., Teo, Y. N., & Cohen, S. M. (2016). *A conformation-induced fluorescence method for microRNA detection.* Nucleic acids research, 44(10), e92-e92.
33. Chen, X., Xu, K., Li, J., Yang, M., Li, X., Chen, Q., & Yang, H. (2020). *Switch-conversional ratiometric fluorescence biosensor for miRNA detection.* Biosensors and Bioelectronics, 155, 112104.
34. Hizir, M. S., Balcioglu, M., Rana, M., Robertson, N. M., & Yigit, M. V. (2014). *Simultaneous detection of circulating oncomiRs from body fluids for prostate cancer staging using nanographene oxide.* ACS applied materials & interfaces, 6(17), 14772-14778.
35. Li, Y., Liang, L., & Zhang, C. Y. (2013). *Isothermally sensitive detection of serum circulating miRNAs for lung cancer diagnosis.* Analytical chemistry, 85(23), 11174-11179.

Overall discussion

The search for reliable tools to detect specific biomolecules quickly and selectively is currently in the spotlight, driven by the need for systems capable of producing quantifiable results in a short period of time. Gated systems offer a distinct advantage, given their unique structural attributes, which enable the efficient loading and controlled release of diverse molecules like dyes, fluorophores, drugs, and their release in response to analytes. This versatility extends their utility across multiple domains, including medicine, agriculture, and sensing applications. Consequently, gated systems has assumed significant relevance in the detection arena, offering viable solutions to persisting challenges such as enhancing detection sensitivity and reducing non-specific effects. More concretely, within the realm of detection, NAA systems merge as notable players, primarily due to their favorable physicochemical characteristics. In this context, the present doctoral thesis has deepened into the design, characterization, and assessment of intelligent nanodevices triggered by biomolecules, leveraging NAA functionalized with various biological entities as molecular gates.

All systems presented in this study share a common structural approach to their preparation and operation. These methods involve the precise functionalization of mesoporous supports to allow oligonucleotides to adhere either covalently or electrostatically. These interactions play a crucial role in regulating the diffusion of a encapsulated reporter molecule, depending on the presence of a specific analyte. The validation of these detection probes in real-world samples has demonstrated their effectiveness, which advances in their potential practical application. The detection systems developed in this study include:

- Environmental application (use as a reporter of climate change):
    1. Development of a gated nanomaterial for a rapid and reliable detection of *Vibrio vulnificus* bacterium in water samples.
- Diagnosis application (use in clinical diagnosis):
    2. Development of an innovative nanoprobe for rapid and precise detection of the Human Papilloma Virus in clinical samples.
    3. Design and optimization of a nanoporous sensor based on anodic alumina for rapid screening of miR-4732-5p.

The current diagnostic techniques to identify diseases in patients are mainly based on the direct evaluation of clinical symptoms, being some of these diverse and variable, which requires the use of different analytical methods. Unfortunately, some conventional diagnostic methods are associated with invasive procedures and can often result in ambiguous results after prolonged analysis, which affects patient care. This problem extends to diseases caused by microorganisms, where innovative and accurate detection technologies are needed. The methods currently used to identify pathogenic microorganisms fall into several categories:

- Molecular biology techniques: These methods are based on the detection of unique nucleotide sequences (DNA or RNA). Examples include RT-PCR (reverse PCR transcription), isothermal amplification, such as LAMP (loop-mediated isothermal amplification), for amplification and detection of miRNA, and PCR, which has high sensitivity and specificity but is associated with long analysis times, expensive equipment and reagents and a demand for highly qualified personnel.
- Microbiological culture: Microorganisms are grown in liquid or solid media under specific conditions with minimum incubation periods of 12 hours, with subsequent visual observation of colonies by experienced personnel. In addition, further confirmation by additional techniques or specific crops is often required.
- Immunological and serological detection: These techniques use antibodies to detect specific biomolecules, often using ELISA assays or specialized kits. However, these methods require expensive eqipment and reagents. Serological approaches also face challenges, as they include delayed immune responses after infection and ineffective outcomes in immunocompromised patients.

In the field of detection techniques, although the previously mentioned methods offer advantages such as sensitivity and selectivity, they are not free from limitations, which requires the development of new, faster, more cost-effective and reliable detection systems. Even commercialized tests, despite their usefulness, are not universally considered 100% reliable. This thesis has been dedicated to making contributions to the development of innovative protocols and nanodevices for the early detection of diseases

and climate change. Notable features of the sensor materials devised in this research include:

- **Versatility**: These systems have been subtly modified for the detection of different bioanalytes, which could allow detect multiple molecules at once, by combining mesoporous supports functionalized by different DNA sequences.
- **Fastness/Speed response:** With less than one hour for gate opening and cargo diffusion, evaluations are more efficient.
- **Robustness/Efficacy:** Developed systems have been validated in real samples, proving to be functional even in complex matrix environments.
- **Signal Amplification:** Signals are self-amplified, where a minimal number of analyte molecules causes a significant amount of fluorescent reporter molecules to be released. Analyte-to-reporter enhancement ratios can be very high, eliminating the need for DNA amplification and replication typically required by other analytical techniques.
- **Cost-effective and easy-to-use solution:** As routine analytical tools, these sensing systems are highly suitable due to their affordability. The instruments are user-friendly, can be portable, and do not require qualified personnel or expensive equipment.

Chapter three of this doctoral thesis presents an innovative collection of 9 coated NAA supports, designed to identify up to 14 different types of high-risk HPV in clinical samples. These sensors, developed by incorporating specific oligonucleotides on the surface of NAA supports, allow the precise and specific detection of viral DNA, based on the delivery of a fluorescent dye in the presence of complementary oligonucleotides. Extensive clinical sample testing demonstrated the ability of these sensors to effectively identify up to 14 high-risk HPV types, offering multiplexing screening for HPV infections with very high negative predictive values. In addition, the production of the sensors was optimized by external modification of the surface of the nanoporous materials, following a protocol that guarantees its reproducibility and scalability, which has the potential to significantly improve HPV screening and prevention programs globally. In the fourth chapter, we have developed and tested a highly selective and sensitive fluorogenic

biosensor to detect *V. vulnificus* using nanoporous materials and specific DNA sequences. This biosensor uses NAA scaffolding loaded with RhB and coated with a specific oligonucleotide for *V. vulnificus.* Interaction with the DNA of the target bacterium causes the opening of pores and the release of RhB, which allows the detection of the pathogen. The biosensor demonstrated high selectivity for *V. vulnificus*, no cross-reactivity with other Vibrio species, and detection limits comparable to the most advanced methods. Effective in clinical and environmental samples, this design is adaptable for the detection of multiple Vibrio species, highlighting its versatility for public health and environmental monitoring.

The fifth chapter of this thesis presents an innovative nanoporous biosensor controlled by DNA for the diagnosis of cardiotoxicity, based on the detection of miR-4732-3p. This biosensor uses a specific oligonucleotide that hybridizes with miR-4732-3p and binds to a NAA nanostructure with pores loaded with RhB. The presence of miR-4732-3p uncap the pores, releasing the reporter and generating a fluorescent signal proportional to its concentration. The biosensor demonstrates high selectivity and sensitivity, with an extremely low detection limit, and is simple and portable, ideal for use in clinical laboratories and patient care points. These nanodevices have great potential to be applied in the diagnosis and monitoring of cardiotoxicity and heart failure, and future research will focus on their clinical validation and adaptation to detect other biomarkers associated with diseases.

The development of nanosensors based on oligonucleotides represents a significant advance in the detection of biomarkers of both clinical and environmental interest, offering notable advantages over traditional methods:

- **Improved accuracy and sensitivity:**
  - ✓ **Superior selectivity:** Oligonucleotide nanosensors can accurately discriminate between the target biomarker and other molecules in the sample, minimizing interference and increasing confidence in the results.
  - ✓ **Low detection limit:** These biosensors allow detecting minimal amounts of biomarkers, improving diagnostic sensitivity even in samples with very low concentrations.

- **Speed and simplicity:**
  - ✓ **Rapid detection:** The detection process is fast and efficient, providing results in a short time and allowing timely clinical decisions.
  - ✓ **Ease of use:** These biosensors are easy to use and do not require complex equipment or techniques, making them accessible to a wide range of healthcare personnel.
- **Versatility and potential:**
  - ✓ **Adaptability to multiple biomarkers:** Oligonucleotide-based nanodevice technology can be adapted to detect a wide range of biomarkers, expanding diagnostic possibilities for various diseases.
  - ✓ **Integration into portable devices:** These biosensors can be integrated into portable devices, allowing the detection of biomarkers at patient care points and decentralized environments.
- **Prospects:**
  - ✓ **Clinical validation:** Future studies will focus on the clinical validation of these nanosensors in large-scale studies, evaluating their effectiveness in actual clinical practice.
  - ✓ **Cost reduction:** Large-scale production and development of new technologies are expected to reduce the costs of these nanodevices, making them more accessible for widespread use.
  - ✓ **Implementation in clinical practice:** The incorporation of these biosensors in the clinical routine could revolutionize the diagnosis and monitoring of various diseases, improving the accuracy, accessibility and efficiency of diagnostic processes.

The outcomes of this thesis should aid in the development of sophisticated detection systems that will greatly enhance biomarker identification and pathogenic species in the future for improved diagnosis and treatme